SPECTROSCOPIC INVESTIGATION OF SIMPLE, MIXED, AND DOUBLE CLATHRATE HYDRATES; PROBE OF DEFECT ACTIVITY

BY

FOUAD ADNAN FLEYFEL

Bachelor of Science

in Chemical Engineering

University of Tulsa

Tulsa, Oklahoma

1985

Submitted to the Faculty of the Graduate College
of Oklahoma State University
in partial fulfillment of the requirements
for the degree of
DOCTOR OF PHILOSOPHY
December, 1990

SPECTROSCOPIC INVESTIGATION OF SIMPLE, MIXED, AND DOUBLE CLATHRATE HYDRATES; PROBE OF DEFECT ACTIVITY

Thesis Approved:

J Paul Devlin
Thesis Adviser

Lionel M. Raff

Donald L. Thompson

James P. Wicksted

Norman N Durham
Dean of Graduate College

1394997

TO MY PARENTS

ACKNOWLEDGEMENT

First and foremost I want to thank God the most gracious and the most merciful for giving me the strength to survive four years of high speed educational roller coaster. I would like to express my utmost love and respect to Dr. J. P. Devlin. I strongly believe that without his unlimited patience, and his fatherly guidance and advice inside and outside the laboratory, I could not have finished, or started this work.

I am indebted to the members of my committee Dr. L. M. Raff, Dr. D. L. Thompson, and Dr. J. P. Wicksted for their effort and assistance. I want to give a special recognition to my labmates and friends Mark Fisher, Robert Wooldridge, Gary Ritzhaupt, Kailash Swarna, Jeff Fuson, and Brad Rowland for making my life and my work at Oklahoma State seem easier.

As for the three brothers that I found when I arrived to the United States Ayman, Bilal, and Sateh words do not describe the love and the place they occupy in my heart. They enjoyed the good moments with me, and they were there to give me a shoulder to lean on when I needed it.

I want to express my love and gratitude to my loving wife, Vicki, who entered into my life two years ago, and encouraged me with her love and understanding to pursue this degree, not to mention her tremendous effort in helping me to put together this thesis. Also, my two step-children Jessica and Derek, whom I love dearly, for providing the recreational time with their presence and love, which makes my life much more joyful.

I want to thank my sisters Rana and Lynn, and their husbands Mustafa Sidani and Hamid Lawand for their support.

Finally, I dedicate this work to my parents Adnan and Mona, that are and will always be my driving force and inspiration for the rest of my life. Dad, Mom the dream has come true.

TABLE OF CONTENTS

Chapter Page

I. INTRODUCTION 1

Historical Perspective 2
Experimental Methods 13
Infrared Spectroscopy and Sample Preparation 13
Dielectric Properties 18
Examples of Clathrate Hydrates 36
Tetrahydrofuran Clathrate Hydrate (THF) 37
Ethylene Oxide Clathrate Hydrate (EO) 42
Carbon Dioxide Clathrate Hydrate (CO_2) 45
Proposed Research 49

II. EXPERIMENTAL PROCEDURES 51

Description of Equipment 51
Vacuum Lines 51
Infrared Cells 51
Instrument 66
Sample Preparation 66

III. RESULTS AND DISCUSSION 76

Mixed and Simple CO_2 Clathrate Hydrate 76
H_2O:CO_2 Deposition on CsI Plate 76
Structure I Mixed H_2O:CO_2:EO Clathrate Hydrate 79
Structure I Simple Hydrate of CO_2 84
Structure II Simple Hydrate of (THF) and CO_2 107
Structure II Simple Hydrate of Chloroform (CF) and CO_2 144
Structure I Methylchloride (meCl) Clathrate Hydrate 154

IV. CONCLUSION AND FUTURE RESEARCH 174

BIBLIOGRAPHY 177

APPENDIX A - NOMENCLATURE 181

Chapter Page

APPENDIX B - UNIT CONVERSION FROM N/m TO $D^2/A^{\circ 5}$ 183

APPENDIX C - DERIVATION OF THE FREQUENCY SPLITTING EQUATION 186

LIST OF TABLES

Table Page

1. Geometry of Unit Cells and Cages 10
2. List of Some Clathrate Hydrate Relaxation Times, Activation Energies and Dipole Moments 31
3. Infrared Frequencies of Vapor, Liquid, and Hydrate (THF) 43
4. Infrared Frequencies of (EO) Clathrate Hydrate 44
5. List of Equipment For Vacuum Line and Diffusion Pump 52
6. List of Equipment For the Glass Cell 56
7. List of Equipment For Cryogenic Cell 59
8. List of Equipment For Dewar and Copper Base 63
9. Similarities and Differences Between FTS-20C and FTS-40 67
10. List of Regular Deposits of Different H_2O:Guest Mixtures 72
11. List of Double and Mixed Clathrate Hydrates 73
12. List of Simple Clathrate Hydrate of CO_2, (CF), and (meCl) 74
13. Splitting and Coupling Constant vs θ_1 and θ_2 108
14. Frequencies of Structures I and II of $^{12}CO_2$ and $^{13}CO_2$ Hydrates in Small and Large Cages, and of (THF) in Large Cages of Structure II at Different Temperatures 145
15. Infrared Frequencies of (meCl) Clathrate Hydrate 155

LIST OF FIGURES

Figure Page

1. Ideal Form of Crystal Ice 5

2. Structure I Clathrate Hydrate 7

3. Structure II Clathrate Hydrate 9

4. Vibrational Modes of CO_2 Molecules 17

5. Hydrogen Atom Arrangement in Ordered Lattice 20

6. Hydrogen Atom Disorder in Ice I Crystal 22

7. Model of Bjerrum L-Defect 25

8. Model of Bjerrum D-Defect 27

9. Formation and Migration of Bjerrum Defects in Ice 29

10. Formation and Migration of Ionization Defects in Ice 33

11. Bulk dc Conductivity and High Frequency Conductivity of Pure Polycrystalline ice 35

12. Second Moment vs. Temperature 39

13. Heat Capacity vs. Temperature of (THF) Hydrate Doped with KOH and Hexagonal Ice Doped with KOH 41

14. Formation of CO_2 Clathrate Hydrate on Icy and Clathrate Surfaces 48

15. Vacuum Line Used For System Evacuation 54

16. Standard Low Temperature Infrared Glass Cell 58

17. Standard Low Temperature Infrared Cryogenic Cell 62

18. Silver Polished Dewar and Copper Base 65

19. Thin Layer Deposition on Substrate 71

20. Infrared Spectrum of Antisymmetric Stretching Frequency of a $H_2O:CO_2$ Vapor Deposit on CsI at 140 K 78

Figure Page

21. Infrared Spectrum of Bending Mode of water of $H_2O:CO_2$ Vapor Deposit On CsI at 140 K 81

22. Infrared Spectra of Antisymmetric Stretching Frequency of CO_2 of a Mixed $H_2O:CO_2$:EO Clathrate Hydrate 83

23. Infrared Spectra of Bending Frequency of CO_2 of a Mixed $H_2O:CO_2$:EO Clathrate Hydrate 86

24. Infrared Spectra of the Antisymmetric Stretching Frequency of a CO_2 Clathrate Hydrate Epitaxially Deposited to (EO) Hydrate Substrate at 120 K 88

25. Infrared Spectra of Antisymmetric Stretching Frequency of $^{13}CO_2$ Clathrate Hydrate Deposited Epitaxially to (EO) Hydrate Substrate at 120 K 91

26. Infrared Spectra of Bending Mode of CO_2 Clathrate Hydrate Deposited Epitaxially to (EO) Hydrate Substrate at 120 K 93

27. Infrared Spectra of Bending Mode of Small Cage Frequency of CO_2 Clathrate Hydrate 95

28. Infrared Spectra of Bending Mode of Large Cage Frequency of CO_2 Clathrate Hydrate 97

29. Subtracted Infrared Spectra of Antisymmetric Stretching Frequency of a Perfect CO_2 Clathrate Hydrate From Partially CO_2 Clathrate Hydrate ... 99

30. Infrared Spectra of Antisymmetric Stretching Frequency of $H_2O:CO_2$ Deposited Epitaxially to (EO) Hydrate at 105 K 102

31. Large Cage Frequency of CO_2 Clathrate Hydrate in the Antisymmetric Stretching Region Fitted to Lorentzien and Gaussien Curves 106

32. Coupling Constant vs. θ_1 110

33. Frequency Splitting vs. θ_1 112

34. Infrared Spectra of (THF) Structure II Hydrate in the C-O Region 115

35. Infrared Spectra of (THF) Structure II Hydrate in the C-H Region 117

36. Infrared Spectrum of CO_2 Structure II Hydrate of Antisymmetric Stretching Mode of a Double Hydrate of $H_2O:CO_2$:THF 119

37. Infrared Spectrum of CO_2 Structure II Hydrate in Bending Mode Region of a Double Hydrate of $H_2O:CO_2$:THF 122

38. Infrared Spectra of Antisymmetric Stretching Frequency of CO_2 of Different Samples Having Different (THF) Hydrate Thicknesses 124

Figure Page

39. Infrared Spectra of the Bending Mode of CO_2 of Different (THF) Hydrate Thicknesses 126

40. Infrared Spectra of Antisymmetric Stretching Mode of CO_2 Structure II Hydrate Compared to the Same Mode of CO_2 Structure I Hydrate 128

41. Infrared Spectra of Antisymmetric Stretching Frequency of CO_2 Clalthrate Hydrate; and of the O-D Stretching Frequency in Relation to H_2O:THF and $H_2O:CO_2$ Deposition Time 130

42. Infrared Spectra of Isolated HOD 132

43. Subtracted Infrared Spectrum in the O-D Stretching Region of Isolated HOD Resulting From Subtracting Infrared Spectra of a Sample Having 6 min. $H_2O:CO_2$ Deposition Time From a Sample Having 25 min. $H_2O:CO_2$ Deposition Time 136

44. Concentration of L-defects vs. Thickness of Sample (in microns). Barrier is Placed. 139

45. Concentration of L-defects in a Thin Substrate Migrating Accross the Boundary vs. Thickness of Sample (in micron). Barrier is Removed. 141

46. Concentration of L-defects in a Thick Substrate Migrating Accross the Boundary vs. Thickness of Sample (in micron). Barrier is Removed. 143

47. Infrared Spectra of (CF) Structure II Hydrate in the C-H Stretching Region 149

48. Infrared Spectra of (CF) Structure II Hydrate in the C-Cl Stretching Region 151

49. Infrared Spectra of Antisymmetric Stretching Mode of CO_2 Clathrate Hydrate, and O-D Stretching Region of Isolated HOD with Respect to (CF) Hydrate Thickness 153

50. Infrared Spectrum of the C-H Stretching Region of the (meCl) Sample Structure I Hydrate 157

51. Infrared Spectrum in the C-Cl Stretching Region of the (meCl) Sample Structure I Hydrate 159

52. Infrared Spectrum in the CH_3 Bending Mode Region of the (meCl) Sample Structure I Hydrate 161

53. Normal Vibrations of the (meCl) Molecule 163

54. Infrared Spectrum of the H_2O:meCl:EO Mixed Clathrate Hydrate Having a Mixture of 6: 0.8: 0.2 166

55. Infrared Spectrum of the H_2O:meCl:EO Mixed Clathrate Hydrate Having a Mixture of 6: 0.6: 0.2 168

Figure Page

56. Infrared Spectrum of the H_2O:meCl:EO Mixed Clathrate Hydrate Having a Mixture of 6: 0.6: 0.15 171

57. Infrared Spectrum of a Clathrate Hydrate of 6:1 H_2O:meCl Deposited On 10:1 H_2O:EO Hydrate Substrate at 127 K Using Alternating Process 173

CHAPTER I

INTRODUCTION

Clathrate Hydrates in the Universe

Clathrate hydrates are solid compounds in which gas molecules, referred to as 'guests', are encaged inside icy crystalline lattices, referred to as 'hosts'. The process of formation of the clathrate hydrates reported by van der Waals and Platteeuw (1) is given by the reaction:

(1) water + gas = clathrate hydrates

The research in the area of clathrate hydrates has become very common in many laboratories because of their several fascinating aspects. Some of these aspects are related to atmospheric sciences, and others are associated with industrial purposes. Nakahara *et al.* (2), using Raman spectroscopy, reported that 'air hydrates' occurred at a depth of 1501 m. in ice cores (Greenland). The dominating guest molecules in these clathrates were identified to be oxygen and nitrogen. Methane, carbon dioxide, and argon are also constituents of the atmosphere, but are not found to dominate in these samples. Davidson (3), using ^{13}C-NMR, claimed that some intact natural gas hydrates occurred in the Gulf of Mexico, confirming speculations about the presence of clathrate hydrates below the sea bottom. In addition, the clathrate hydrates of methane and ammonia are found in comets, planets and satellites such as Neptune, Titan (4), and Miranda (5), the smallest moon of Uranus, causing unexpected geological behavior. Barraclough (6) claims that if the trapped gases forming clathrate hydrates in the Arctic regions, and at the bottom of the sea could be released, they would become a large potential energy resource with a volume of 10^7 trillion cubic feet. This large volume of gas could make clathrate hydrate reserves a possible source of energy.

In natural gas transportation, the formation of clathrate hydrates inside pipelines can cause problems in the production and transmission of natural gases. In an effort to better understand clathrate hydrate formation in pipelines, Sloan *et al.*(7) experimentally measured the chemical potential difference $\Delta\mu$, and the enthalpy difference ΔH between the empty clathrate hydrate and ice at 273 K and zero pressure, and used this data to predict the conditions under which clathrate hydrates might form in pipelines. Later, the same workers developed a mathematical model that enabled the measurement of the clathrate hydrate dissociation rates (8). Other important proposed means of preventing clathrate hydrate growth in pipelines is to inject inhibitors such as ethanol and methanol in the pipelines (9,10,11). It is claimed however, that under certain conditions methanol, ethanol, and tert-butyl alcohol have a tendency to form clathrate hydrates (12-14), a finding which requires more attention to the growth of the alcohol clathrate hydrate.

Historical Perspective

On November 15, 1810, and during his Bakerian lecture to the Royal Society, Sir Humphry Davy (15) was the first to introduce the term 'hydrates'. He explained that during one of a series of his many experiments, he burned potassium in oxygen to form potassium peroxide. He then added water to the product and observed that the mixture "heated violently, became white, and converted into hydrates." By performing another set of experiments he concluded that the solution of oxymuriatic gas (which he later named chlorine) in water froze quicker than pure water itself.

In 1823, Faraday (16) followed up this study with several experiments and found that by mixing chlorine and water at 233 K and in a ratio of 1:10, (Cl_2:10 H_2O), a solid was formed. He also recognized that there was a possibility that the solid was not 100%

dry. The composition of this mixture was adjusted, and was found to vary between Cl_2:7.27 H_2O and Cl_2:6.04 H_2O (17). Since this discovery, other molecules have been shown to form clathrate hydrates.

In 1948, Powell (18) introduced the term 'clathrates' when he studied the compounds formed by hydroquinone with a large number of gases and volatile liquids. He showed that because of hydrogen bonding in "these compounds", spherical cavities in a ratio of one cavity to every three hydroquinone molecules were formed. When certain molecules like O_2, N_2, CH_4, C_2H_2, Kr, Xe, or any molecules ranging in size from He to CCl_4 occupied these cavities, a molecular complex would form. Powell named these complexes clathrate compounds. According to him, they were "two or more components associated without ordinary chemical union but through complete enclosure of one set of molecules in a suitable structure formed by another".

In 1952 von Stackelberg (19) studied the structures of the clathrate hydrates using X-Ray crystallographic techniques. His results were obtained by studying simple crystals of single and double hydrates. He introduced these structures and found that they were a kind of ice in which each water molecule had four water neighbors that surrounded it tetrahedrally as shown in Fig. 1, and which contained holes or voids of two different geometries large enough to hold the gas molecules. These structures are called structure I and structure II hydrates and represented in Figs. 2 and 3. More studies on the structure I hydrate were performed on a hydrate of ethylene oxide (EO) at 258 K (20), whereas the studies of the structure II hydrates were done on a double hydrate of tetrahydrofuran-hydrogen sulfide (THF-H_2S) (21). It is found that cubic unit cells form the structure I and the structure II clathrate hydrates. Each cell in structure I hydrates has a 12 A° diameter, whereas the one in structure II hydrates has a 17 A° diameter. Structure I is described by the space group Pm3n and contains 46 water molecules per unit cell. Moreover, 8 cages per cell are available in the structure I, in which 6 are large and the other two are small. The structures and cages characteristics are presented in Table 1 (19). The small cages are

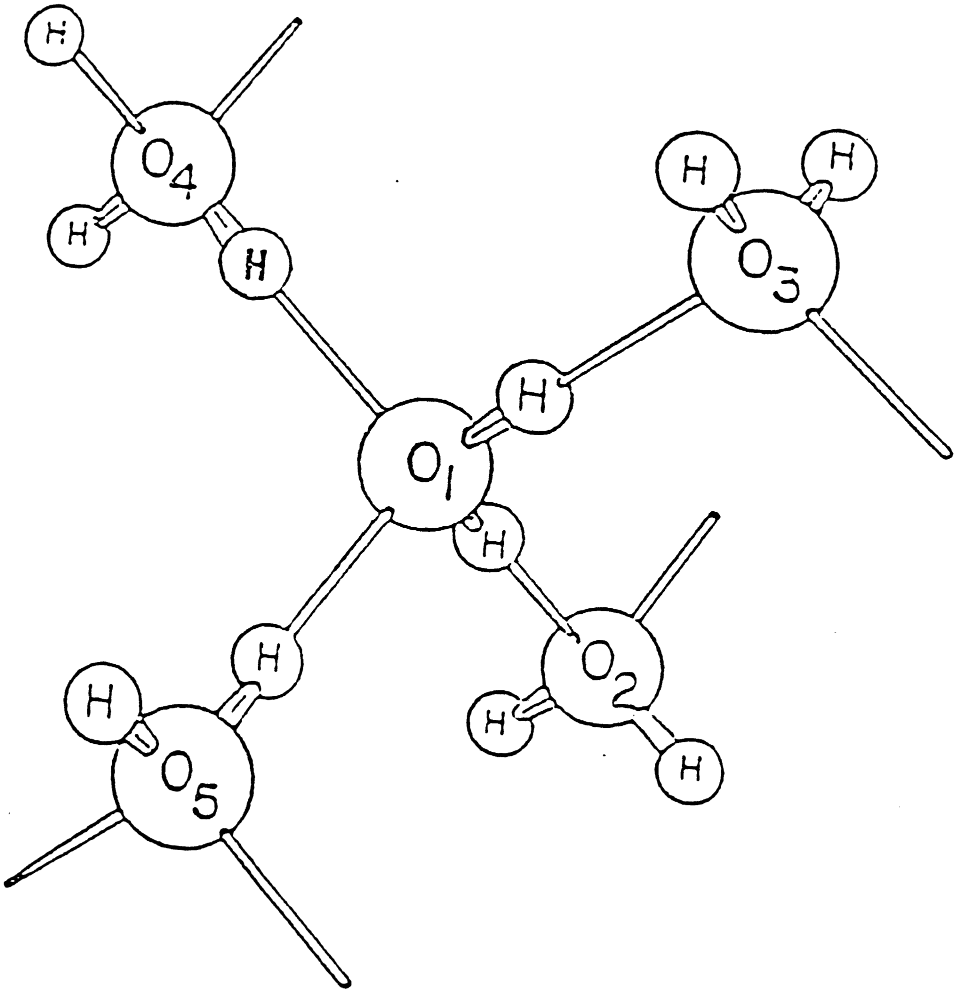
H
O4
H
H
H
H
O3
H
O1
H
H
O2
H
H
H
O5
H

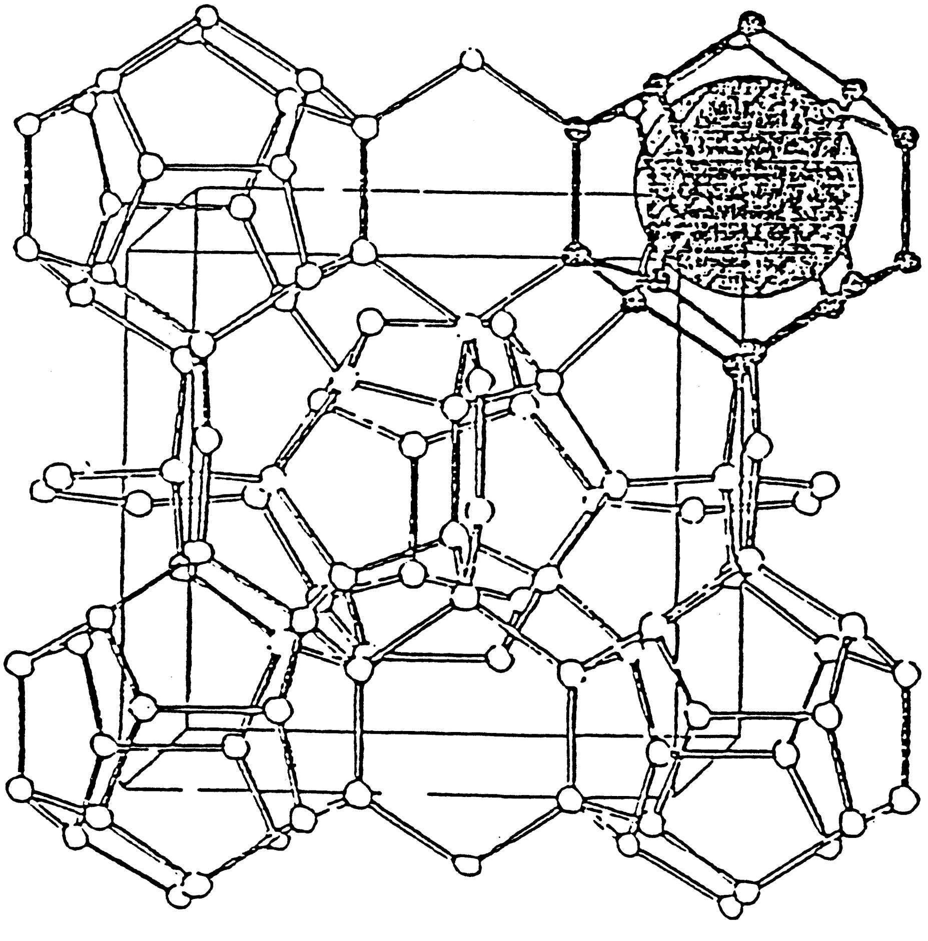

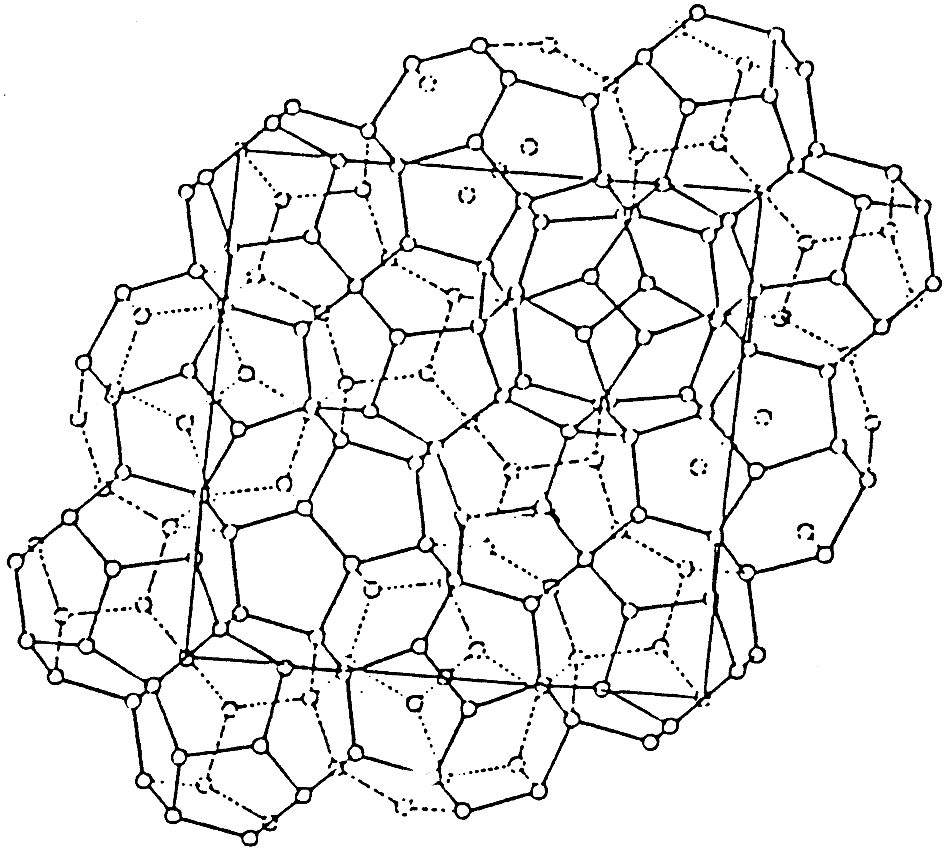

TABLE 1

GEOMETRY OF UNIT CELLS AND NUMBERS OF CAGES FOR STRUCTURE I AND STRUCTURE II

	Structure I	Structure II
Space group, cell parameter	Pm3n, 12.03 A°	Fd3m, 17.31 A°
Number of water molecules	46	136
Nonequivalent O sites	6(c),16(i),24(k)	8(a),32(e),96(g)
Oxygen site symmetry	$\bar{4}$2m,3m,m	$\bar{4}$3m,3m,m
Departure from the O-O-O angle from tetrahedral:		
Average at O site	1.2°,1.2°,5.1°	0°,2.1°,3.6°
Average in structure	3.7°	3.0°
Average O-O length,A°	2.793	2.790
Small cages:		
	pentagonal dodecahedral 12 pentagons (5^{12})	pentagonal dodecahedral 12 pentagons (5^{12})
Number, symmetry	2,m3	16,$\bar{3}$m
Oxygen sites	8(i),12(k)	2(a),6(e),12(g)
Distance to center,A°	3.83,3.96	3.748,3.845,3.956
Average cage radius,A°	3.91	3.902
Large cages:		
	tehakaidecahedral 2 hexagons, 12 pentagons ($5^{12}6^{2}$)	hexakaidecahedral 4 hexagons, 12 pentagons ($5^{12}6^{4}$)
Number symmetry	6,$\bar{4}$2m	8,$\bar{4}$3m
Oxygen sites	4(c),8(i),8(k),4(k)	4(e),12(g),12(g)
Distance to center, A°	4.25,4.47,4.06,4.645	4.729,4.715,4.635
Average cage radius,A°	4.33	4.683

pentagonal dodecahedrals (5^{12}) formed by 20 water molecules. Their average diameter is about 5.1 A°. The large cages are tetrakaidecahedrals ($5^{12}6^{2}$) assembled of two parallel hexagons and 12 pentagons. When all the cages are occupied the maximum theoretical composition obtained by one guest molecular substance, M, is M: 5.75 H_2O. This composition is increased to M: 7.66 H_2O when only the large cages (14-hedra) are filled. Structure II hydrate, which belongs to the space group Fd3m, has unit cells containing 136 water molecules. This structure has 24 cages per cell, in which 16 are small and 8 are large. The small cages in structure II are also pentagonal dodecahedrals (5^{12}). They have the same geometry as the small cages in structure I, except they are slightly deformed, and their average diameter is reduced to about 5 A°. The large cages are hexakaidecahedrals, ($5^{12}6^{4}$) consisting of 4 hexagons and 12 pentagons. Their average diameter is 6.7 A°. When all the large cages are filled, the ideal composition is M: 17 H_2O (other dimensions, characteristics, and parameters are mentioned in Table 1). It is important to note that the size of the cages are practically independent of the size of the trapped molecules. By using the diameter of oxygen given by van der Waals (d=2.8 A°) as the diameter for a water molecule, the diameters of the small cages of structures I and II become 5 A°, and the diameters of the large cages become 5.8 and 6.6 A°, respectively (22). Therefore, it has been concluded that structure I forms because of molecules that have a van der Waals diameter of less than 5.3 A°, where structure II forms because of molecules having a diameter d, such that d is between 5.5 and 6.6 A°. If d is between 5.3 and 5.6 A°, most of the structures that form are of type I.

Recently, it was claimed by Holder and Manganiello (23) that small non polar molecules were an exception to this rule. This claim was confirmed by Tse and co-workers (24-28). They reported that argon, krypton, and later oxygen and nitrogen molecules, having molecular diameters ranging from 3.83 up to 4.2 A°, could form the structure II hydrate, and their lattice parameters were in the order of 17.07 ± 0.04 A°. The cell dimensions seemed to agree with other known structure II hydrates studied earlier by

Sargent and Calvert (29). Also, Sloan (30) reported that 0.5% of impurities (i.e., C_3H_8) in a CH_4:H_2O mixture caused the hydrate structure to change from type I to type II.

As it was mentioned before, the clathrate hydrates have an ice-like structure because of the tetrahedral oxygen atom surroundings, and the hydrogen bonding of the four water neighbors as shown in Fig. 1. However, this structural similarity is not the only one that proves that clathrates and ices are alike. The average 'departure angle' of the O-O-O angle in the clathrate is 3.7° and 3.0° for types I and II respectively (19), which are a lot closer to the tetrahedral values of the hexagonal ice, Ih, and of the cubic ice, Ic, than the high-pressure ices II, III, V, and VI. Another similarity is the average length of the O-O bond, which is about 1% higher than the one in Ic and Ih. However, one of the major differences between the clathrates and the ices is the perfect planarity of the pentagons in the structure II, and the almost perfect planarity in structure I, whereas the five edged rings in ice IX are non planar. The same is true concerning the hexagons as they are completely flat in type I, and very close to flat in type II. However, the hexagons are "puckered" in the ice structure.

In addition to the two hydrate structures the clathrate hydrates are classified into three categories.

a) Simple hydrates: This term is applied only when a single kind of guest molecule is present. An appropriate example would be H_2O-trimethyleneoxide (TMO).

b) Double hydrates: This term is used only when two kinds of guest molecules are present, and where the large molecules occupy the large cages and the small molecules occupy the small cages. An example would be H_2O:H_2S:THF.

c) Mixed hydrates: This term is used when two or more kinds of guest molecules are present, and also when any of these molecules can occupy either cage. An example would be H_2O:CO_2:EO.

Experimental Methods

Infrared Spectroscopy and sample preparation

Infrared spectroscopy has become an important tool to study clathrate hydrates. Bertie(31-34) contributed to the field by applying x-ray powder diffraction and IR techniques to the same bulk grown (EO) sample, determining the structure as well as the absorption bands in mid and far IR, building a bridge relating both methods, that opened a door to more infrared investigation of more clathrate hydrates. From the x-ray results at 120 K, he characterized the sample as being a structure I (EO) clathrate hydrate because the unit cell parameter was 11.88 ± 0.03 A°, which was 1% different from the value listed by Davidson for the structure I hydrate parameter (19). Then he collected the IR spectrum of that same sample and assigned the frequencies, which eased the identification of the infrared spectrum of other clathrate hydrates.

This identification is not straight forward because the host "ice" spectrum is very similar to the IR spectrum of ice I (31). However, the relative range of the O-O near neighbor distances between the clathrate hydrate and ice I, reflecting the difference in the hydrogen-bond length distributions (52% are at 2.75 A°, 26% are at 2.79 A°, and the rest are either 2.74 or 2.82 A°, whereas in ice I, all the H-bonds are close to 2.75 A° at 100 K), is reflected in the IR spectra by a difference in the O-D stretching band of the isotopically isolated HOD units in the sample (31,35). The band half width in the clathrate hydrates is between 40-80 cm^{-1}, compared to 18-20 cm^{-1} in ice I. Combined with distinctive characteristics of encaged guest-molecule spectra, this behavior of the O-D stretching mode band normally permits the reliable recognition of a crystalline clathrate hydrate.

The guest-molecule infrared pattern is usually significantly different than observed for other phases. Besides this unique pattern, the temperature dependence of certain guest bands may also be informative since reduced temperatures, that limit rotational motion, often cause a pronounced shifting, narrowing, and peak intensity enhancement (36). If these aspects of the spectrum of a certain sample do not allow a firm judgement regarding the samples clathrate hydrate nature, a powerful alternative is to incorporate a few percent of (EO), since the IR spectra of that particular ether hydrate is now readily recognized. Therefore, (EO) has become a 'help gas', which by incorporating a few percent of it in a water:guest mixture, the IR spectrum of that guest clathrate hydrate could be easily determined. Later, Bertie also extended the far IR study to investigate the spectra of other clathrate hydrates such as cyclopropane, cylcobutanone, Tertrahydrofuran (37), and especially the detailed work done with Wright (38) on structure I and structure II clathrate hydrates of (TMO).

One disadvantage they could have encountered is the preparation of the sample mulls because the experimental procedure is long and tedious, and requires quite drastic treatment of the sample. The clathrate hydrate solid has to be ground to a fine powder, and if a disc is being prepared, subsequently compressed at low temperatures, where by then, the sample may be partially decomposed, which is a big disadvantage to the work (39). Therefore, jointly with Devlin (40), Bertie introduced the molecular vapor beam deposition technique, where, in a matter of a few minutes, the clathrate hydrate sample is prepared and ready for spectroscopic investigation.

Richardson *et al.* (36) took advantage of the simplicity of this new technique and extended the IR study to the growth of the simple, double, and mixed clathrate hydrate of some additional gases such as H_2S, THF/H_2S, EO/C_2H_6. They found by comparing the IR spectra of the simple H_2S hydrate and the double THF/H_2S hydrate that the frequencies of the H_2S in the large cage absorbed at 2550 cm^{-1} while the small cage molecules absorbed at 2560 cm^{-1}. In the case of the EO/C_2H_6 mixed hydrate the 10 cm^{-1} split in the degenerate υ_7 (e_u) mode was attributed to the split in the degeneracy as a result of nonsymmetric interactions with cage walls. Also, the authors went further in their IR investigation to probe the proton transfer rate, and the L-defect activity in the (EO) hydrate by observing the direct conversion of the isolated D_2O molecules in the clathrate samples (41), to isolated HOD units, and found that the activation energy for this reaction was approximately 5 kcal. in the temperature range of 105-120 K.

Infrared spectroscopy and clathrate hydrates cryogenic sample preparations are not spared from disadvantages. The workers encountered some problems because of the selection rules governing the activity of vibrations in IR, and the volatility of the guest molecules. To summarize these problems:

i) A diatomic molecule must possess a permanent dipole moment for its vibration to be IR active (42). Thus, it would not be possible to observe the IR spectra of 'air hydrates', which contains [O_2, N_2] clathrate hydrate etc...

ii) For polyatomic molecules (i.e., CO_2), vibrations will be IR active if there is a change in the dipole moment during vibration (42). Thus, the IR band of the CO_2 symmetric stretch mode, as shown in Fig. 4, will not be observed.

iii) Small nonpolar molecules such as ethane, methane, carbon dioxide, cyclopropane, and acetylene are found to resist the clathrate hydrate growth on a salt plate without a 'help' gas (36,43-44), rather growing as an amorphous compound at low temperature ~ 90 K, or being lost to the vacuum if the temperature is higher than 120 K.

The third disadvantage is very easily overcome by incorporating few percent of (EO) gas in the mixture as mentioned earlier, or by overpressurizing the system; such as the case of acetylene (44). The second disadvantage is not a major factor, since most molecules have more than one vibrational mode. Therefore, the study of the other modes (i.e., antisymmetric stretch, and bending) would easily allow the detection of the clathrate hydrate IR spectrum. The first disadvantage is impossible to overcome in IR spectroscopy. The only possibility is to observe the O-H stretching region, or the bending mode band in

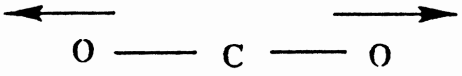

IR inactive

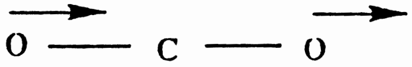

IR active (high freguency)

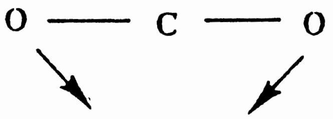

IR active (low frequency)

water (35) to detect the formation of a clathrate hydrate sample. However, other means like Raman spectroscopy combined with IR, fulfill the needs to overcome the problem.

Dielectric Properties

Since clathrate hydrates are very similar to hexagonal ice in structure, a study of the dielectric properties of ice is suggested to help understand the properties of clathrate hydrates. When the idea of hydrogen - bonded water molecules in ice was accepted, an image of an idealized lattice or a "perfect" ice crystal was constructed. This perfect crystal followed the Bernal-Fowler rules (45-46).

i) Each oxygen atom is bonded to two hydrogen atoms. The O-H bond length is about 0.95 A° and thus, they form a water molecule.

ii) The two hydrogen atoms of this molecule are directed towards two of the four oxygen atoms that surround the central water molecule tetrahedrally.

iii) Only one hydrogen atom lies between each pair of oxygen atoms.

However, in reality ice crystals show a disorder (47), in that the hydrogen atom lying along the O_1-O_2 axis (2.76 A°), is 50% of the time closer to O_1 (at a distance of 0.95 A°), and 50% closer to O_2. This is seen from the results of the neutron diffraction techniques, the electron diffraction studies, and Debye's theory. Debye suggested that the cause of this disorder was the frequent turning of the water molecules from one position to another in the presence of an applied electric field. Pauling also studied this problem when he calculated the zero-point entropy of ice and found it to be $S_0 = R \text{ Ln } 3/2$, which corresponded to 0.814 e.u (48). Figure 5 shows the hypothetical perfect ice, where the arrow indicates the direction of the polarity, and Fig. 6 represents the disordered ice crystal. The polarity in the ice is caused by the presence of a permanent dipole moment in the water molecule that has a value of 1.84 D (46). This dipole moment vector bisects the

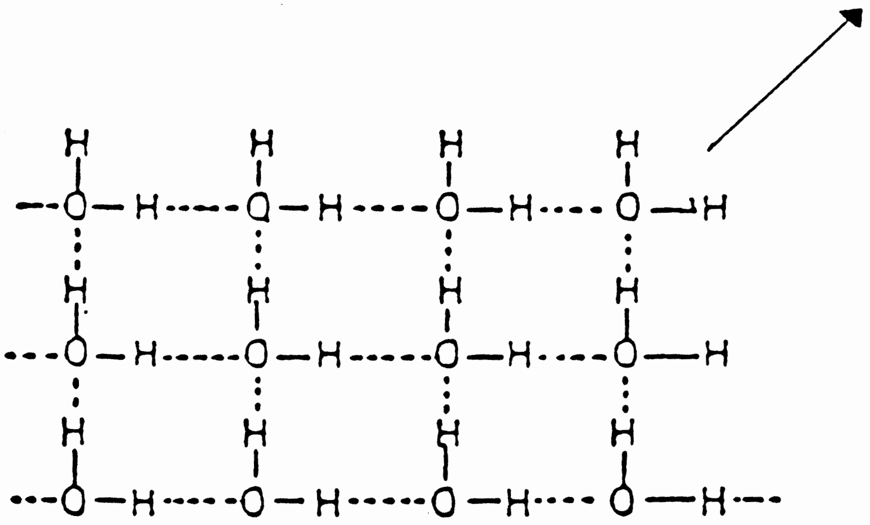
H
O
H

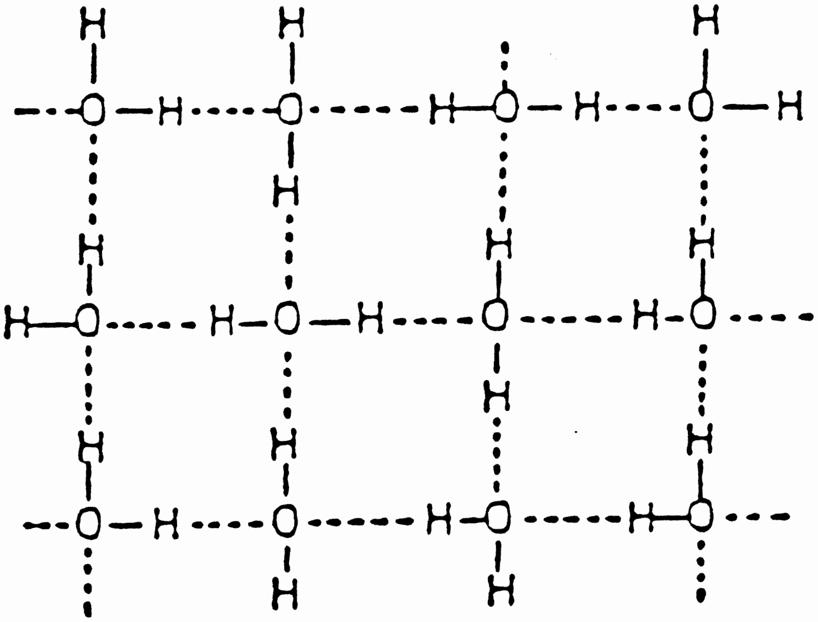
H
O
H

H-O-H angle (104.74°), and is directed from the negative region, where the oxygen atom is situated to the positive region where the hydrogen atoms are located. After the removal of the applied electric field the water molecules relax, and their relaxation time, τ, is the time required for the dipole moment in ice to revert to a random distribution after the removal of the electric field. For a single relaxation process, τ is represented by an Arrhenius form equation:

$$(2)\quad \tau = A \operatorname{Exp} (Ea/kT)$$

The presence of the dipole reorientation, the mass transport, and the charge transport resulted in many suggestions about mechanisms to describe the procedure. The best mechanism that explained the problem was introduced by Bjerrum (45). He suggested that the reason for this transport was a low concentration of lattice defects. The concentration of these orientational defects is in the order of 10^{-7} mole defects per mole of ice at a temperature of 263 K, and their energy of formation is about 16 kcal per mole pair of defects, which means a small fraction of the crystal ice is maloriented. This misorientation could occur either from the absence of a hydrogen atom on the O-O axis, or the presence of a second hydrogen atom on the O-O axis. (This misorientation violates the third rule of Bernal-Fowler). When the hydrogen is missing from the O-O axis the defect is called an 'L-defect' as in Fig. 7, and when there are two hydrogens on the O-O axis the defect is called a 'D-defect ' as in Fig. 8. Figure 9 (a-d) shows the perfect ice crystal that follows the Bernal-Fowler rules, and the formation and migration of the L and the D-defects. This formation is caused by a rotation of the central water molecule of 120°, when enough thermal energy is gained to allow the rotation. However, there is a probability that the water molecule goes back to its initial position, and thus, the L and the D-defects cancel each other. If the rotation of the other central water molecule occurs as shown in Fig. 9 (c,d), the L and the D-defects start to migrate inside the crystal, which reduces the probability of self cancellation. In ice I formation of defects is represented by the following equation:

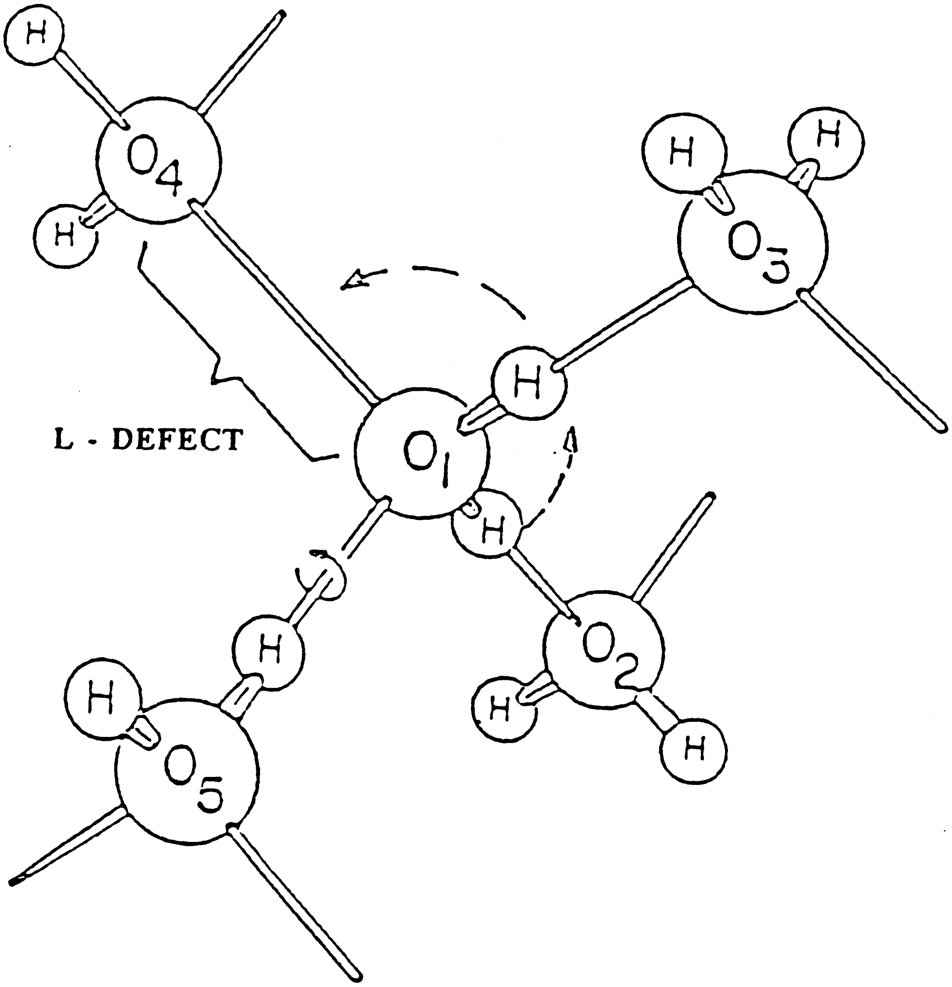
H
H
O4
H
H
O3
H
L - DEFECT
O1
H
H
H
O2
H
H
O5

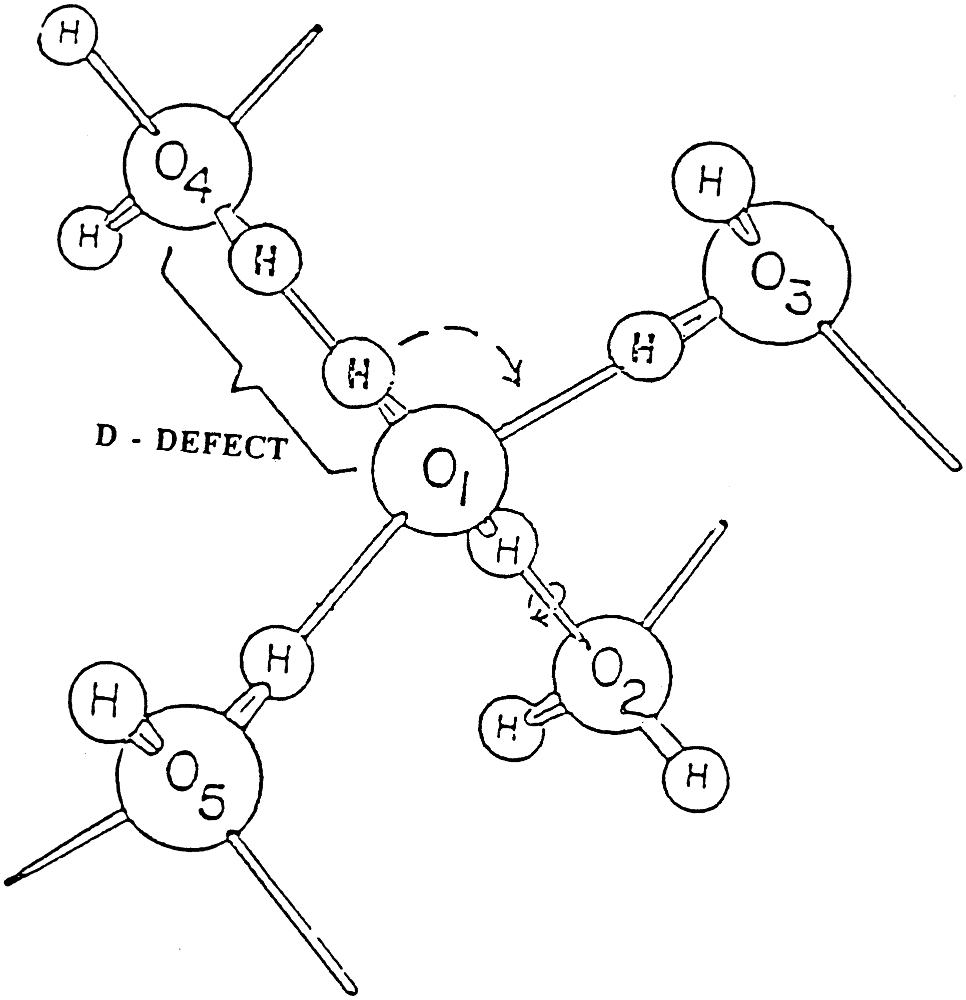
H
O4
H
H
H
H
O3
H
D - DEFECT
O1
H
O2
H
H
H
H
O5

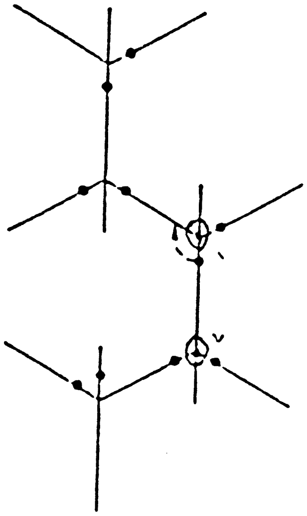

a

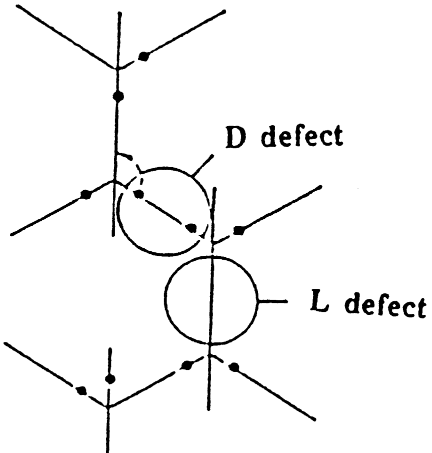
D defect
L defect

b

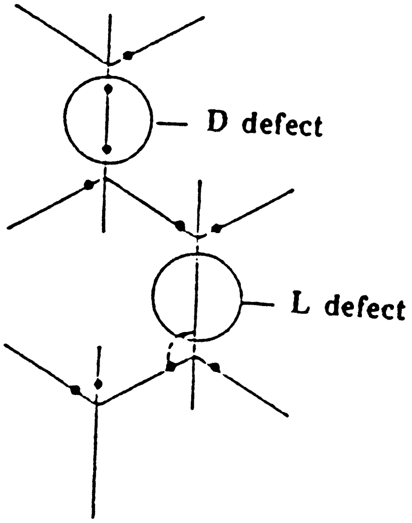
D defect
L defect

c

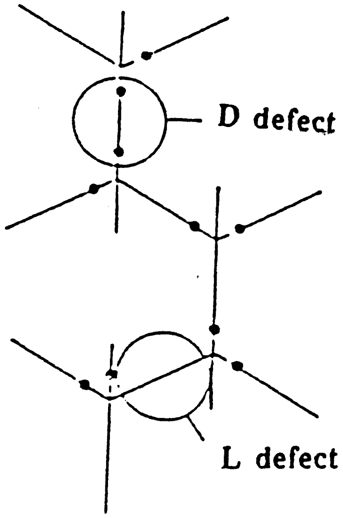
D defect
L defect

d

$$(3)\ \ 2N = D + L$$

where N the normal hydrogen bonds.

Another defect that exists in ice is called the ionization defect. Figure 10(b) shows the formation of the hydronium ion and the hydroxide ion, which are caused by a proton shift from one position to another. The same argument about the defect self cancellation is also true in this case. Figure 10(c) shows the migration of the ions inside the deformed ice crystal.

Camp *et al.*'s (49) experimental work describes the major charge carriers in ice samples as illustrated in Fig. 11. At low temperatures and at high frequencies (σ_∞), the majority charge carrier is the process of proton hopping, whereas at low frequencies (σ_S), it is the L-defect process. At high temperatures the opposite is true.

Davidson *et al.* (50) used the structural similarities between the clathrate hydrates and ice I, and considered the dielectric properties of the former to be close to the latter. Therefore, they used dielectric measurements to study the relaxation times of ice and several clathrate hydrates of different structures. They found that at 233 K the relaxation times of structure I (EO) hydrate, $\tau = 0.33\ \mu s$, and structure II (THF) hydrate, $\tau = 1.0\ \mu s$, were smaller than the argon and nitrogen hydrate values, $\tau = 96$ and $180\ \mu s$ respectively, which in turn relaxed much faster than ice I, $\tau = 1420\ \mu s$ as listed in Table 2. To explain this particular behavior (51), they suggested that the clathrate hydrates might also relax by diffusion of orientational defects, since the hydrogen bonding in the hydrate structures I and II lattices resembled more the hydrogen bonding in ice I, than did the hydrogen bonding in ices III, V, VI, and VII; especially since these high pressure ices were also suggested to relax by the same mechanism as ice I. They found that the fraction of normal bonding converting to defect was 300 times larger in the (EO) clathrate hydrate than in ice I, at 263 K. The other explanation to why some isostructural hydrates relaxed faster than others was because the guests of the fast relaxing solids (i.e.; EO, THF) might hydrogen bond with the lattice walls, which could result in more L-defect activity in the

TABLE 2

LIST OF SOME CLATHRATE HYDRATE RELAXATION TIMES, ACTIVATION ENERGIES, AND DIPOLE MOMENTS

Guest (structure)	τ_0(233.2K)	E_D[a]	μ[b]
Ice	1420	13.2	-
Xe (SI)	330	12	0
Cyc.propane (SI)	310	11.4	0
N_2 (SII)	180(1.2Kbar)	-	0
Ar (SII)	96(2.0Kbar)[c]	-	0
CH_3Cl (SI)	-	10.5	1.87
CO_2 (SI)	14.9	7.55	0
EO (SI)	0.33	7.7	1.90
TMO (SI)	0.03	5.8	1.93
SF6 (SII)	780	12.3	0
CCl_3F (SII)	450	-	0.46
CCl_2F_2 (SII)	230	-	0.51
$CClF_3$ (SII)	160	-	0.5
$CHCl_2F$ (SII)	130	-	1.3
$CBrClF_2$ (SII)	60	-	-
1,3-dioxolane (SII)	5.4	8.7	1.47
1,4-dioxane (SII)	4.6	9.1	0
Propylene oxide (SII)	2.0	8.0	2.0

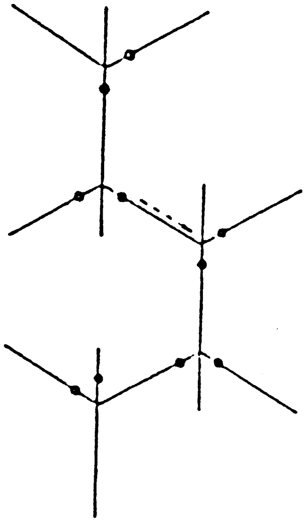

a

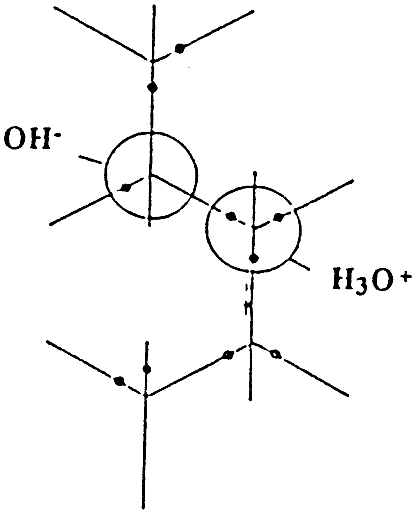

b

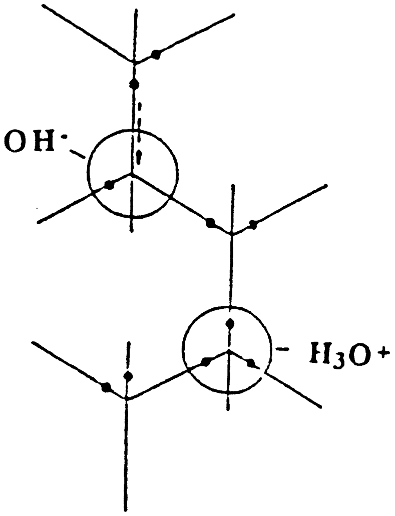

c

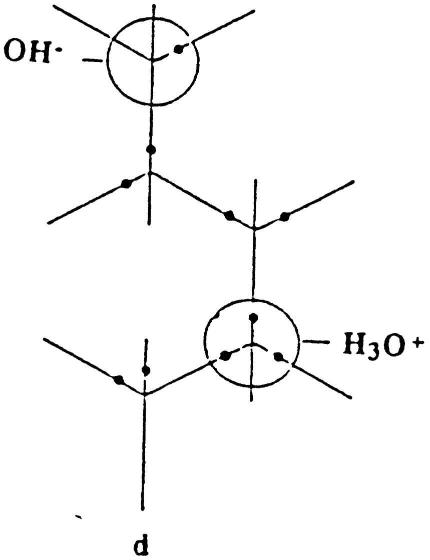

d

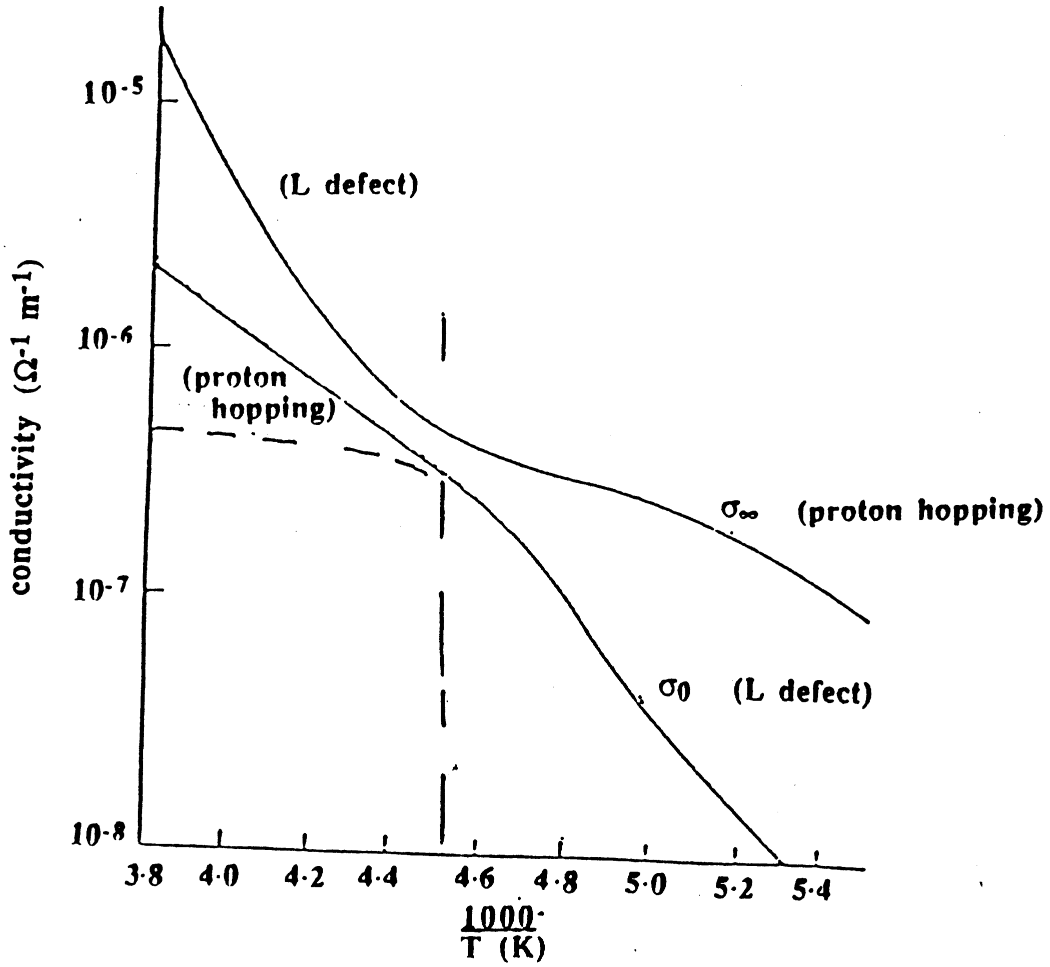

conductivity (Ω^{-1} m^{-1})
10^{-5}
10^{-6}
10^{-7}
10^{-8}
(L defect)
(proton hopping)
σ_∞ (proton hopping)
σ_0 (L defect)
3·8
4·0
4·2
4·4
4·6
4·8
5·0
5·2
5·4
$\frac{1000}{T\ (K)}$

crystalline sample, whereas argon and nitrogen might substitute for water molecules as impurities. The reason why the relaxation time for (EO) hydrate is three times faster than that for (THF) hydrate was not explained, but since the structure II hydrate has more icy characteristics than structure I hydrate, the results seem consistent (43).

The defect process mechanism for clathrate hydrates is modified from the one suggested for ice, to supply for the difference in the enthalpy and entropy values between the two compounds. The mechanism suggested (51) is:

$$(4) \quad M + N = M...H\text{-}O + L$$

where M, N, and L represent a guest molecule, a normal H-bond, and an L-defect. Figure 7 explicitly shows that process. A guest molecule (i.e.; EO) steals the H-atom situated on the O_1 - O_4 axis to form a vacancy in the O_1 - O_4 bond and creates an L-defect. That structural distortion causes instability in the crystal, which allows the neighboring water molecule to rotate with relative ease around the O_1 - O_5 axis for 120° to fill the vacancy, which in turn creates an L-defect around the O_1 - O_2 axis, etc...

By combining the FT-IR and the dielectric data, it is suggested by Devlin (43) that the clathrate hydrate containing ethers as guest molecules are relatively rich in defects compared to other hydrates, or especially compared to ice.

Examples of Clathrate Hydrates

In this section a brief presentation of some experimental results and a brief discussion about three clathrate hydrates, tetrahydrofuran (THF), ethylene oxide (EO) and carbon dioxide (CO_2) is given. The experimental techniques that have been used are (a) Dielectric and NMR, (b) Calorimetric, (c) FT-IR, and (d) X-ray.

Tetrahydrofuran Clathrate Hydrate (THF)

McMullan et al. (21), using x-ray analysis, studied the double hydrate of

THF/H_2S. They reported that the H_2S molecules (which are the small molecules in the clathrate) occupy the small cages of the type II hydrate formed, filling about 48% of them. The large cages, are obviously occupied by the (THF) molecules. Those hexakaidecahedrals are almost spherical in shape, and their diameter is 6.6 A° where the molecular diameter for (THF) is 5.9 A°, which led to the conclusion that the THF molecules possess a rotation inside the large cages. The structural result was confirmed by Sargent and Calvert (29). Davidson (50,52) ensured these results by conducting dielectric experiments on three different (THF) clathrates. H_2O-THF, D_2O-THF, and H_2O-THF_{d8}. The experiments were performed on various modes of motion of guest and host molecules. The measurements indicate that the second moment (SM), representing the mean square of the band shapes, in all cases falls with increasing temperatures as seen in Fig. 12. This decrease in (SM) is attributed to the averaging of the inter and intra-molecular proton interactions. The superposition of the curves at high temperatures was caused by 1) reorientation of the molecules, and 2) translational diffusion of the molecules. This study was followed by the observation of the complex permittivity vs. the frequency. At low frequencies it seems that the reorientation of the water molecules is the major factor, and at high frequencies, where the curve falls, the reorientation of the guest molecules takes place. The reorientation of the (THF) molecules was observed also by Leaist (53), and White and MacLean (54) using heat capacity measurements in the temperature range of 17 K to 260 K. Above 120 K, the measurements are consistent with free guest rotations, which agree with the dielectric measurements discussed earlier. At lower temperatures, the rotation of the (THF) molecules became hindered. Suga *et al.* (55) observed a first order phase transition of the (THF) clathrate hydrate doped with KOH at 62 K, which was 10 K lower than that of Ih as in Fig. 13. In another work done by the same group (56), a smaller jump in heat capacity occurred about 80 K, which was comparable to Mac Lean's maximum heat capacity value of 85 K. At this temperature, Suga presumed that the jump was caused by the reorientation of the protons, which represents also the onset of mobile

Figure 12. Plot of the second moment with respect to temperature. (Taken from reference 50)

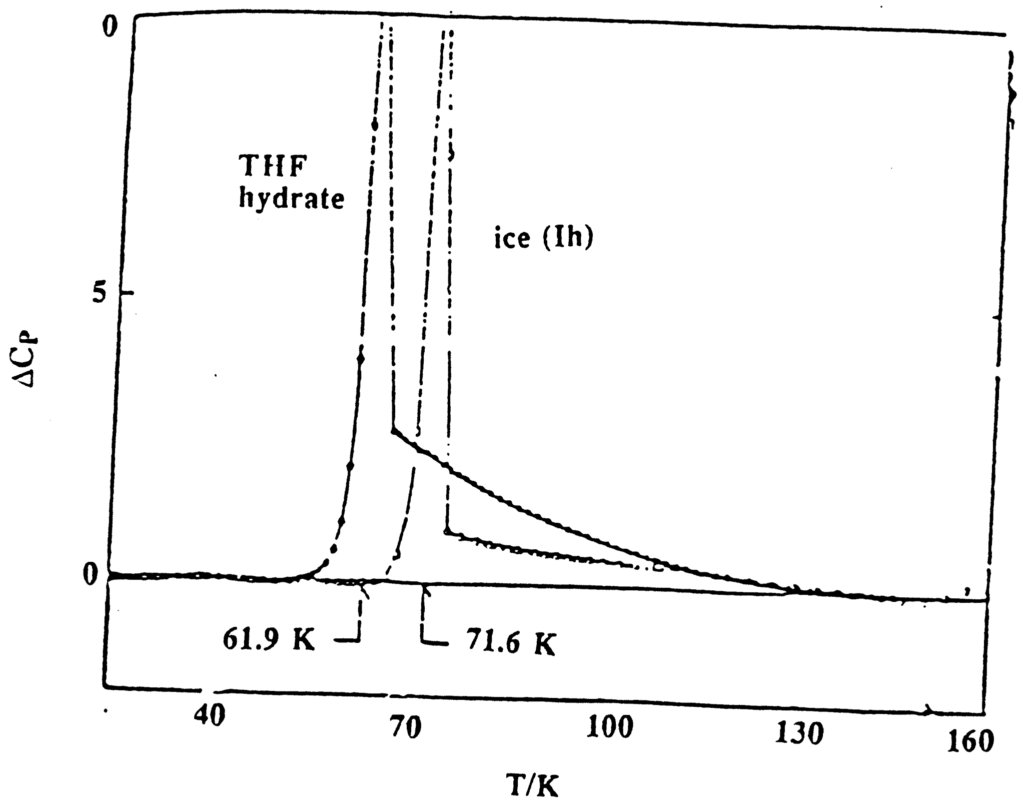
0
5
0
ΔCP
THF
hydrate
ice (Ih)
61.9 K
71.6 K
40
70
100
130
160
T/K

Bjerrum defects. This conclusion is parallel to that of Fujara (57), when he studied the reorientation of the protons for different doped ices.

Spectroscopically, using FT-IR, Richardson *et al.* (36) monitored the IR spectra of (THF) clathrate hydrates by growing the crystalline sample from an annealed (THF) amorphous layer deposited at 90 K. The C-O stretching frequency of the amorphous sample showed a doublet at 1052/1034 cm^{-1} and the frequency of the crystalline (THF) clathrate hydrate was at 1073 cm^{-1}, which was 7 cm^{-1} lower than the gas phase value (58), and 5 cm^{-1} higher than the liquid phase value (59). The frequency values of (THF) clathrate hydrates are listed and compared to the frequency values of liquid (THF) in Table 3.

Ethylene Oxide Clathrate Hydrate (EO)

X-ray powder diffraction was used (20) to identify that the hydrate structure of (EO) was of type I. Richardson *et al.* (36) extensively used FT-IR spectroscopy to study the IR spectrum of (EO) hydrate samples, which were prepared by the means of cryogenic deposition techniques. The IR spectra were obtained in the range of 4000-500 cm^{-1}. Assignments were given to some particular frequencies following Bertie's results for bulk grown clathrate hydrates. The Evans holes in the spectra of the (EO) were noted and assigned in Table 4. In an amorphous deposit of H_2O:EO, a single hole appeared around 2536 cm^{-1}. This was due to the overlap of the overtone of the (EO) $\upsilon_3(a_1)$ ring vibration, and the "association" band of ice and water located at 2240 cm^{-1}. In a crystalline deposit of the same mixture three holes appeared in the spectrum. The side band frequency at 1281 cm^{-1} is interpreted as being the frequency $\upsilon_3(a_1)$, which corresponds to (EO) molecules encaged inside the small cages of structure I hydrate, and the 1268-1266 cm^{-1} doublet belongs to the large cages. This doublet is interpreted by Bertie as being caused by a multiple site effect (31,34). The 2548 cm^{-1} hole is reported to be the combination mode

TABLE 3

FREQUENCIES (cm^{-1}) IN THE INFRARED SPECTRA OF (THF) CLATHRATE HYDRATES AT 10 K

THF hydrate (10 K)	Gas Phase THF	Liquid Phase THF
2981	2980	2975
2952	-----	-----
2938	-----	-----
2880	-----	-----
2867	-----	-----
2852	2850	2852
2840	-----	-----
1310	-----	-----
1289	-----	-----
1278	-----	-----
1208	-----	-----
1192	-----	-----
1168	-----	-----
1152	-----	-----
1144	-----	-----
1131	-----	-----
1073[a]	1080	1068
1071[a]	-----	-----
1055	-----	-----
1025	-----	-----
-----	915[b]	900

a) correspond to υ_a (C-O) of (THF)

b) correspond to υ_s (C-O) of (THF) not shown in the hydrate case because of band overlap with water.

TABLE 4

FREQUENCIES (cm^{-1}) IN THE INFRARED SPECTRA OF (EO) CLATHRATE HYDRATES AT 90 K

Wavenumbers (cm^{-1})	Interpretation
2562	Evans holes (2 x 1281)
2548	Evans holes (1281 + 1267)
2535	Evans holes (2 x 1267)
2455	$\nu_3(D_2O)$
2428 b_1	$\nu_{OD}(HOD)$
2423	(1281 + 1143)
2412	(1267 + 1143)
2380	$\nu_1(D_2O)$
1480	$\nu_2(HOD)$
1281 w	ν_3(small cage)
1268 m	ν_3(large cage)
1266 vs	ν_3(large cage)
1217	$\nu_2(D_2O)$
1153	ν_{11},ν_{14}(small cage)
1143 w	ν_{11},ν_{14}(large cage)

of (EO) molecules in the adjacent small and large cages (1281 + 1266 = 2547) in resonance with the water lattice. This coupling is also seen by Tse *et al.* (60). The hole at 2562 (1281 + 1281) is very weak and usually disappears quickly. The 2535 cm^{-1} is interpreted to be: a) a combination of neighboring molecules in the large cages (intermolecular coupling), or b) an overtone of a single molecule. The first interpretation is more satisfactory since the band intensity decreased with the increase of the dilution factor.

The proton hopping rates in (EO) clathrate hydrates were also analyzed using the two step reaction:

(5) $D_2O + H_2O$ -------> $(HOD)_2$ rate constant: k_1

(6) $(HOD)_2$ -----------> 2 HOD rate constant: k_2

The first reaction is caused by the proton hopping, whereas the second is caused by the L-defect migration. Knowing that $k_2 >> k_1$, the first equation would be the rate determining reaction. The activation energy of the proton hopping is calculated by plotting the ln k_1 vs. 1/T and found to be 5± 1.8 kcal, which is almost half the activation energy of cubic ice (9.5 Kcal). This results seems to agree with Davidson's (61), in which he proposes that this value might lead to a greater concentration of L-defects in the sample.

Carbon Dioxide Clathrate Hydrate (CO_2)

The studies concerning the clathrate hydrates of CO_2 are not very numerous. Spectroscopically, Ripmeester and Ratcliffe (62) applied the ^1H and ^{13}C NMR to measure the relaxation time of the CO_2 clathrate hydrate lattice molecules in the temperature range of 77-250 K. They found that at temperatures higher than 200 K the guest molecules, occupying only the structure I hydrate large cages, picked up a rotational motion inside the lattice cavities making a maximum angle of 31° with the equatorial plane of the cage. At 233 K, the relaxation time, τ, of the lattice molecules was measured to be 14.9 μs, possessing an activation energy of 31.6 kJ/mol corresponding to 7.55 kcal/mol.

Schmitt (63) conducted kinetic studies on the formation of CO_2 clathrate hydrates by gas-ice interaction phenomena at low temperatures (~ 200 K) and moderate pressures. During the study, he observed three "evolutionary" steps involved in the process. a) The incubation step: in which during this period no variation in the pressure of the system is observed, b) the nucleation step: a fast decrease in pressure, and a large increase in the absorption rate, until the latter reaches a maximum value, and than decreases progressively while the pressure approaches the CO_2 clathrate hydrate dissociation pressure ~ 255×10^{-3} bar, and c) the growth step: characterized by a high rate of absorption and a strong dependence on initial pressure. The first two steps were defined by Sloan (30) as being the primary and secondary nucleation steps. Figure 14 shows the growth of CO_2 clathrate on ice and on clathrate surfaces. Schmitt concludes that the dissociation pressure of CO_2 clathrate is reached faster when the surface is a clathrate rather than ice. This is caused by the large reduction in the incubation time, which leads to a faster nucleation start. When the dissociation pressure is reached, the curve shows an asymptotic behavior which describes an indefinite growth of the clathrate hydrate. The maximum rate of absorption on ice at 195 K was measured to be 1.7×10^{-12} mol/cm^2 sec. after 100 min. Also, by varying the initial pressure of the CO_2, Schmitt found that by getting closer to the dissociation pressure the incubation time increased, whereas the nucleation process seemed to behave the same, and even overlap after 1000 min. The rate of absorption slows down when the pressure gets closer to the dissociation pressure. Therefore, he concluded that the formation of CO_2 clathrate hydrate depends strongly on the gas initial pressure. He suggests in his mechanism that the mobility of the water molecules indicates that the first CO_2 clathrate species are constructed by the migration of water molecules, and the trapping of the adsorbed guest molecules. Then, the CO_2 clathrate hydrate formation continues either by a growth on the clathrate surface caused by the trapping of the gas molecules by water molecules from the clathrate free area, or by nucleation on the ice surface. This last process reduces the icy surface area. Finally, the formation process of the CO_2 clathrate stops

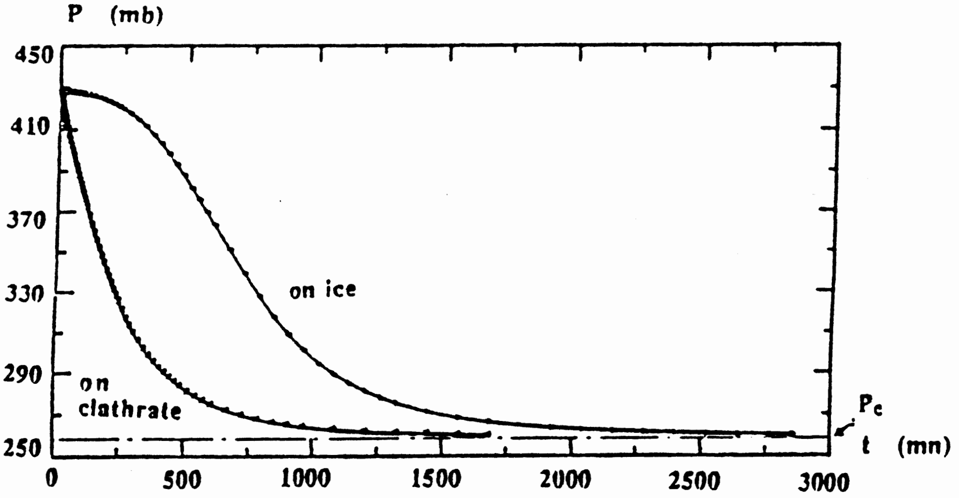
P (mb)
450
410
370
330
290
250
on ice
on clathrate
Pe
t (mn)
0
500
1000
1500
2000
2500
3000

when the clathrate layer of ~ 1μ thick, corresponding to approximately 800 unit cells, forms a continuous screen forbidding the diffusion of water molecules toward the surface.

Proposed Research

The spectroscopic investigation of clathrate hydrates has been greatly facilitated by the introduction of the vapor beam deposition method by Devlin and Bertie (40). This method enabled the quick formation of clathrate hydrate samples in the temperature range of 100-150 K to allow the examination of some of the factors that control the hydrate formation. For example, the epitaxial growth of some clathrate hydrates could be examined with respect to temperature, guest species, acid/base dopant molecules, concentration of Bjerrum defects, and the thickness of the clathrate substrate. The growth of some non-polar-molecule clathrate hydrates could also be examined as mentioned earlier by incorporating a few percent of (EO).

The key to this research is to be able to grow the CO_2 simple clathrate hydrates by depositing the $H_2O:CO_2$ vapor mixture epitaxially to hydrate substrates such as (EO) or (THF), or as mixed or double compounds by mixing with a few percent (EO). The investigation of the FT-IR spectra of the samples allows the determination of the CO_2 hydrate small and large cage frequencies of the antisymmetric and bending modes, which in turn helps the determination of the CO_2 clathrate type that might form. Also, the incorporation of 4% HOD permitted the observation of the υ (O-D) stretching frequency for both hydrate structures. A major part of this work deals with the question, whether the epitaxial growth of the clathrate hydrate is determined by the nucleation process, or by growth via the presence of mobile L-defects in the system. The work done to approach the answer was based on the fact that (EO) and (THF) hydrate substrates are considered to be a rich source of L-defects. Therefore, the probe of defects in the system was achieved by testing the epitaxial growth of the 6:1 $H_2O:CO_2$ mixture on the substrate and by varying the experimental procedure accordingly. Some of the variations are:

1) Grow the mixed CO_2 and (meCl) clathrate hydrate by mixing the H_2O:CO_2 and H_2O:meCl with few percent (EO) gas.
2) Vary the relative concentration of EO:CO_2 and EO:meCl to be able to determine small and large-cage frequencies.
3) Epitaxially grow the H_2O:CO_2 to (EO) and (THF) clathrate hydrate substrate.
4) Varying the thickness of the hydrate substrates by varying the deposition times at the deposition temperatures of 150 K and 105 K for (THF) and (EO) hydrates, respectively.
5) Epitaxially growing a chloroform (CF) clathrate hydrate layer,with a variable thickness from one experiment to another, to a (THF) hydrate substrate having a constant layer thickness, and the use of this layered sample to examine the defect activity in the clathrate hydrate.

CHAPTER II

EXPERIMENTAL PROCEDURES

Description of Equipment

Vacuum Lines

Two vacuum lines were used during this study. The first, is for loading the gases in the glass bulbs (the loading technique will be discussed later). The second, which is illustrated in Fig. 15 and described in Table 5 is joined to the cell by extremely well fitted glass joints to keep the cell under vacuum. Inlet #1 on the very left is connected to a SV.1 Hastings vacuum gauge to monitor the gas pressure inside the line. The pressure ranges from 10^{-6} to atmospheric. Inlets #3 and #4 are joined to the upper and lower part of the infrared cell, respectively. The last joint is connected to a GPH-320C ionization gauge to provide a better pressure reading accuracy. Some of this work was done without the help of ionization gauge because of an electronic malfunction. The vacuum in the line is achieved by mechanical pumping using a Welch Duo-Seal model 1402 roughing pump. Both lines are kept under vacuum almost constantly without being exposed to the atmosphere to avoid unnecessary contamination. The valves used in the loading line are grease sealed stop-cocks, which did not seem to contaminate the mixtures, and the second line was sealed from the atmosphere by Teflon valves that do not require the use of grease.

Infrared Cells

During this work two infrared cells were used; the standard glass IR low

TABLE 5

AN ITEMIZED LIST OF EQUIPMENT FOR VACUUM LINE AND DIFFUSION PUMP PRESENTED IN FIGURE 15

Number of Units	Representation; Function
1	O-ring seal ball glass joint.
2	(0-3)mm orifice Teflon vacuum valve; connects line to cell for back pumping.
3	(0-10)mm orifice Teflon vacuum valve; connects the vacuum line to expander unit.
4	(0-3)mm orifice Teflon vacuum valve; connects the vacuum line to the pressure gauge.
5	(0-5)mm orifice Teflon vacuum valve; connects both parts of the vacuum line.
6	(0-3)mm orifice Teflon vacuum valve; connects the vacuum line to ionization gauge.
7	Liquid nitrogen trap; traps impurities when dipped in liquid nitrogen.
8	(0-5)mm orifice Teflon vacuum valve; connects the vacuum line to the oil diffusion pump.
9	(0-5)mm orifice Teflon vacuum valve; connects the vacuum line to the mechanical pump.
10	Rubber hose; connects the vacuum line to the mechanical pump.
11	Heater connection wires; heat the oil.
12	Oil reservoirs.
13	Diffusion column; cools the oil at the upper tip and condenses it.

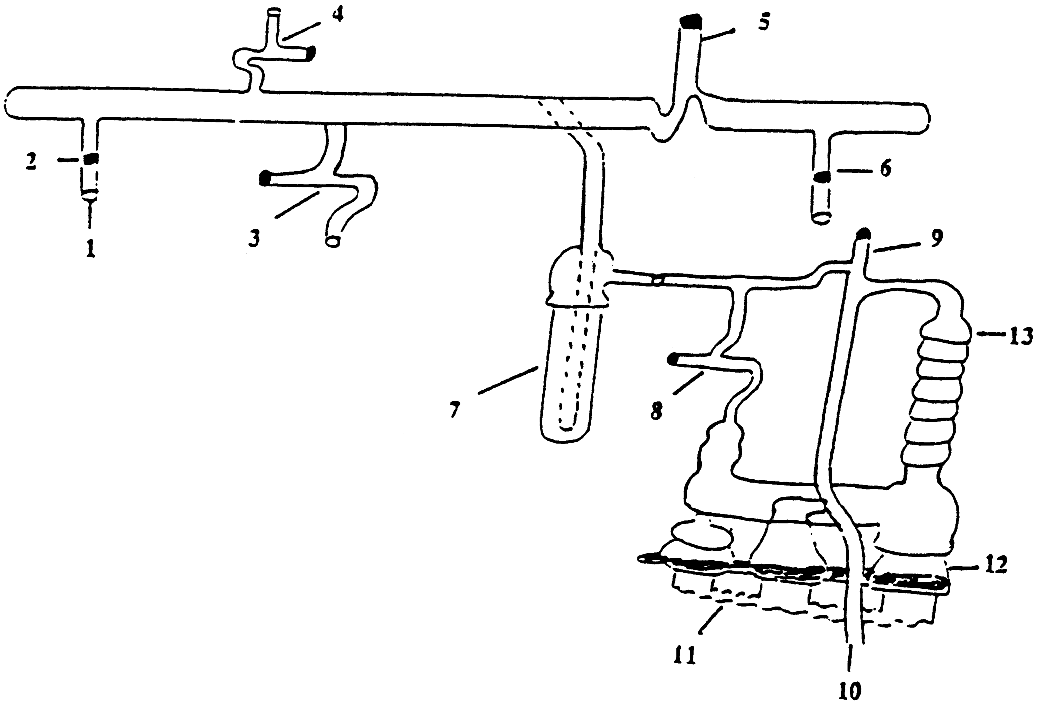

temperature cell as in Fig. 16 and described in Table 6, and the cryogenic cell in Fig. 17 and Table 7. In principle, both cells operate similarly, but the cryogenic is more sophisticated than the glass because of its cooling system and design. When the cells are off the vacuum rack, the cryogenic cell could be left off for at least an overnight for data collection, since it is cooled by an Air Product HC-2 water cooled closed cycle helium cryogenic refrigerator. The glass cell however, needs frequent checking, since it is cooled manually with liquid nitrogen. Both cells on the other hand, could be closed securely to avoid any leaks for several hours. The cooling of the sample in the glass cell is done by pouring liquid nitrogen into a silver coated dewar fitted to the cell by the means of a glass taper joint, and extending through the cell chamber by a stem, which is soldered to a copper base using a Kovar seal as shown in Figure 18 and described in Table 8. The copper base holds the Cesium Iodide salt plate substrate, on which the water:gas mixture deposits to form a clathrate hydrate thin film. Between the salt plate and the copper base an indium wire is placed to improve thermal contact with the coolant. The temperature is read by inserting an iron-constantan thermocouple into the copper base. Before and during the deposition the salt plate faces the vapor beams exiting from glass delivery guns, and after the deposition the stem has to be rotated 90°, so that the salt plate parallels the outer polished KBr windows, that allow the IR beam to pass through the sample.

The cryogenic cell design is more complicated. It is divided into two parts, the shroud and the expander unit. The shroud; a brass piece that plays the role of an outside vacuum jacket, which could rotate around the expander unit to give the IR beam a straight path. The shroud is designed with four entry ports, in which two on the side serve as window ports. The back entry is connected to the vacuum line by a glass joint as a back pumping resource, and the front entry could be linked to gas bulbs and reservoirs by glass joints, and by precision bore flowraters. The expander unit is composed of the cylinder assembly and the motor assembly. The major part of the first assembly is the stem. A heater wire and a gold doped with iron thermocouple are wrapped around the stem, and

TABLE 6

AN ITEMIZED LIST OF EQUIPMENT FOR THE GLASS CELL PRESENTED IN FIGURE 16

Number of Units	Representation; Function
1	18/7 female glass socket; vacuum connection.
2	(0-3)mm orifice Teflon valve; isolates glass from vacuum line.
3	3 cm diameter glass window; plug bottom opening of the cell.
4	40/50 male glass taper joint; base for liquid nitrogen dewar.
5	Thermocouple wire vacuum seal; allows temperature measurements.
6	34/45 female glass taper joint; holds gas delivery tubes.
7	4 cm diameter KBr outer window; plug side openings and serves as a pattern for IR beam.

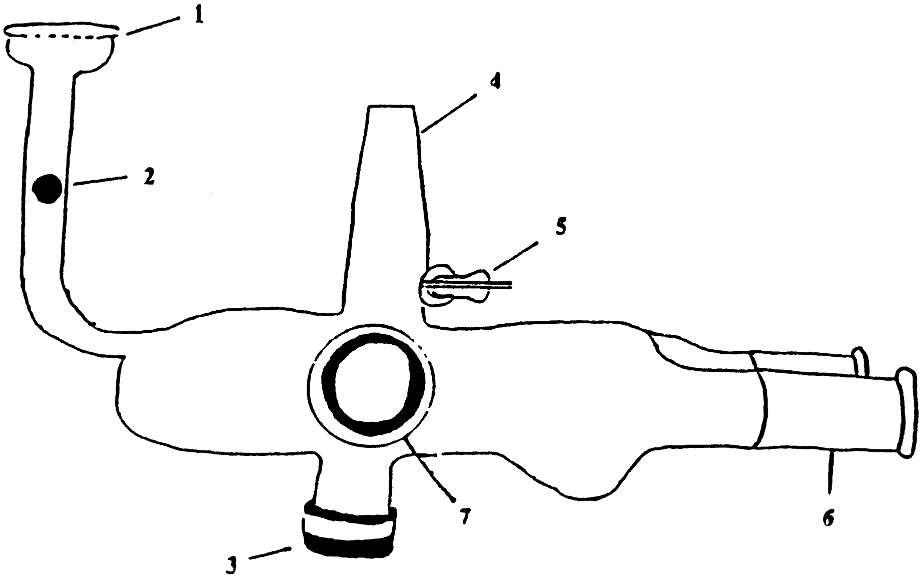

TABLE 7

AN ITEMIZED LIST OF EQUIPMENT FOR THE CRYOGENIC CELL PRESENTED IN FIGURE 17

Number of Units	Representation; Function
1	Gas bulb; gas mixture storage.
2	Grease sealed stop-cocks; seal gas bulbs.
3	(0-3)mm orifice Teflon valve; connects the bulb to flowrater.
4	Flowraters; measure flow rate.
5	18/9 fork shaped glass joint; allows more gas inlets.
6	(0-3)mm orifice Teflon valve; connects the glass joint to gas delivery tube.
7	Glass tube; gas delivery.
8	Metal joint; houses the delivery tube and connects to the front end of the shroud.
9	(0-3)mm orifice Teflon valve; connects metal delivery pipe to mixtures reservoirs.
10	Kovar seal; glass-metal joint.
11	Metal delivery pipe.
12	Shroud; houses the substrate and cold stem.
13	2.2 cm sides window brass retainer; protects KBr windows from damaging.
14	KBr side windows.
15	Back port for back pumping.
16	(0-3)mm orifice Teflon valve; connects the vacuum line to the cryogenic cell backport.
17	Metal valve; allows pumping on expander unit.

TABLE 7 (Continued)

Number of Units	Representation; Function
18	Metal-glass joint; connects the vacuum line to the expander unit.
19	Helium gas connectors; connects the refrigerator to the cell by hoses.
20	Expander unit.
21	Golden thermocouple feed through; measure temperature of lower part of the cell.(a)
22	Iron-constantan thermocouple; measure temperature of substrate.(b)

(a), (b) = the difference in temperature measurement is about ± 1 K.

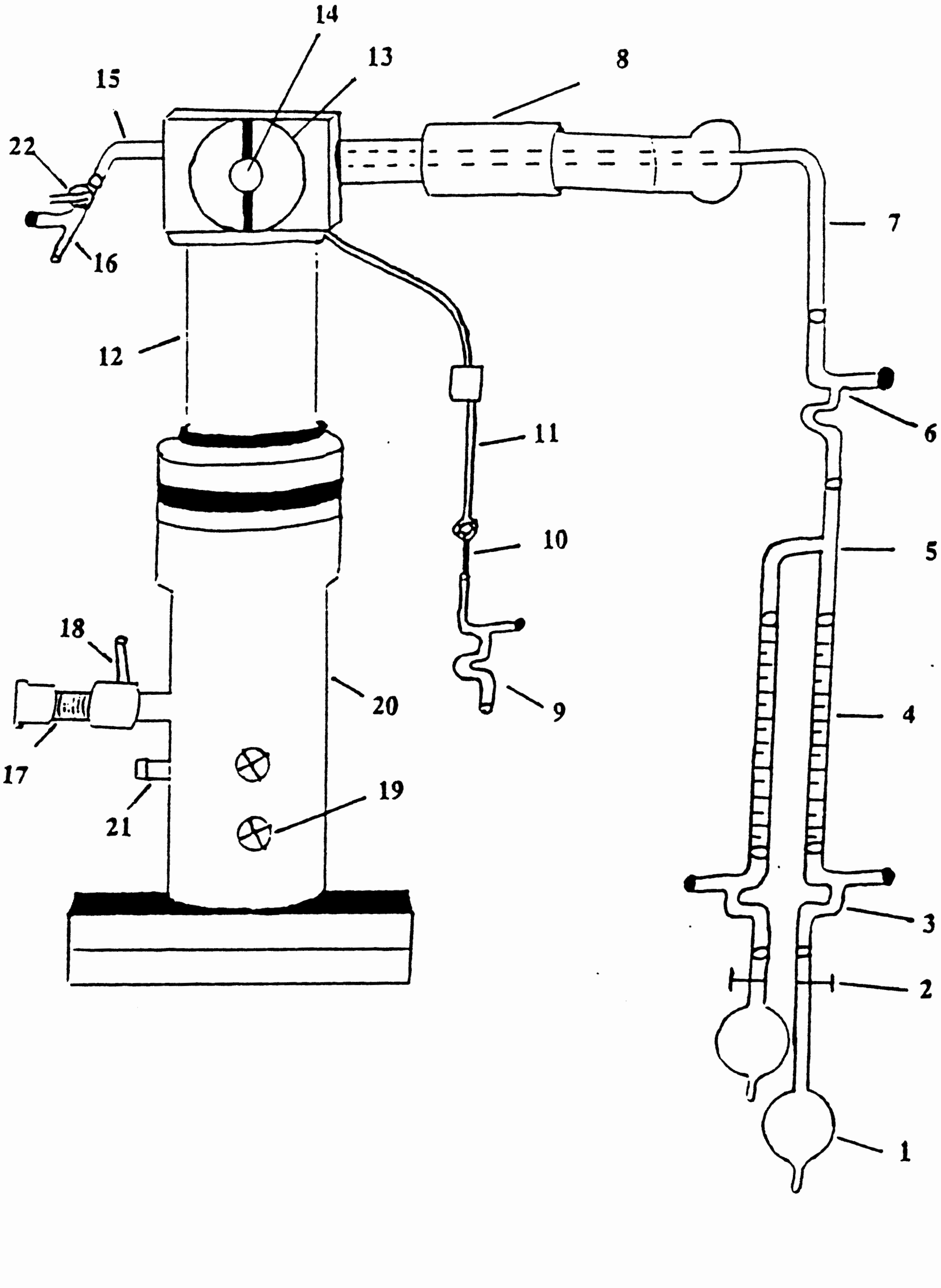

TABLE 8

AN ITEMIZED LIST OF EQUIPMENT FOR THE DEWAR, AND THE COPPER BASE PRESENTED IN FIGURE 18

Number of Units	Representation; Function
1	Silver polished glass liquid nitrogen dewar.
2	40/50 female glass taper joints.
3	9 cm dewar cold stem; extends through glass cell.
4	1 cm Kovar seal; glass metal connection.
5	Iron-constantan thermocouple wires.
6	Copper base; holds the CsI salt plate.
7	Screws; tighten the copper base to back up copper plate.
8	Gas delivery gun; allows gas flow and directed to the center of the substrate.
9	3 x 1.5 x 0.2 cm CsI plate; substrate for thin film samples.
10	Copper plates; sandwich the CsI substrate.
11	Indium wires; keep better thermal contact between plate and substrate.

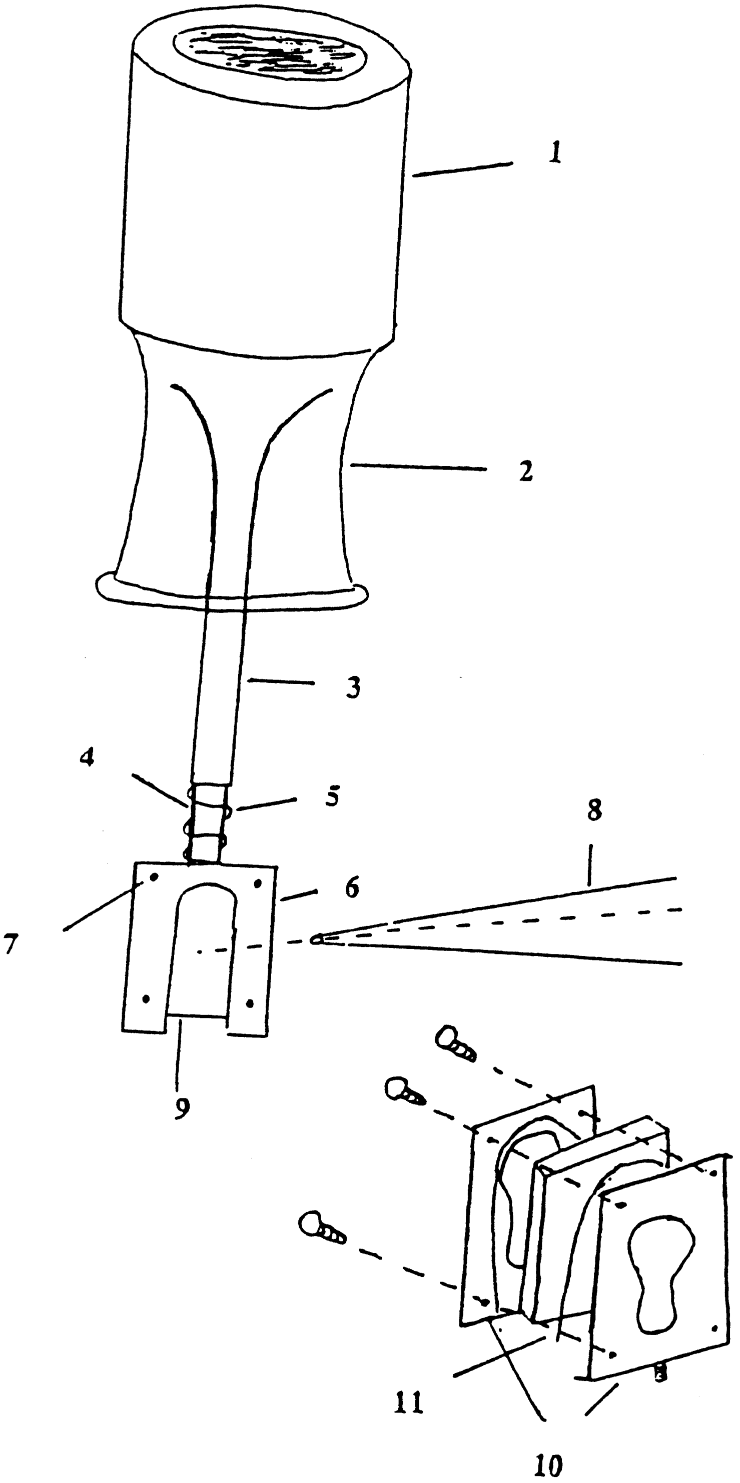

separately connected to the sample finger at the tip. The other end of the heater is connected to a set of two 2PF1010 variacs to control the heating process. The main variac is set constantly at 20V, whereas the settings of the second vary according to the temperature needed. The maximum difference in temperature read from the gold thermocouple and the iron-constantan thermocouple is ± 1 K, which is considered to be insignificant. The bottom part of the cell assembly shows two fittings one for gas supply, and one for gas return. The fittings are connected to the refrigerator by hoses, through which the He gas flows. The actual temperature reading is done by converting a voltage reading to temperature using a voltage table and a Honeywell 2745 potentiometer with a built-in compensator, or by using a DP80 Omega digital indicator.

Instrument

Two water cooled Digital single beam FT-IR spectrometers are used throughout this work; the FTS-20C and the FTS-40 spectrometer. Table 9 describes a few similarities and differences between both systems.

Sample Preparation

In this section a general idea on how the clathrate hydrate samples are prepared is described, and in the following sections particular examples will be given and variations of the experimental procedures will be discussed in detail.

The gas mixtures are first prepared and stored in two-liter gas bulbs mounted to the loading vacuum rack. The water:guest pressure ratio is taken according to the desired clathrate hydrate, which in most cases is determined by the size of the guest molecule. Therefore, if a structure I is needed the H_2O:guest ratio is approximately 6:1, and if a structure II is needed the H_2O: guest is around 17:1.

First, the bulb is evacuated, and deionized water, which is outgassed by freeze-pump-thaw cycles, is introduced from a glass reservoir connected to another inlet of the

TABLE 9

SIMILARITIES AND DIFFERENCES BETWEEN THE FTS-20C AND THE FTS-40

	FTS-20C	FTS-40
Type of interferometer	single	single
Spectral range	4000-500 cm^{-1}	4000-500 cm^{-1}
Interferometer	Michelson interferometer	Michelson interferometer
Type of beam splitter	KBr	KBr
IR Source	Nernst graphite glow bar	Ceramic glower
Detector	Triglycine Sulfate Detector (TGS)	(TGS)
Converter	Analog-to-digital	Analog-to-digital
Random access memory	32 K	1 M
Data Storage	5 M disc cartridge	80 M hard-drive
Purging	Vacuum pumped	Dry Air
Plotter	Digitally controlled	Digilab Laser Printer/Plotter
Apodization	Triangular	Triangular
Computation	Fourier transform system	Fourier transform system
Resolution at which the spectra are collected	1 or 2 cm^{-1}	1 or 2 cm^{-1}

loading line. After the introduction of water, the bulb is closed and cooled by dipping its tip into liquid nitrogen. The guest gas, coming mostly from Matheson bottles and Fisher Scientific, is added to the cooled bulb according to the appropriate ratios. The volume of the bulb to the line is taken into consideration by using the equation:

$$(7)\ \frac{\text{V bulb}}{\text{V line}} = \text{x} - 1 \qquad \text{where x} = \frac{\text{P line}}{\text{P(bulb + line)}}$$

This ratio is found to be 3.1 for the two-liter bulbs. After the mixture is prepared the filled bulbs are mounted to the infrared cell, where the whole system is evacuated overnight with the bulbs closed. The total pressure in a bulb did not exceed 20 torr. The cell is then cooled to a temperature ranging between 100 and 120 K according to the sample needed. When the temperature is reached, the stored vapor mixture in the bulbs is discharged through a flowrater, and directly deposited at a rate of 0.16/min. on a CsI substrate located inside the cell as described earlier. The deposition times varied from 10-20 minutes.

During the deposition of the H_2O:CO_2 mixture the dynamical pumping is eliminated by closing the valve connecting the cell to the vacuum line. This method is applied because of the high vapor pressure of carbon dioxide. The volatility of CO_2 led to overpressurizing the system with CO_2 by overlapping mixtures for one minute. The pressure inside the cell caused by the overlap reached a maximum of 0.25 torr. This deposition followed the formation of the clathrate hydrate substrate and preceded the H_2O:CO_2 deposit. Its presence suppressed the volatile guest molecule escape factor, which eased the epitaxial growth of the clathrate films.

Occasionally, isolated D_2O, occupying approximately 5% of the total sample, is incorporated in the clathrate hydrates. To avoid isotopic exchange from D_2O to HOD, the presence of 7-Azindole is required to trap the protons generated from the water. At the end of the deposit, the valve connecting the line to the back entry of the cell is reopened to allow the nonreacted gas to pump out. The temperature is then dropped to 13 K, and the cell is positioned in the Bio-Rad spectrometer for scanning, at 13 K or higher temperatures, using a nominal resolution of 1.0 or 2.0 cm^{-1}.

The total sample consisted of a single or several layers deposited on the CsI plate as shown in Fig. 19. If a layer is deposited to a clathrate substrate layer (i.e., CO_2 to EO hydrate), the deposit is epitaxial because the substrate imposes its structure on the new growing phase. If the CsI salt plate is the substrate, the deposit is regular. Tables 10, 11 and 12 show the different experimental conditions that have been used throughout this work that enabled the successful growth of clathrate hydrate samples. The nomenclature is defined in Appendix A.

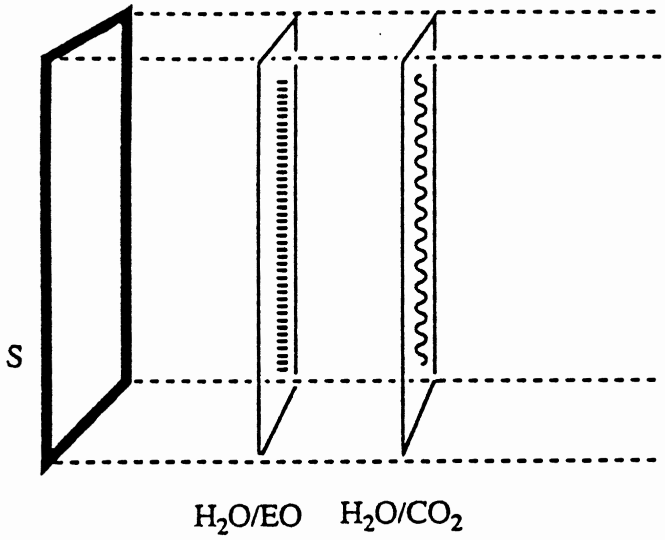
S
H_2O/EO
H_2O/CO_2

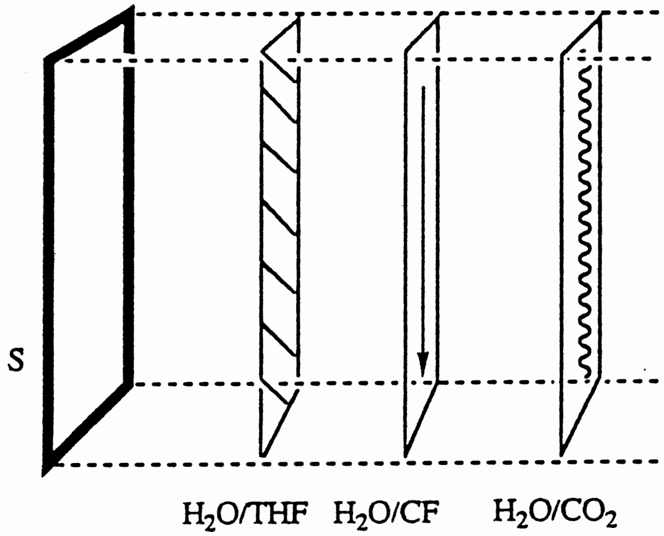
S
H_2O/THF
H_2O/CF
H_2O/CO_2

TABLE 10

A LIST OF ALL THE REGULAR DEPOSITS OF DIFFERENT H_2O:GUEST MIXTURES

Sample	Mixture	T_d; T_s	P	t_d; f	$(HOD)_i$	Structure	Type
H_2O:EO	6:1	100-120; 13-140	10^{-6}	12; 6.5	N	S I	simple
H_2O:TMO	6:1	140; 13-140	10^{-6}	12; 6.5	N	S I	simple
	7:1	150; 13-140	10^{-6}	12: 6.5	N	S I + S II	simple
H_2O:THF	17:1	150; 13-90	10^{-6}	12: 6.5	N	S II	simple
H_2O:meCl	8:1	90; 90	10^{-6}	15; 5	N	amorphous	--------
	5:1	120; 90	$4x10^{-4}$	15; 5	N	amorphous	--------
H_2O:CF	17:1	150; 13	10^{-6}	12; 6.5	Y	CF diluted in crystal ice	--------
H_2O:CO_2	6:1	120; 13	$7x10^{-4}$	12; 6.5	Y	CO_2 diluted in amorphous ice	--------

TABLE 11

A LIST OF ALL THE DOUBLE AND MIXED CLATHRATE HYDRATE SAMPLES FORMED BY MIXING WATER AND SEVERAL GUEST MOLECULES (H_2O:M_1:M_2)

Sample	Mixture	T_d; T_s	P	t_d: f	$(HOD)_i$	Structure	Type
H_2O:CO_2:EO	5.2:0.25:0.75	120; 90	10^{-6}	15; 6.5	N	S I	almost mixed
	5:0.5:0.5	120; 90	10^{-6}	15; 6.5	N	S I	mixed
	5:0.66:0.33	120; 13-140	10^{-6}	15; 6.5	N	S I	mixed
	6:0.91:0.09	120; 90	10^{-6}	15; 6.5	N	S I + amorphous	--------
H_2O:meCl:EO	6:0.4:0.15	133; 90	10^{-6}	20; (4,2)	Y	S I	mixed
	6:0.6:0.15	116; 90	10^{-6}	20; (5,2)	Y	S I	mixed
	6:0.6:0.2	123; 90	10^{-6}	20; (6,2)	Y	S I	mixed
	6:0.4:0.1	125; 90	10^{-6}	20; 6	Y	S I	mixed
	6:0.8:0.2	127; 90	10^{-6}	20; 6	Y	S I	mixed
H_2O:THF:CO_2	17: .75: .25	150; 13-90	10^{-6}	10; 6.5	N	S II	double
H_2O:THF:CF	17: .376: .765	140; 90	10^{-4}	15; 3.5	N	mostly ice	--------

TABLE 12

A LIST OF THE SIMPLE CLATHRATE HYDRATES OF CO_2, CF AND meCl GROWN BY EPITAXAL APPROACH ($S:L_1:L_2:L_3$)

Sample[(a)]	$M(L_1)$	$M(L_2)$	$M(L_3)$	T_d; T_s	$t_d(L_1)$	$t_d(L_2)$	$t_d(L_3)$	$(HOD)_i$	Overlap	Structure
H_2O:EO, $H_2O:CO_2$	6:1	6:1	-------	120; 13-140	6	6	-------	Y	N	S I
	6:1	6:1	-------	120; 13-140	2	6	-------	Y	N	S I
	6:1	6:1	-------	120; 13-140	0.166	6	-------	Y	N	S I
	6:1	6:1	-------	120; 90	3	21	-------	Y	N	S I + amorphous
	6:1	6:1	-------	114; 13-140	6	6	-------	Y	N	S I
	6:1	6:1	-------	114: 13-140	2	6	-------	Y	N	mostly S I + little ice
	6:1	6:1	-------	105; 13-140	6	10	-------	Y	N	S I
	6:1	6:1	-------	105; 13-140	0.166	10	-------	Y	N	S I + ice
H_2O:EO, H_2O:meCl	10:1	6:1	-------	127; 90	10 (2.5x4)	10 (2.5x4)	-------	N	alternating process	S I
D_2O:EO, D_2O:meCl	10:1	6:1	-------	127; 90	3	21	-------	N	--------	S I
H_2O:THF, $H_2O:CO_2$	17:1	6:1	-------	150; 13-140	6	6	-------	Y	THF/CO_2	S II

TABLE 12 (Continued)

Sample[(a)]	$M(L_1)$	$M(L_2)$	$M(L_3)$	T_d; T_s	$t_d(L_1)$	$t_d(L_2)$	$t_d(L_3)$	$(HOD)_i$	Overlap	Structure
	17:1	6:1	-------	150; 13-140	1	6	-------	Y	THF/CO_2	mostly ice
	17:1	6:1	-------	150; 13-140	6	--	-------	Y	THF/CO_2	S II
	17:1	6:1	-------	150: 13-140	6	6	-------	Y	N	ice
	17:1	6:1	-------	150; 13-140	6	25	-------	Y	THF/CO_2	little S II + mostly ice
	17:1	6:1	-------	150; 13-140	14	6	-------	Y	THF/CO_2	S II
H_2O:THF, H_2O:CF	17:1	17:1	-------	150; 13-140	6	6	-------	Y	N	S II
H_2O:THF, H_2O:CF, H_2O:CO_2	17:1	17:1	6:1	150; 13-140	6	0.5	6	Y	CF/CO_2	S II
	17:1	17:1	6:1	150; 13-140	6	3	6	Y	CF/CO_2	mostly S II + little ice
	17:1	17:1	6:1	150; 13-140	6	6	6	Y	CF/CO_2	S II + ice
	17:1	17:1	6:1	150; 13-140	6	9	6	Y	CF/CO_2	little S II + mostly ice
	17:1	17:1	6:1	150; 13-140	1	6	6	Y	CF/CO_2	ice

CHAPTER III

RESULTS AND DISCUSSION

Mixed and Simple CO_2 Clathrate Hydrates

In the field of spectroscopy, the IR spectra of CO_2 clathrate hydrates have not been reported, even though numerous publications report the IR data of gas phase CO_2, pure amorphous CO_2 (64), pure crystalline CO_2 (65), or solid CO_2 clusters (66-68). This work with mixed EO-CO_2 hydrate, and simple CO_2 clathrate hydrate epitaxially grown to ether clathrate substrates, reveals the unique and distinctive spectrum of enclathrated CO_2 molecules, and gives strong insight to the role of mobile Bjerrum defect activity in these particular ice-like materials.

The work is divided into several sections to simplify the understanding of the logic followed throughout this chapter. The sections will discuss in detail the different types of clathrate hydrate samples. Such samples are summarized in Tables 10, 11, and 12 and their infrared spectra are illustrated in different figures. In each figure containing more than one curve, the absorbance scale of these curves in that figure is constant.

H_2O:CO_2 Deposit on CsI Salt plate

To confirm what is reported by Richardson *et al.*(43), a mixture of 6:1 H_2O:CO_2 was deposited on a CsI plate at 140 K. It is seen that the CO_2 antisymmetric stretch frequency, υ_3, has an absorption band at 2340 cm^{-1} as shown in Fig. 20. However, the IR frequency value of the bending mode of ice, being at 1556 cm^{-1}, does not agree with the 1600 cm^{-1} regular value of the clathrate hydrates, it is closer to the crystalline ice value as

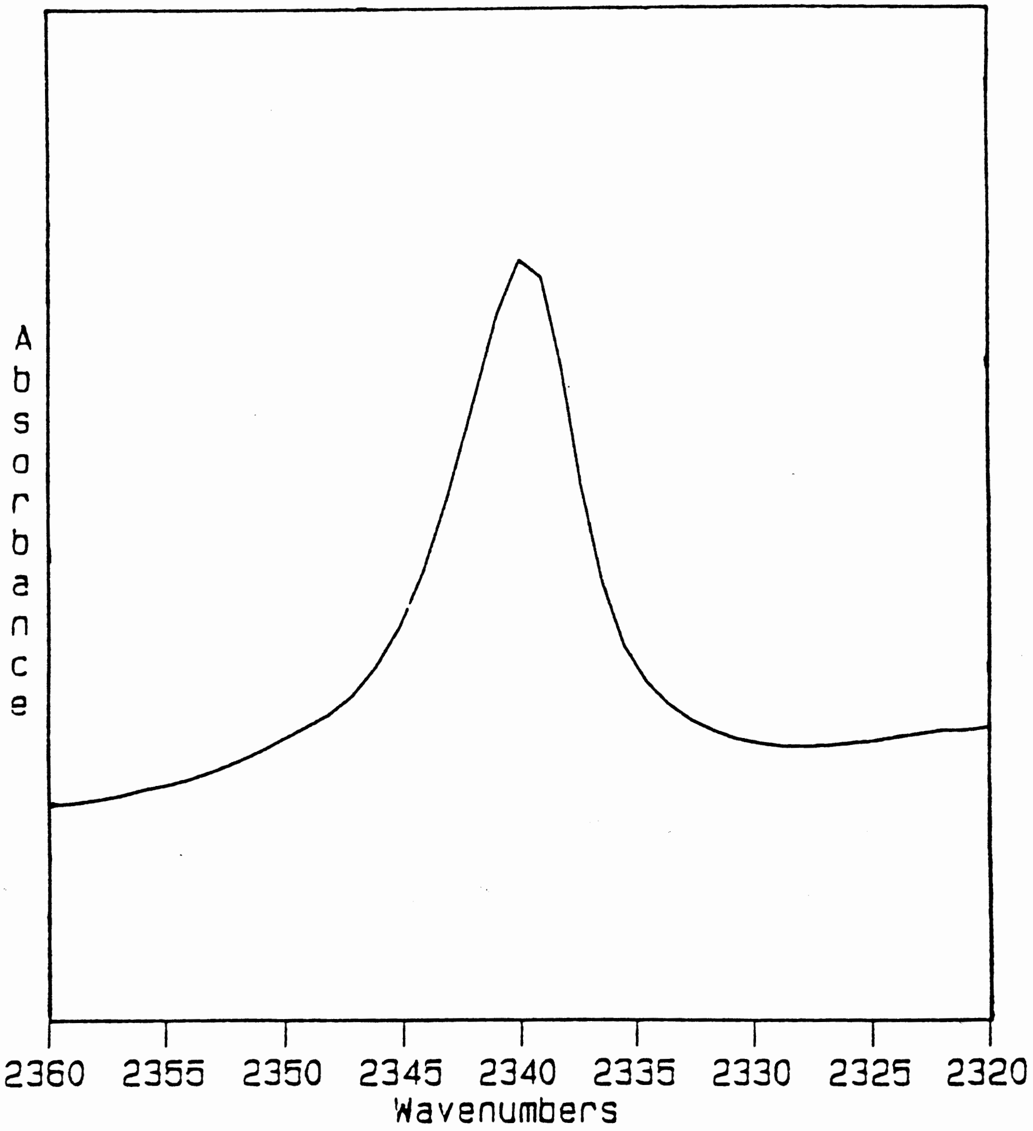
Absorbance
2360
2355
2350
2345
2340
2335
2330
2325
2320
Wavenumbers

represented in Fig. 21. Since Falk and Seto report the value of pure crystalline CO_2 and pure amorphous CO_2 to be at 2344.8 and 2342.3 cm^{-1} respectively, and since it is known that the gas phase value of υ_3 of CO_2 is 2349.14 cm^{-1}, the value found in our work could only be explained as being for solid carbon dioxide diluted in crystalline ice, which confirms the idea that CO_2 resists the clathrate hydrate growth under low temperatures.

Structure I Mixed H_2O:CO_2:EO Clathrate Hydrate

The FT-IR spectra of thin-films of (EO) clathrate hydrate matched what has been available and documented (31, 40, 69). Therefore, it is unnecessary to present new results for that particular clathrate. As for the CO_2 clathrate hydrate it was evident that the enclathration of the CO_2 molecules in the clathrate hydrate cages under cryogenic conditions could be realized only by using a help gas (i.e., EO). For that matter, several vapor mixtures of H_2O:CO_2:EO have been prepared and deposited at 120 K to investigate the IR bands of the guest molecules of the mixed clathrate hydrate. These mixtures have a constant dilution factor of approximately 5:1 (host:guest), but the relative concentration of the guest molecules have been changed as listed in Table 10. Thus, Fig. 22 illustrates the IR spectra of the CO_2 antisymmetric stretch band of the mixed clathrate hydrates for the H_2O:CO_2:EO mixtures having the compositions 5.0: 0.25: 0.75 curve (a), 5.0: 0.5: 0.5 curve (b), and 5.0: 0.66: 0.33 curve (c).

The ratio of the doublet at 2346 cm^{-1} and 2337 cm^{-1} varies enormously going from a ratio of 2:1 CO_2:EO to 1:3 CO_2:EO. In curve (a), where the ratio is 1:3 CO_2:EO, the sample has almost the characteristics of a double hydrate because the CO_2 occupies mostly one cage type. By changing the relative concentration ratio to 1:1 and to 2:1 as in curves (b,c), the CO_2 molecules seem to occupy both the small and the large cages, which is easily detected by observing the increase in intensity of the 2335 cm^{-1} band. This indicates that the CO_2 successfully competes with the (EO) in cage occupation. Knowing that the CO_2 is

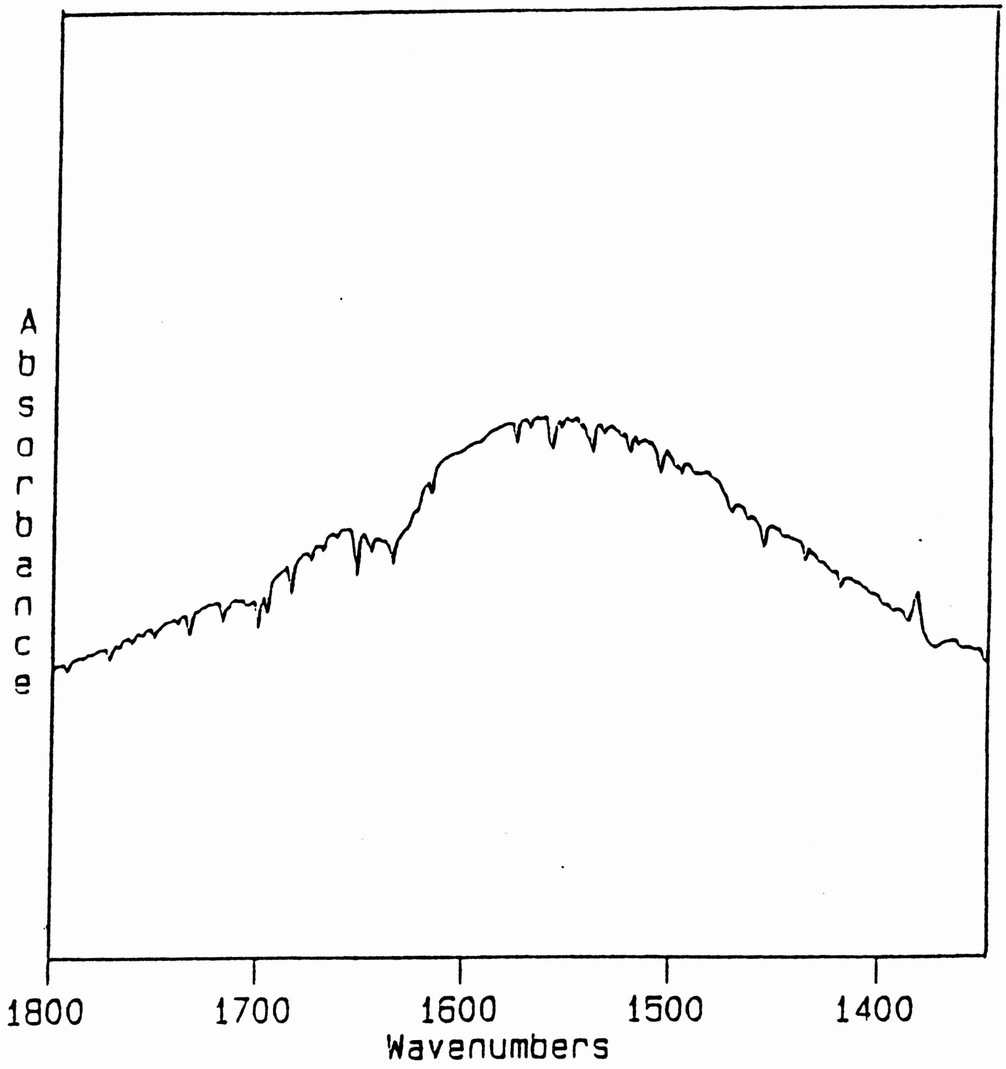
Absorbance
1800
1700
1600
1500
1400
Wavenumbers

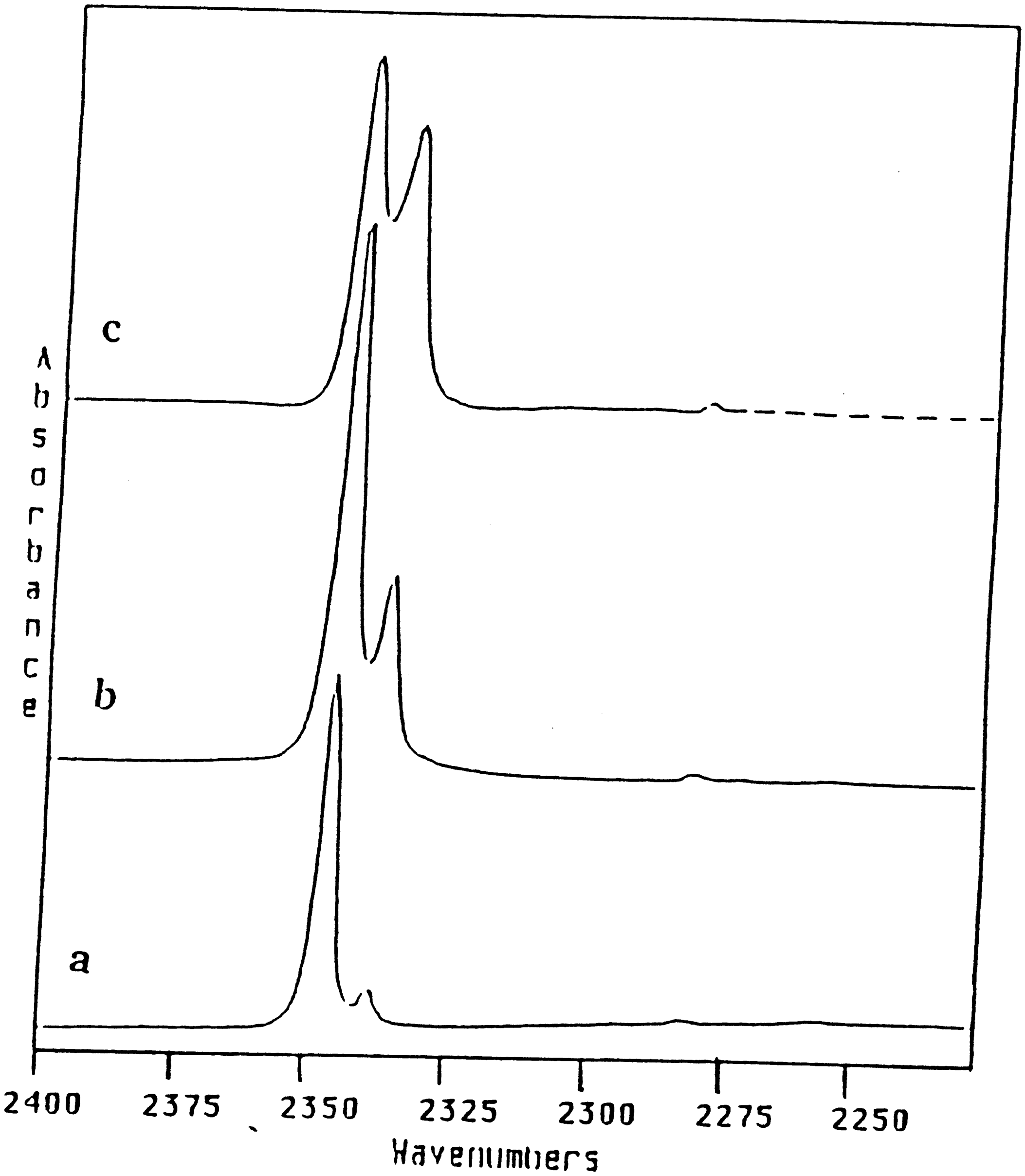
c
b
a
Absorbance
2400
2375
2350
2325
2300
2275
2250
Wavenumbers

smaller in size than the (EO), it is logical to assign the large-cage frequency at 2337 cm^{-1}, and the small-cage frequency at 2346 cm^{-1}.

In the region of the degenerate mode frequency, υ_2, corresponding but opposite changes occurred, which suggest that the small-cage value of CO_2 clathrate hydrate is at 655 cm^{-1}, and the large-cage value is at ~661 cm^{-1} as shown in Fig. 23. An overlap of the small-cage band with the large-cage band makes it difficult to observe a degeneracy splitting if this occurs at 90 K.

Another mixed sample of H_2O:CO_2:EO having relative ratio of 6: 0.91: 0.09 (not shown) failed to grow as a crystalline clathrate hydrate. This result could suggest that a minimum amount of (EO) is required in the mixture to grow this thin non-stoichiometric solid.

Structure I Simple Hydrate of CO_2

After having been successful growing the mixed clathrate hydrate of EO-CO_2, and assigning the small and the large-cage frequencies of the antisymmetric stretch and bending modes of CO_2, the idea of probing the growth of CO_2 clathrate hydrate by an epitaxial approach seemed possible. Therefore, at 120 K a thin film of (EO) clathrate hydrate was deposited, and then followed by another thin film of H_2O:CO_2.

The frequency values of the υ_3 mode of the CO_2 molecules in the (5^{12}) cages and the ($5^{12}6^2$) cages of the epitaxially grown type I hydrate at 13 K are 2347 and 2335 cm^{-1} respectively, as shown in Fig. 24 curve (a). These values are closely comparable to the ones measured earlier for the mixed CO_2 clathrate hydrate, despite a difference in temperature, indicating that both approaches, mixed and epitaxial, successfully yield the type I structure having both kinds of cages occupied, in contrast to what has been reported about the CO_2 molecules occupying the structure I tetrakaidecahedrals only (62). The dominant absorption by the molecules in the large cavities is expected because of the 1:3

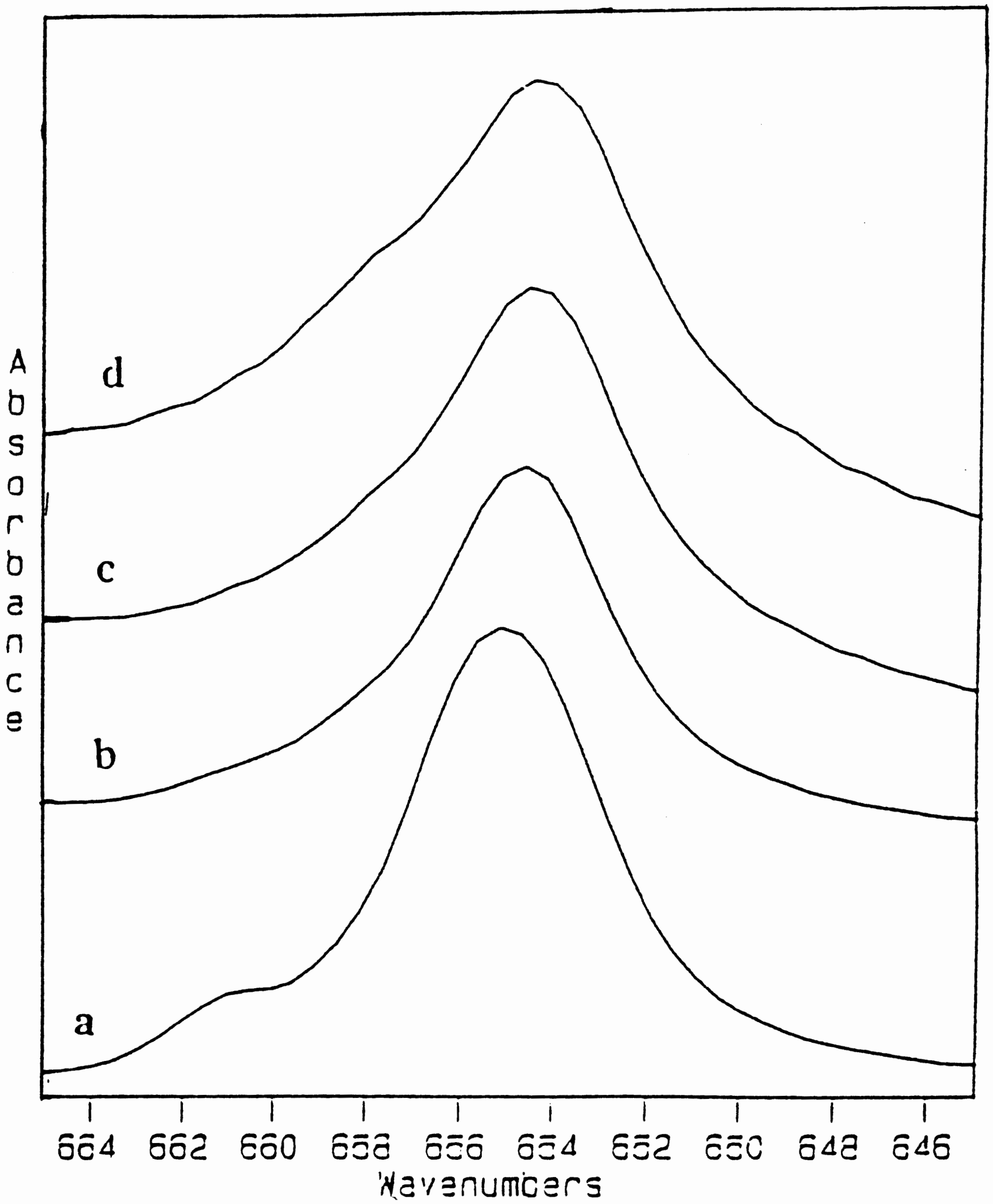

A
b
s
o
r
b
a
n
c
e
d
c
b
a
664
662
660
658
656
654
652
650
648
646
Wavenumbers

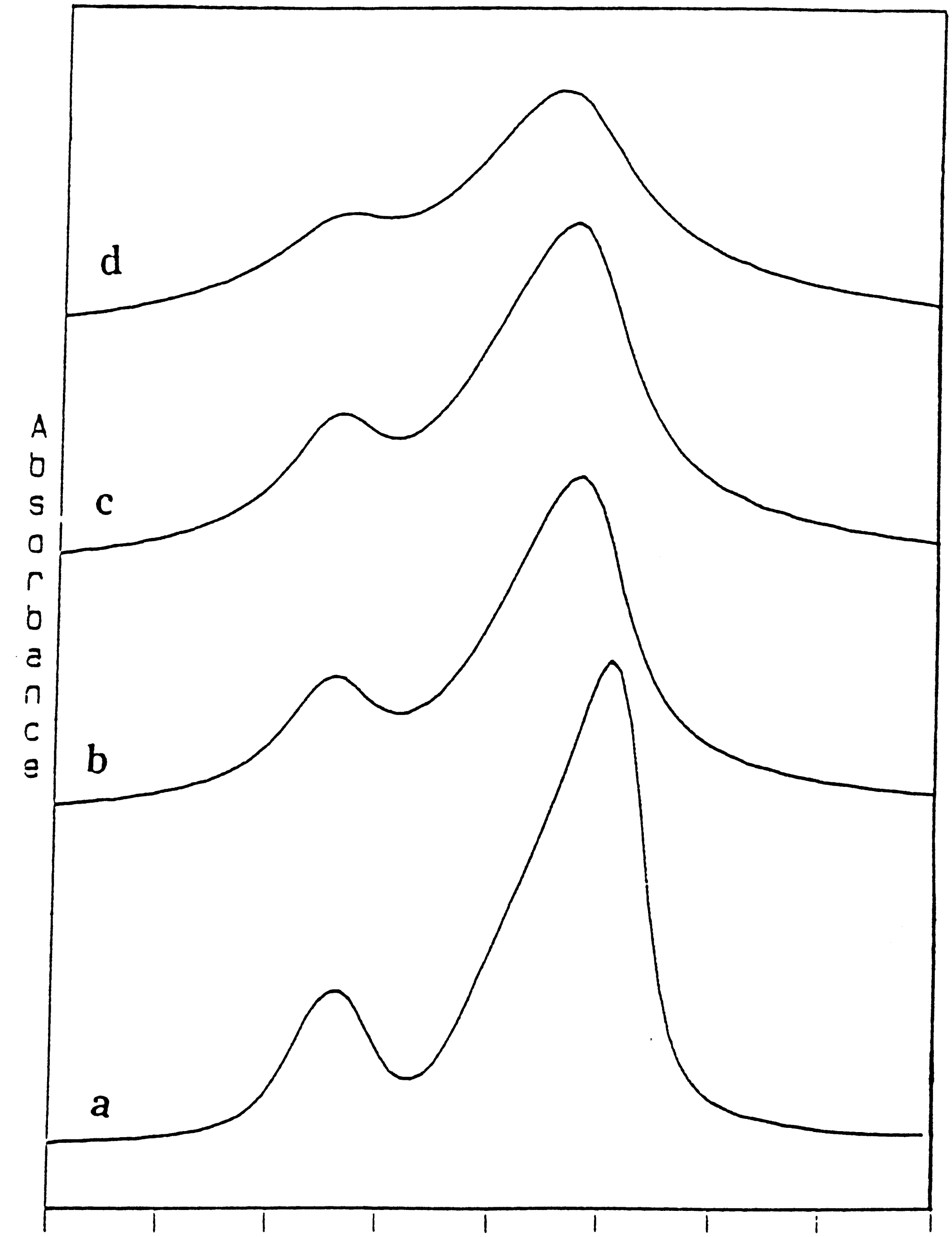
d
c
b
a
Absorbance
2360
2355
2350
2345
2340
2335
2330
2325
2320
Wavenumbers

ratio of structure II small-cages to large-cages. The same behavior is seen for the $^{13}CO_2$ molecules in Fig. 25, which has the small and the large-cage frequencies at 2281 and 2272 cm^{-1}, respectively.

In the degenerate bending region the small-cage CO_2 value at 655 cm^{-1} in Fig. 26 also seems to agree with the early results, but since the temperature, Ts, at which the sample is scanned is 13 K, and since the small-cage band does not dominate, the degeneracy splitting of the υ_2 mode large-cage band is more easily seen as a doublet at 658/661 cm^{-1}. The separate view of the small cage and large cage CO_2 bands in Figs. 27 and 28 are obtained by subtracting the IR spectra of EO-CO_2 hydrate rich in (EO), with CO_2 occupying primarily the small cages, from the IR spectra of an epitaxial sample rich in CO_2 molecules residing in the large cages and vise versa. The subtraction level is determined by monitoring the vanishing of the small or large cage υ_3 absorption bands to allow the clear observation of the separate υ_2 bands. These results indicate that the H_2O:CO_2 mixture, when deposited epitaxially to the (EO) hydrate, does nucleate and form the simple type I clathrate hydrate.

Once the epitaxial growth of the structure I CO_2 clathrate hydrate was mastered the influence of deposition temperature and sample thickness on the L-defect mobility in the sample was probed.

By gradually decreasing the deposition time of the (EO) clathrate hydrate thin-film from 6 min. (film a), to 2 min. (film b), to 0.2 min. (film c) at 120 K results in the decrease of substrate thickness. The collected IR spectra of these samples showed the same characteristics presented in Fig. 24. However, by subtracting 76% of the IR spectrum of (film a) from the IR spectrum of (film b) the 2340 cm^{-1} band appears weakly as shown in Fig. 29, which suggests that the quality of the clathrate hydrate in (film b) degraded from the quality of the clathrate hydrate in (film a). By the same manner, subtracting 76% of the IR spectrum of (film b) from the IR spectrum of (film c) results in the appearance of the 2340 cm^{-1} band, which also leads to the same conclusion. A similar subtraction in the

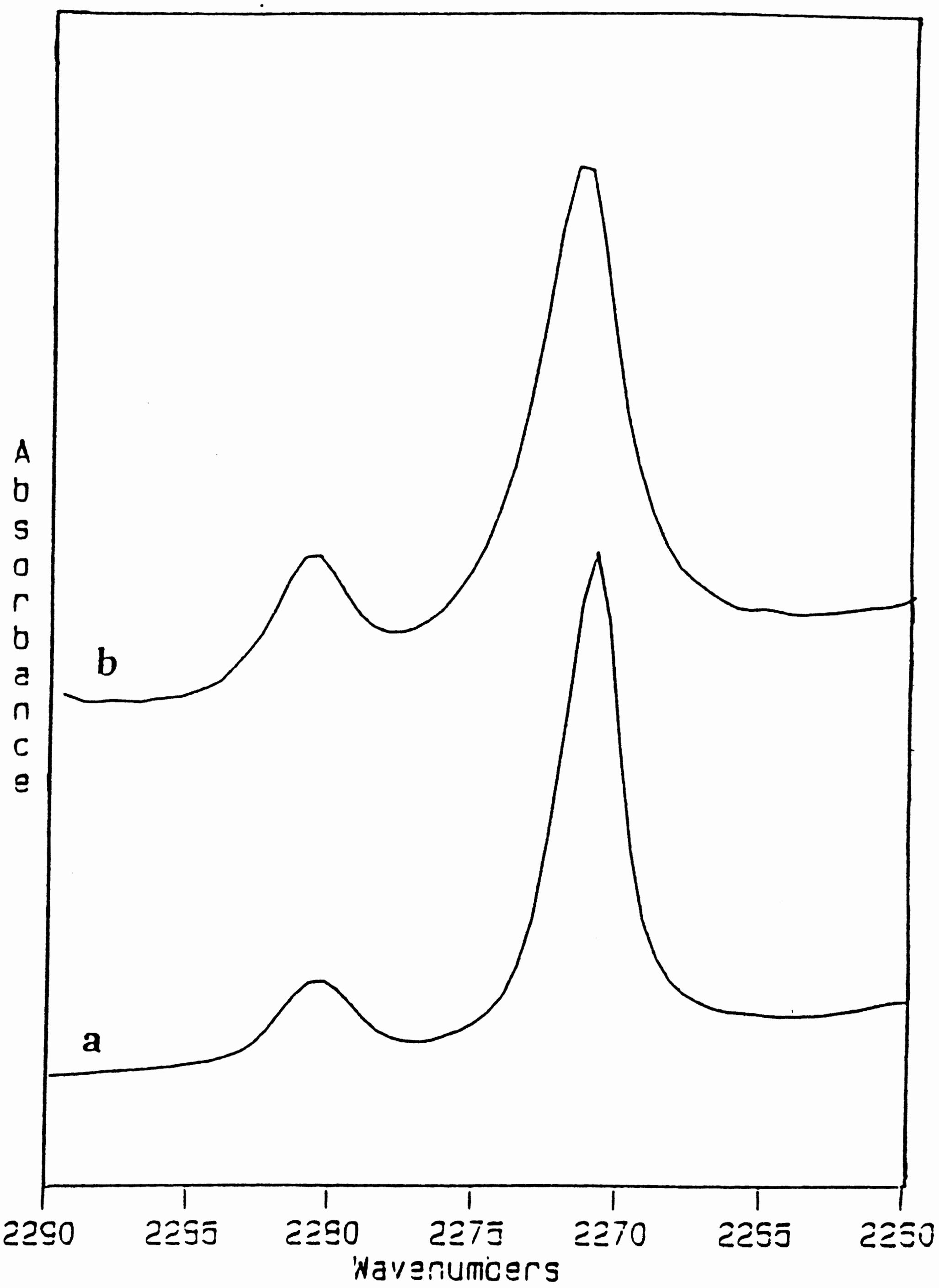
Absorbance
b
a
2290
2285
2280
2275
2270
2265
2260
Wavenumbers

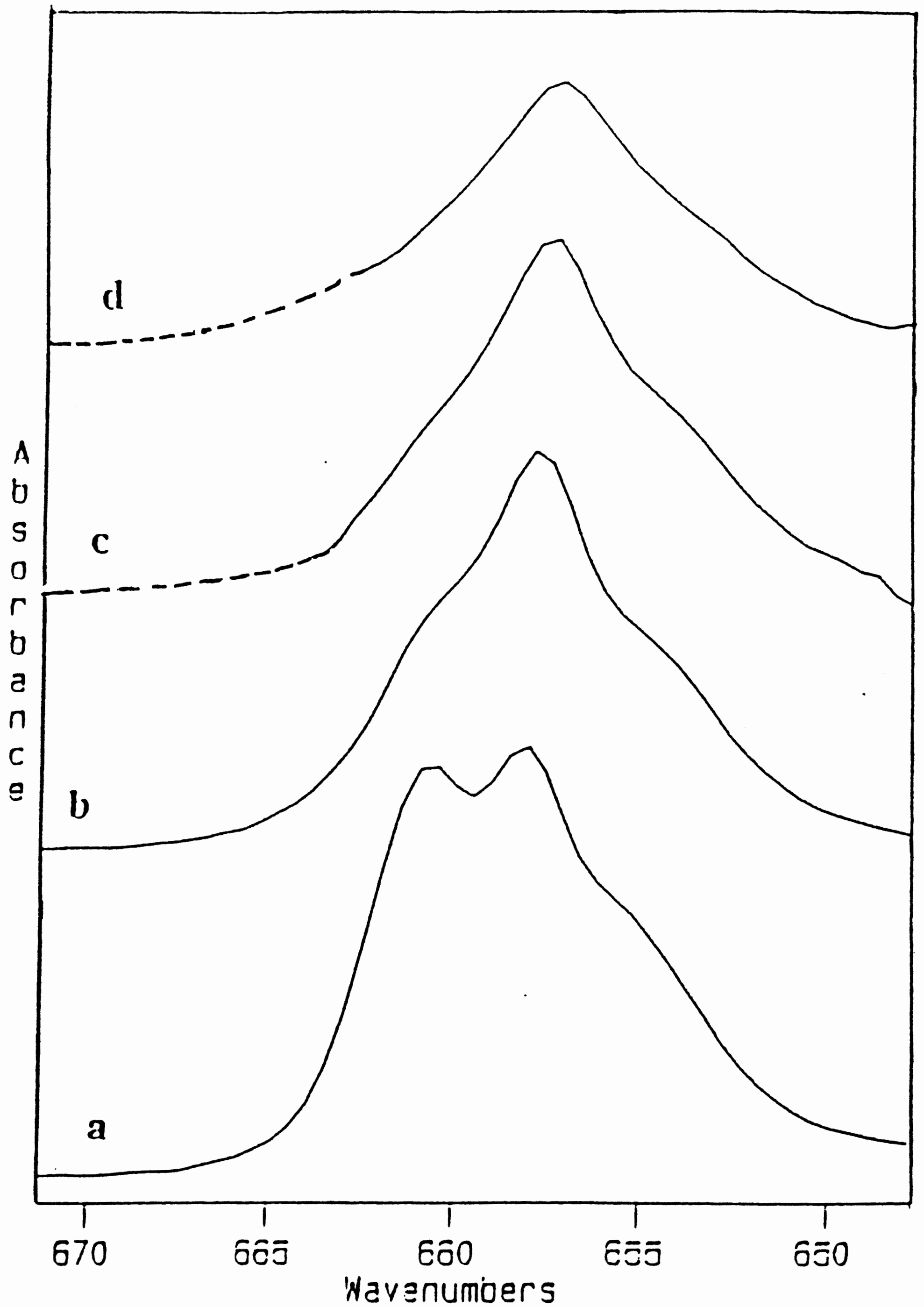
d
c
b
a
Absorbance
670
665
660
655
650
Wavenumbers

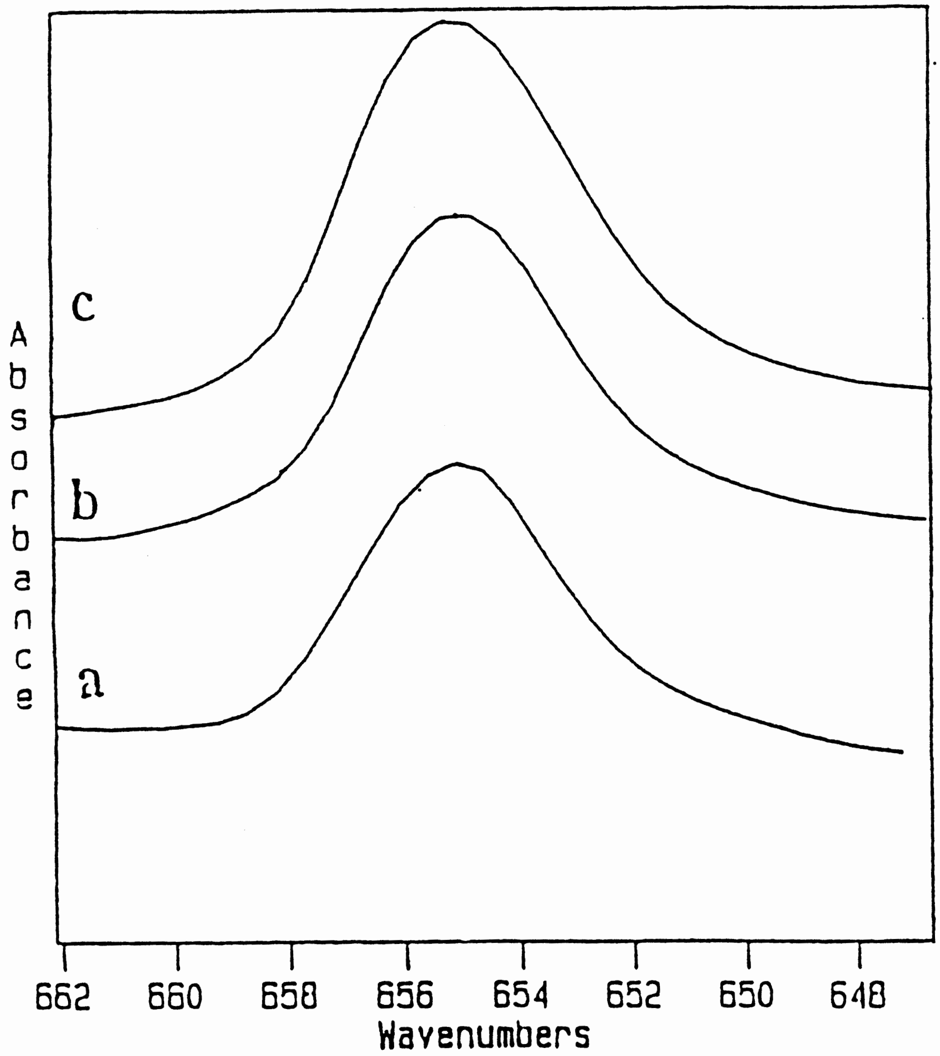
c
b
a
Absorbance
662
660
658
656
654
652
650
648
Wavenumbers

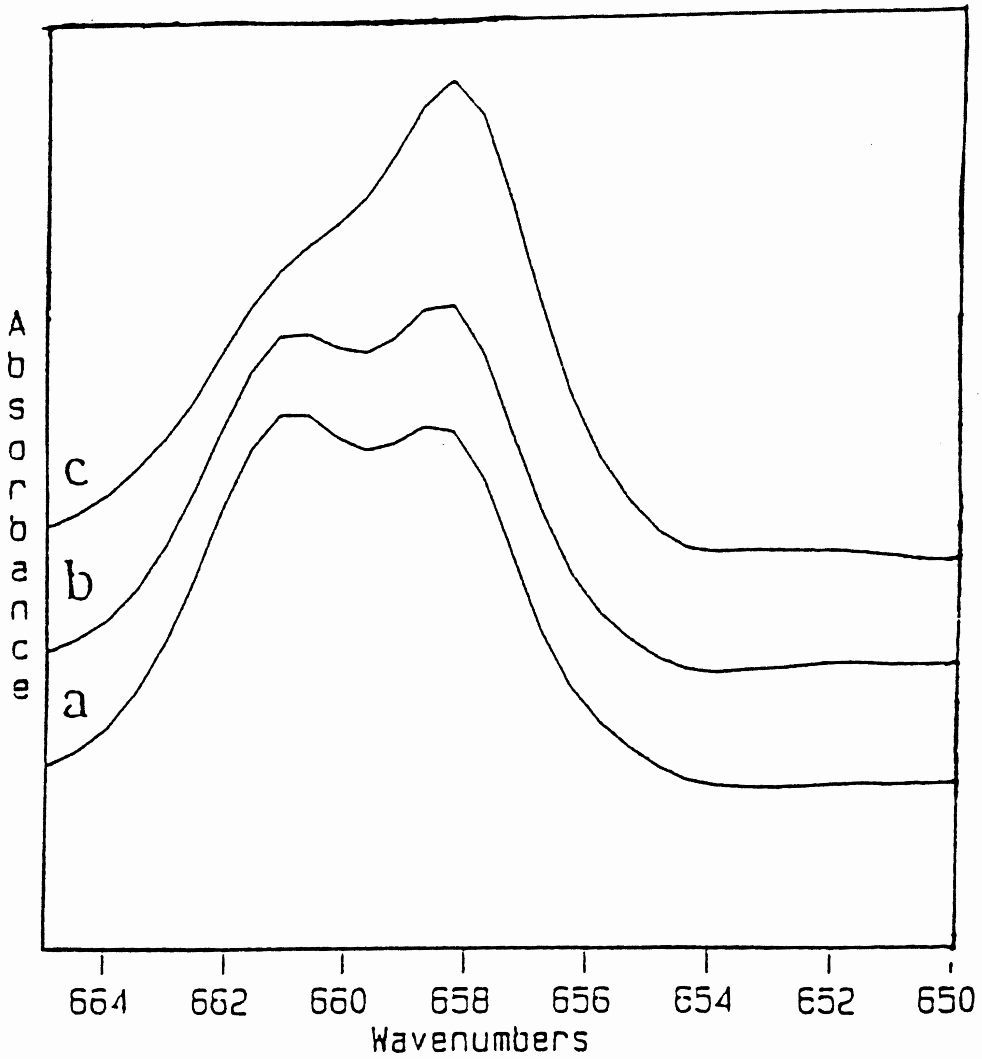
Absorbance
c
b
a
664
662
660
658
656
654
652
650
Wavenumbers

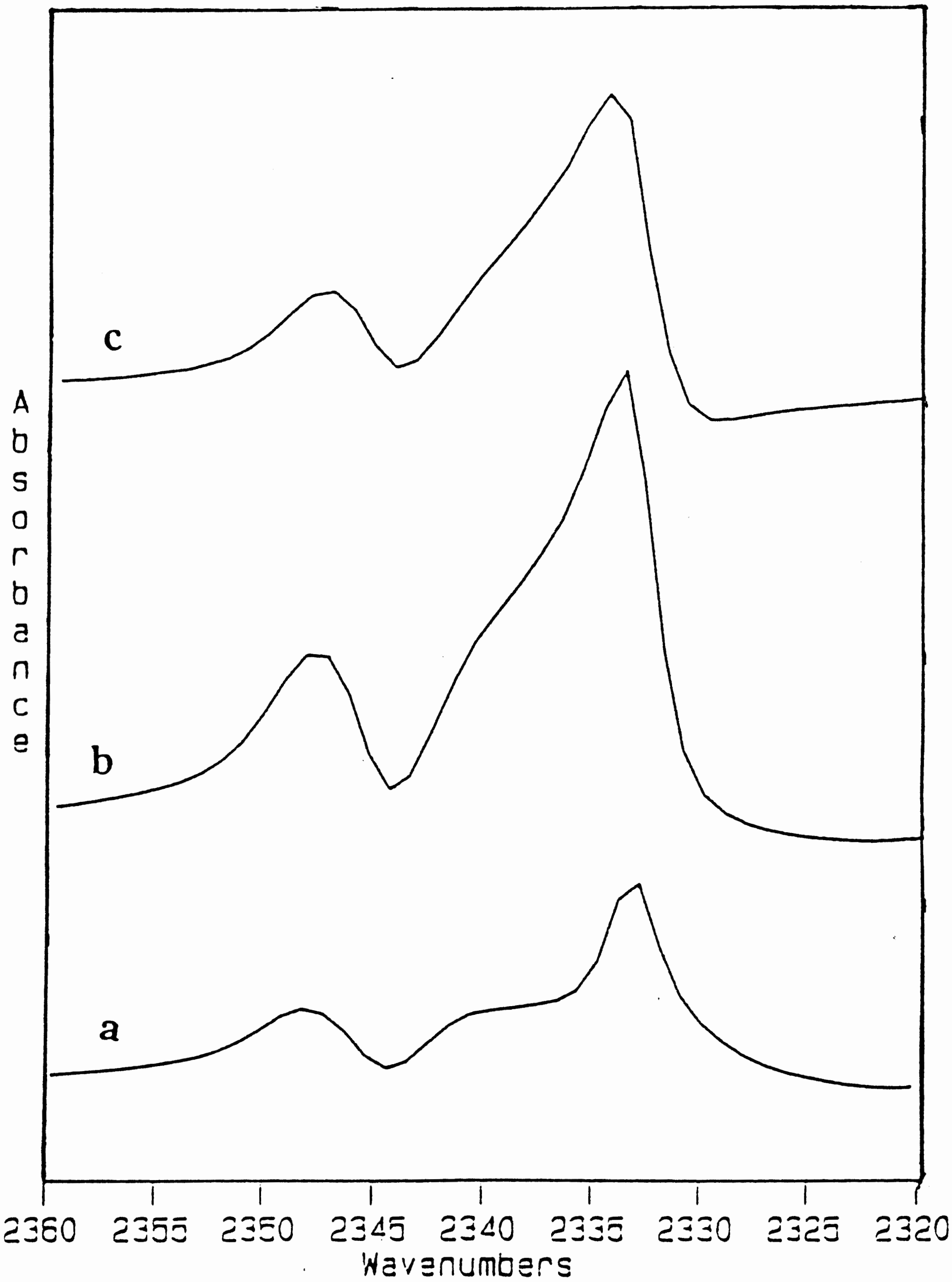
c
b
a
Absorbance
2360
2355
2350
2345
2340
2335
2330
2325
2320
Wavenumbers

antisymmetric stretching region of the $^{13}CO_2$ favors this conclusion because the band at 2274 cm^{-1}, which describes the amorphous characteristics of the carbon dioxide clathrate hydrates in the $^{13}CO_2$ appeared. To explain these results the three possibilities noted by Devlin *et al.* (43) about L-defects in clathrate hydrate samples may apply: a) the ether clathrate hydrates (i.e. EO, THF clathrate hydrate) are relatively rich in defects compared to ice and other clathrate hydrates, b) L-defects in the solid phase control the rate of formation of that phase, and c) besides the L-defects produced by the condensation of the $H_2O:CO_2$ mixture on the CsI plate, the (EO) clathrate hydrate thin film is a major source of L-defects contributing to the epitaxial growth of the CO_2 clathrate hydrate phase. Therefore, by decreasing the thickness of the (EO) clathrate substrate we decrease the total number of defects in the source, which directly affects the ability to grow the CO_2 clathrate hydrate.

To examine this explanation, advantage is taken from the fact that L-defects are much more mobile at higher than lower temperatures (45). The same kinds of experiments were carried out at 105 K, at which temperature the (EO) clathrate hydrate still grew very easily. The υ_3 bands in Fig. 30 show from the broad large-cage band that the CO_2 sample represented by curve (a) (containing 6 min. H_2O:EO deposit) is partially clathrate hydrate and partially amorphous. The CO_2 sample film represented by curve (b) (containing 0.2 min. H_2O:EO deposit) is 100% amorphous. These results are justified by the fact that L-defects are less mobile at 105 K than at 120 K, which slows down their transfer from the (EO) hydrate substrate and damages the quality of the clathrate hydrate epitaxially growing to the substrate. The spectrum in Fig. 30 curve (b) looks exactly like the one in Fig. 20. This suggests that at 105 K, and with H_2O:EO deposition time of 0.2 min. the L-defects from that ultrathin substrate are inadequate for the growth of the solid $H_2O:CO_2$ sample. This again indicates clearly that the L-defects coming from the $H_2O:CO_2$ condensation are not enough to grow that particular hydrate, even when nucleated by a hydrate substrate.

To study the effect of the sample temperature on the host-lattice molecular behavior, the temperature was gradually raised from 13 K to 135 K. The IR spectra are shown in

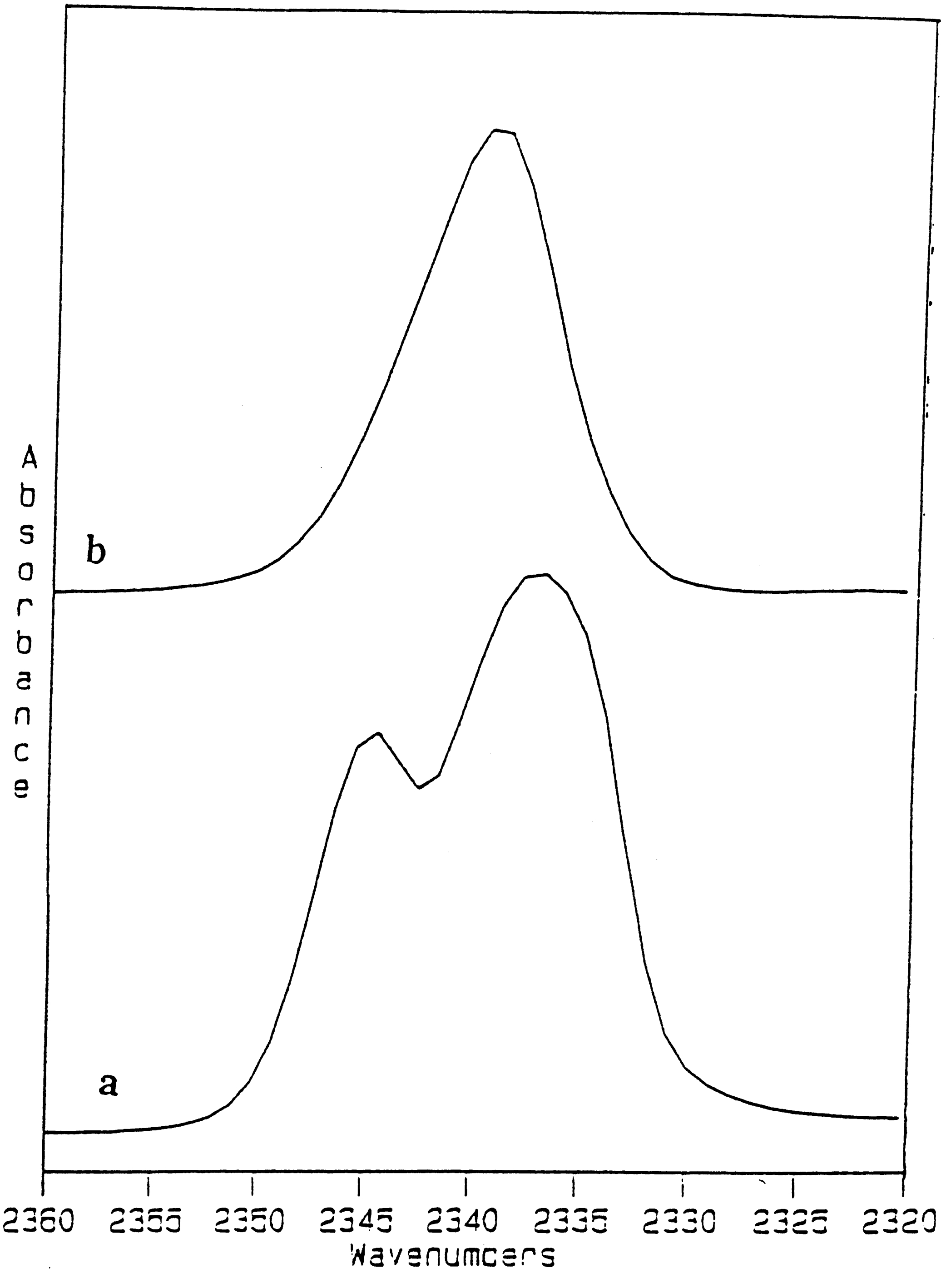
Absorbance
b
a
2360
2355
2350
2345
2340
2335
2330
2325
2320
Wavenumbers

Fig. (24-28). In the structure I clathrate hydrate no major changes occurred in the υ_3 and υ_2 bands of small-cage CO_2 in this temperature range. The van der Waals interactions between the guests and the cage walls are stronger and more symmetric in the small cages than for the large cages, which limits: a) guest molecule distortion, b) the possible sites available to the guest, and c) the guest molecule reorientational motion. In particular, the degenerate bending vibrational energies are not split by the interaction of CO_2 with the small cages (Fig 27), but the degeneracy appears to split in the large cages at low temperatures. A change in (degeneracy) splitting may explain the behavior seen in Fig. 28 where the doublet fades somewhat with increasing temperature. However, the indication that only the 661 cm^{-1} band of the large cage is weakening, indicates that the CO_2 molecules, rather than being distorted are subjected to inequivalent site effects, and are shifted toward the site of lower frequency with increasing temperature. This behavior is also consistent with that seen earlier for mixed H_2O:CO_2:EO clathrate hydrates, but because the small-cage band dominated over the large-cage band, in that mixed hydrate, the degeneracy splitting of this mode did not show. However, the increase in temperature of the sample from 13 K to 150 K shows that the large-cage band vanishes under the small-cage band, indicate that the 661 cm^{-1} large-cage band is shifting to another value at high temperatures, that could not be determined because of band overlap.

At 13 K the $^{12}CO_2$ large-cage band in the υ_3 region is structured and shows a FWHM of 6 cm^{-1}, whereas absorption by the more dilute $^{13}CO_2$ molecules is very narrow with a FWHM of 2 cm^{-1}. For crystalline thin films and cluster CO_2 (66-68) studies similar behavior is attributed to the effects of transition-dipole dynamical coupling that is large in pure solid CO_2, but is expected to decrease if the intermolecular CO_2 distance increases, as in a clathrate hydrate. Also, at that same temperature, the splitting between the small-cage and the large-cage bands for the $^{12}CO_2$ is 25% larger than the band splitting in the $^{13}CO_2$. This again indicates that the $^{12}CO_2$ molecules in the large cages are subject to dynamical coupling. Nevertheless, coupling effects are apparent in the clathrate hydrates, especially when the temperature is increased. Upon warming the sample to 135 K, the $^{12}CO_2$ dipole coupling is disrupted somewhat by molecular reorientation, as reflected in the IR spectrum by changes in large cage absorption near 2335 cm^{-1} while the $^{13}CO_2$ band is relatively insensitive to temperature. This is additional strong evidence that the $^{12}CO_2$ molecules in the large cages are subject to significant dipole-dipole interactions.

By fitting the υ_3 band in Fig. 24 curve (a) to mixed Lorentzian and Gaussian curves as in Fig. 31, it is seen that the large cage band can be decomposed into two bands with frequencies at 2337.2 and 2334.14 cm^{-1} with a splitting $\Delta\upsilon$, of 3 cm^{-1}. This particular splitting is attributed to the transition dipole vibrational coupling.

Theoretically, the splitting could be calculated for two coupled CO_2 molecules using the models described by Decius (70) and Hornig (71). The dipole moment function expressed by Ewing (72) is:

$$(7)\quad \mu_{i\delta} = \mu_i^{\circ} l_{i\delta} + \left|\frac{\partial \mu_i}{\partial Q_i}\right| Q_i l_{i\delta}$$

The dipole moment μ_i° is the permanent dipole of the molecule i, and it is zero for CO_2. The unit-vector component for the normal coordinate Q_i is $l_{i\delta}$, where δ represents the coordinates of the system.

From Yamada and Person (73), the bond moment parameter, $\left|\frac{\partial \mu_i}{\partial Q_i}\right|$ is found to be 4.0 D/A° for the Q_3 mode for crystalline CO_2.

The interaction energy caused by the coupling of two CO_2 molecules is discribed by Decius:

$$(8)\quad V' = -\frac{\mu_1 \mu_2}{R^3}\,(2\cos\theta_1\cos\theta_2 - \sin\theta_1\sin\theta_2\cos\chi)$$

where μ_1 and μ_2 are the magnitudes of the two dipoles and R is the distance between two large-cage centers (~ 5.8A°).

Using a simple coupling potential, the total potential energy of the system is:

$$(9)\quad V = \frac{1}{2}\,\beta\,(x_1^2 + x_2^2) + \alpha\, x_1\, x_2$$

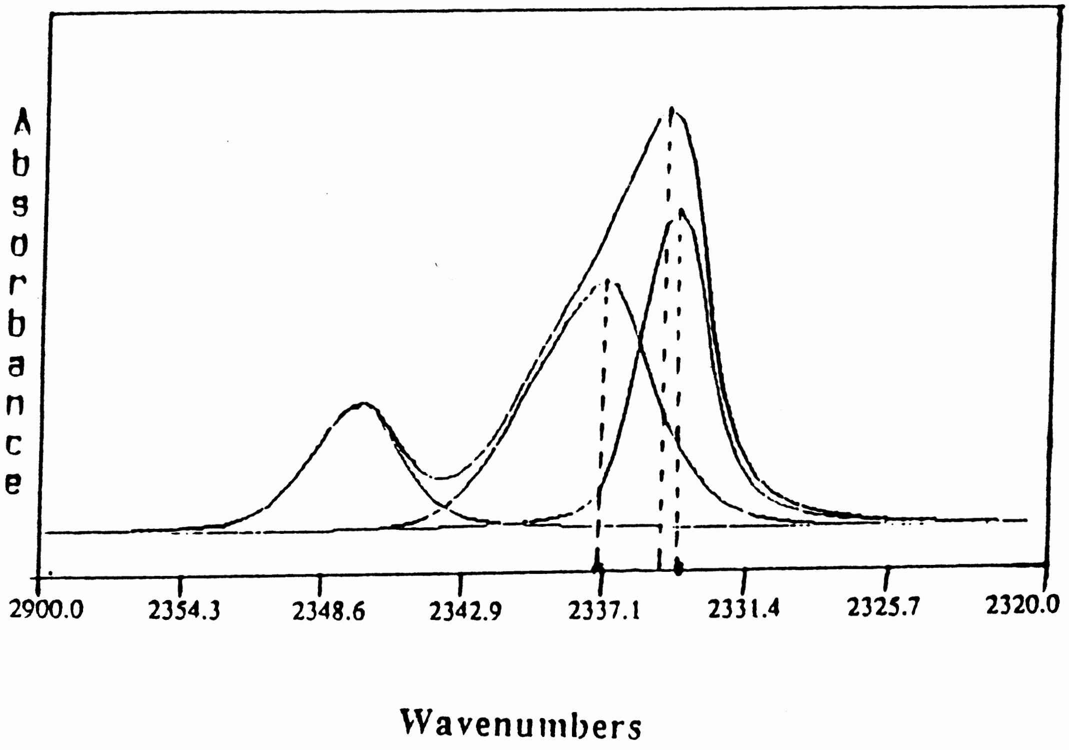
Absorbance
2900.0
2354.3
2348.6
2342.9
2337.1
2331.4
2325.7
2320.0
Wavenumbers

where β and α are the bond constant and the coupling constant, respectively. The angles θ_1 and θ_2 describe the inclination of the dipole moments from the line between the centers. The angle χ is between the projections of the dipoles in the plane perpendicular to the line between the centers and taken to be zero. Therefore, α is expressed by Decius as:

$$(10)\quad \alpha = \frac{-1}{R^3}\left(\frac{\partial \mu_i}{\partial Q_i}\right)\left(\frac{\partial \mu_i}{\partial Q_i}\right)(2\cos\theta_1\cos\theta_2 - \sin\theta_1\sin\theta_2\cos\chi)$$

By varying θ_1 and θ_2 the coupling constant changes, which in turn changes the splitting since from appendix C:

$$(11)\quad |\Delta\upsilon| = |\upsilon^+ - \upsilon^-|$$

where, $\upsilon^+ = \upsilon_o\,(1 + \frac{\alpha}{2\beta})$ and $\upsilon^- = \upsilon_o\,(1 - \frac{\alpha}{2\beta})$, where υ_o is the large-cage harmonic oscillator frequency, having a value of 2336 cm^{-1}. In our calculation θ_2 is always equal to $180-\theta_1$, assuming that the CO_2 molecules have the same orientation in all the cages, and since the data fit was obtained at 13 K, no rotation of the CO_2 molecule inside the cages is taken under consideration. As an example, if $\theta_1 = 0$ and $\theta_2 = 180$, then $\alpha = 0.16$ and $|\Delta\upsilon| = 2.69$ cm^{-1}. Since the splitting experimentally is 3 cm^{-1} the error found is 8%. By taking the orientation of the CO_2 molecules described by Tse *et al.*, (62) $\theta_1 = 60°$ and $\theta_2 = 120°$, then $\alpha = 0.10$, and the splitting is 1.7 cm^{-1}. The error found here is 43.3%. Table 13, and Fig. 32 and 33 show the variation of the coupling constant with respect to θ_1 and θ_2.

The splitting and the coupling constant take minimum values of 1.35 cm^{-1} and 0.084 $D^2/A^{\circ 5}$ respectively, which designates the minimum interaction between the oscillators. This occurs when when $\theta_1 = \theta_2 = 90$, suggesting that the oscillators are perpendicular to the equatorial plane of the large cage, and have the same direction.

Structure II Simple Hydrate of THF and CO_2

The growth of the CO_2 clathrate hydrate epitaxially to the (EO) clathrate substrate

TABLE 13

SPLITTING AND COUPLING CONSTANT VERSUS θ_1 and θ_2

θ_1	θ_2	α	$\Delta\upsilon$
0	180	0.17	2.70
10	170	0.16	2.66
20	160	0.15	2.54
30	150	0.14	2.36
40	140	0.13	2.14
50	130	0.12	1.96
60	120	0.10	1.70
70	110	0.09	1.50
80	100	0.085	1.40
90	90	0.08	1.30

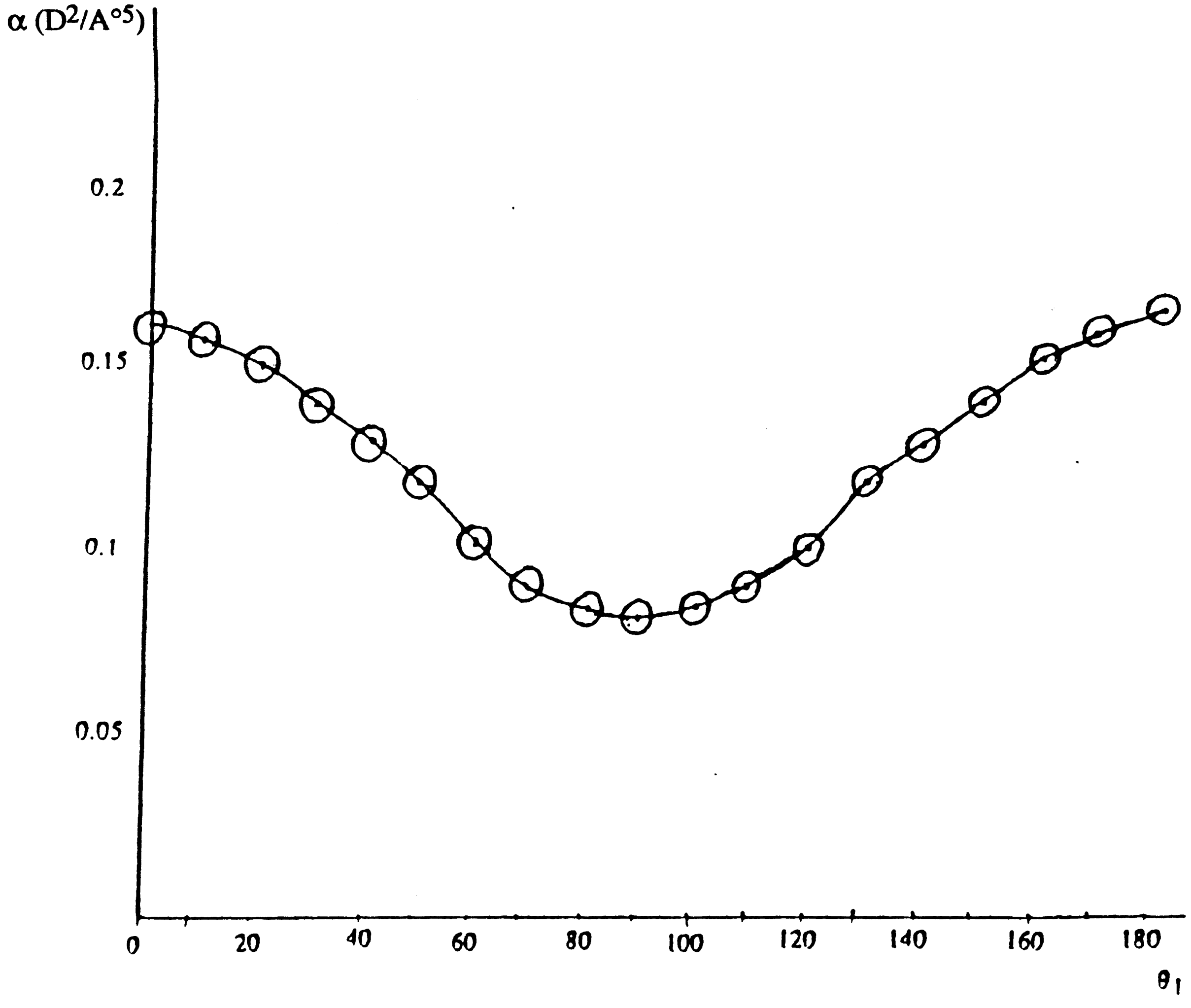
α (D²/A°⁵)
0.2
0.15
0.1
0.05
0
20
40
60
80
100
120
140
160
180
θ1

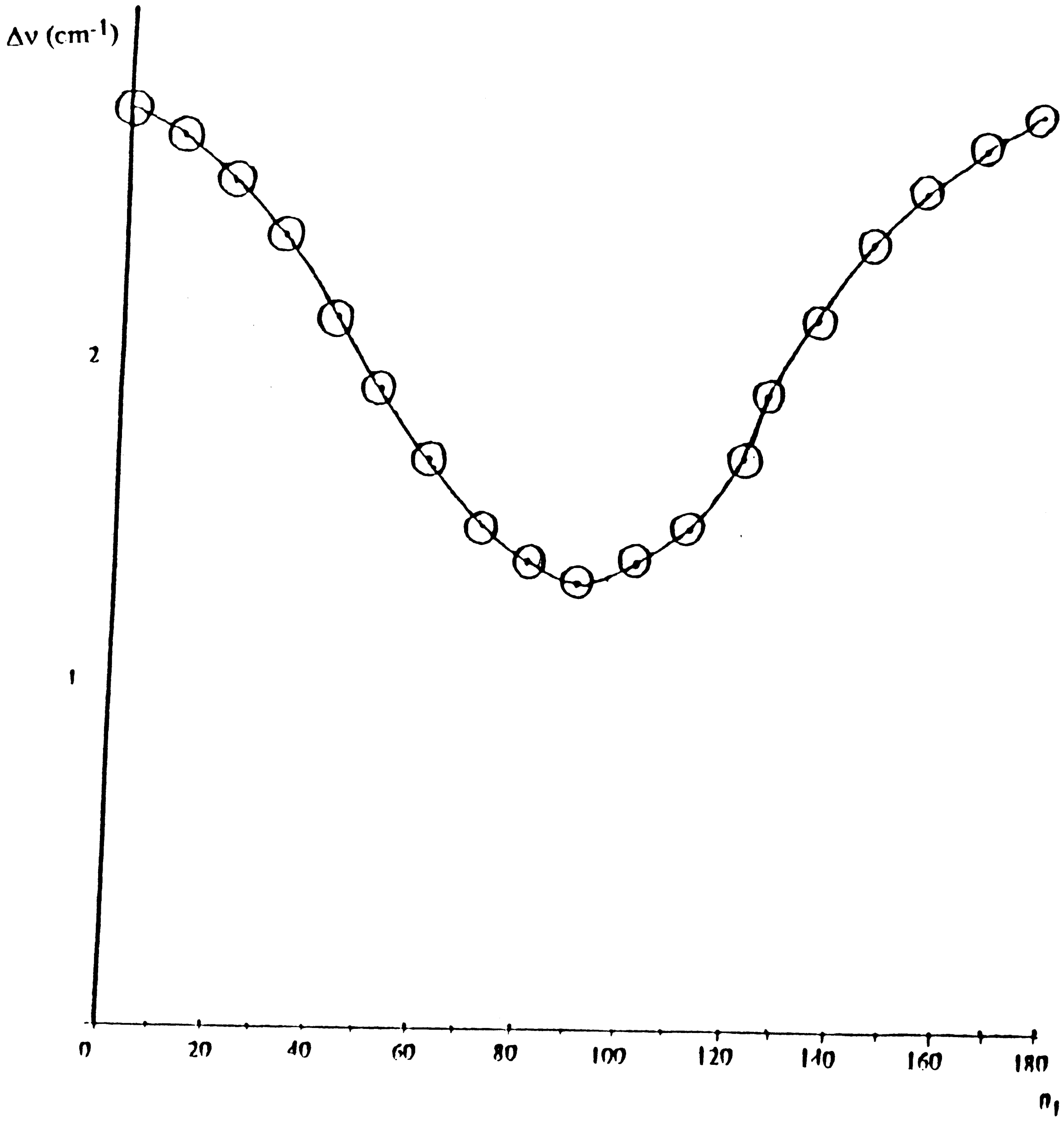
Δν (cm-1)
2
1
0
20
40
60
80
100
120
140
160
180
n1

did not conclusively separate the nucleation process from the L-defect mobility, and therefore did not prove which factor is responsible for the clathrate hydrate formation from the vapor phase; especially since both clathrate hydrates have a tendency to grow as structure I hydrates. Therefore, it was decided to grow the CO_2 clathrate hydrate using the (THF) as a help gas. If CO_2 failed to grow as a structure I clathrate hydrate, then the nucleation process appear to be dominant.

First, a mixture of H_2O:CO_2:THF was deposited onto the CsI plate at 150 K to observe the IR bands of both guest molecules. Unlike (EO) clathrate hydrate, there has been no available reports on the IR spectrum for the ring C-O stretching mode region of a (THF) crystalline clathrate hydrate for temperatures below 90 K. Tetrahydrofuran is known to form a stable structure II simple hydrate as well as structure II double hydrate with small (H_2S) molecules (20).

The spectra of the C-O, and C-H stretching regions of the (THF) clathrate hydrate at 13 K are presented in Figs. 34 and 35 curve (a). The spectrum in the C-O region is easily recognized as that of the crystalline clathrate hydrate, since the difference between the crystalline (THF) clathrate hydrate spectrum and the amorphous (THF) spectrum is noticeable. The major peak and the shoulder in Fig. 34 sample are at 1071/1076 cm^{-1}, whereas bands occur at 1052/1034 cm^{-1} for glassy H_2O-THF films. The frequency values of the crystalline (THF) hydrate agree well with published results (36), but the doublet structure appears only at this lower temperature. This doublet nature of the (THF) hydrate C-O stretching mode band is attributed to the distribution of the (THF) molecules over two unequal positions in the hexacaidecahedral cages, as has been suggested for (EO) hydrate (71), and confirmed during this work by the presence of a doublet in the ^{13}C-O stretching region (not shown).

Upon looking at the spectrum in the CO_2 υ_3 region in Fig. 36 only one band appears at 2345 cm^{-1}. This suggests that the H_2O:CO_2:THF is a double hydrate, just like the H_2O:H_2S:THF clathrate hydrate (20). The CO_2 molecules in this clathrate hydrate

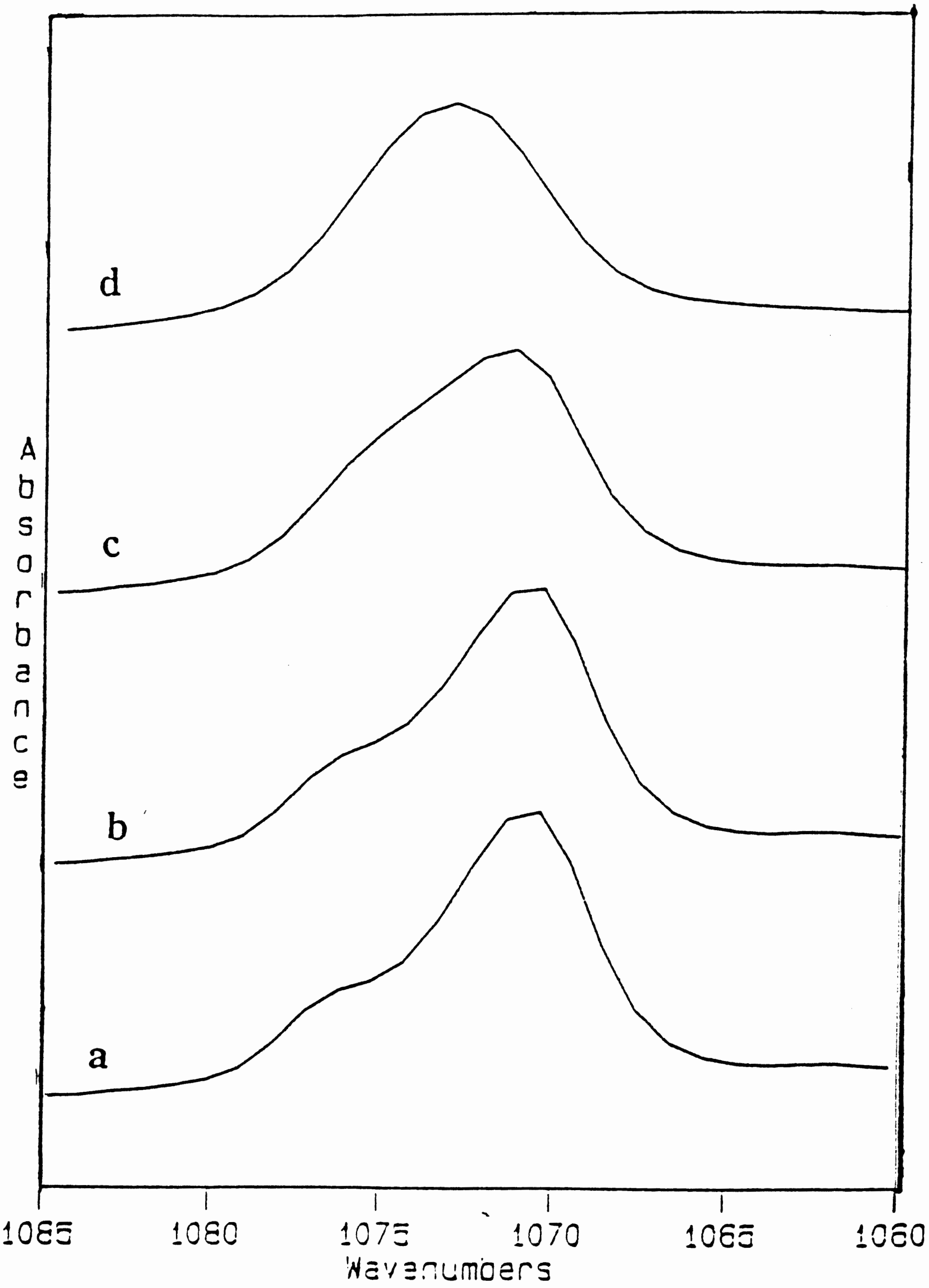
d
c
b
a
Absorbance
1085
1080
1075
1070
1065
1060
Wavenumbers

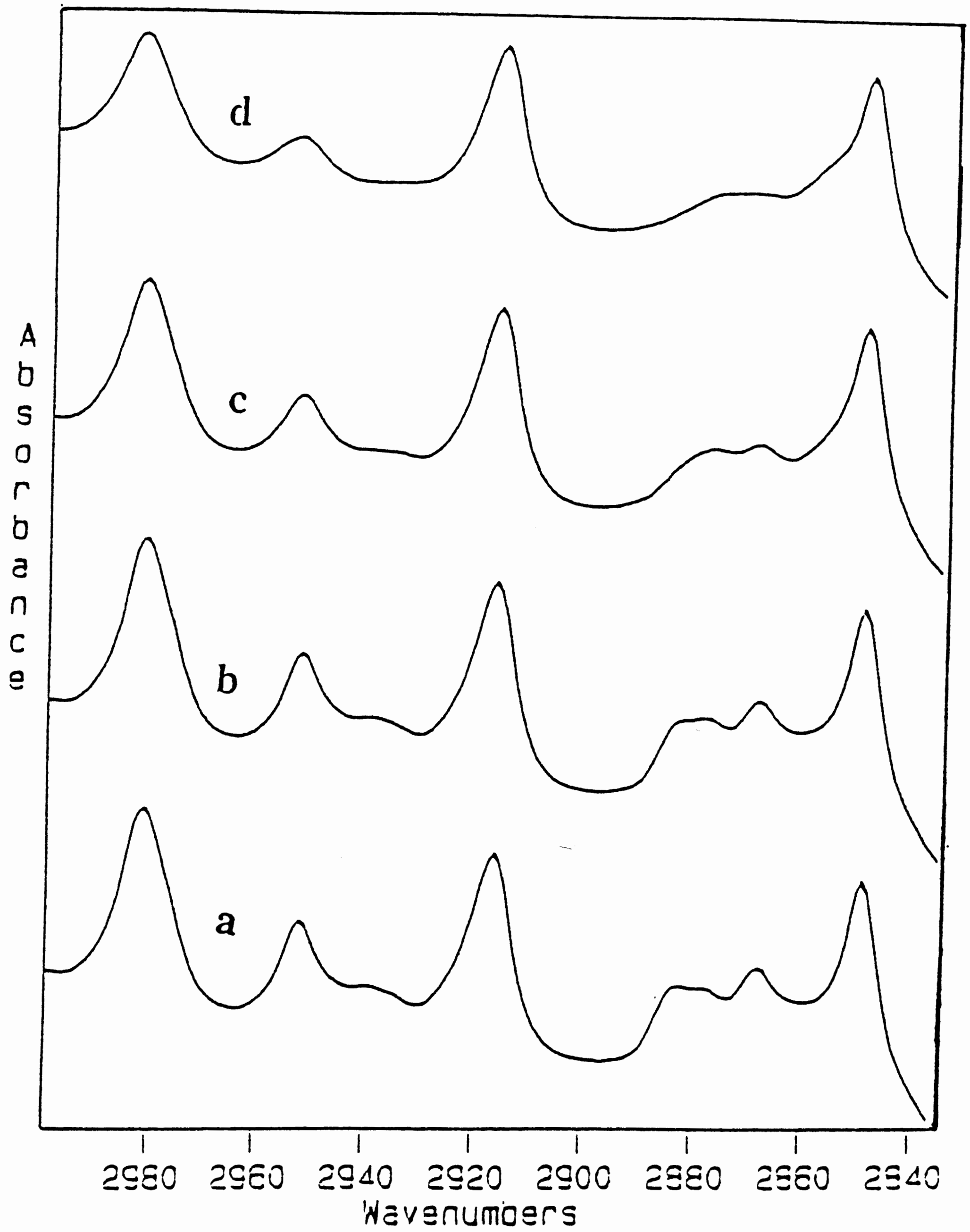
d
c
b
a
Absorbance
2980
2960
2940
2920
2900
2880
2860
2840
Wavenumbers

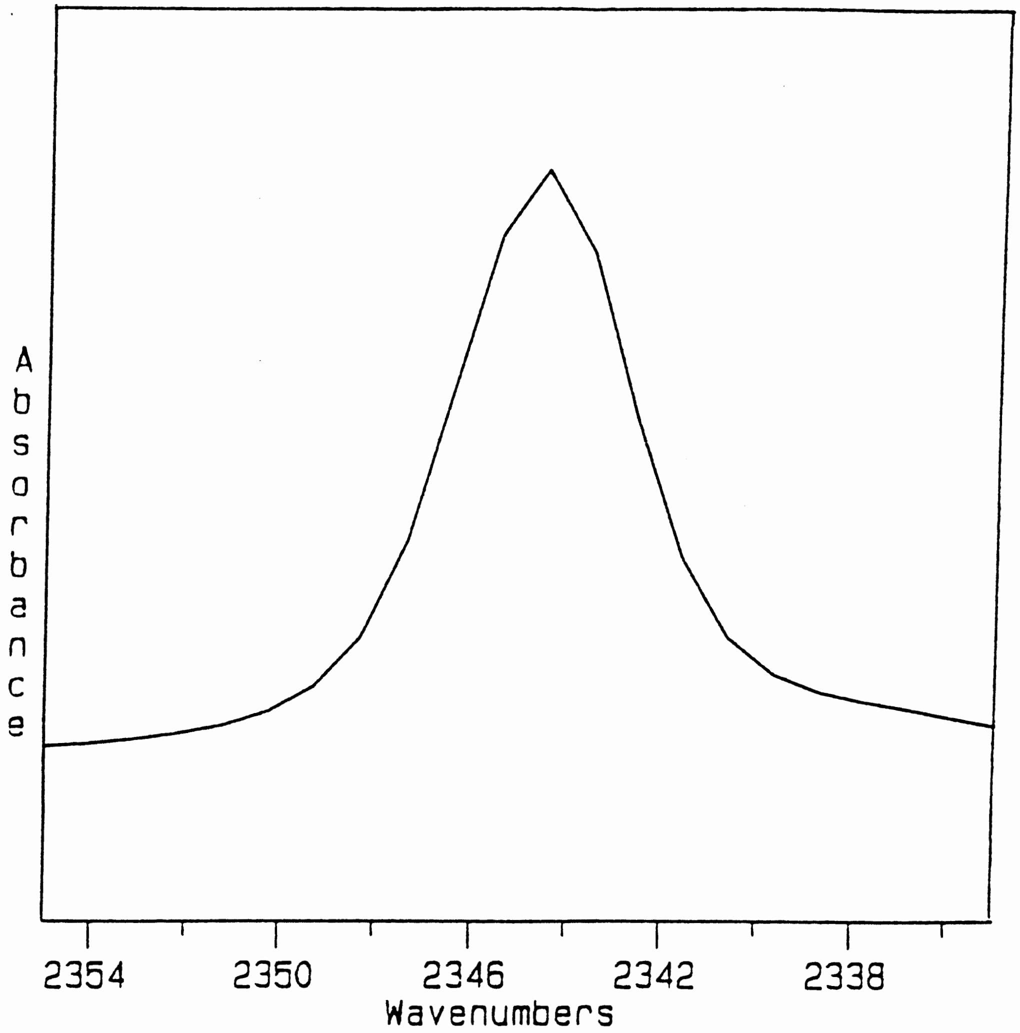
Absorbance
2354
2350
2346
2342
2338
Wavenumbers

reside in the small cages. This is also confirmed by the singlet at 655 cm^{-1} in Fig. 37, which corresponds to the small-cage frequency in the υ_2 degenerate region. The same result is observed when the H_2O:CO_2 mixture is deposited on the (THF) clathrate hydrate substrate at 150 K, as presented in Figs. 38 and 39 curves (a). These band frequencies match exactly with the mixed H_2O:CO_2:THF band values, and are also similar to the small-cage structure I value. However, unlike the structure I hydrate, all the CO_2 molecules are in the small cages as evidenced by the absence of the large cage band (at 2335 cm^{-1} for υ_3), even though the gas phase H_2O:CO_2 ratio is still 6:1. Since stabilizing van der Waals interactions exist between the structure I large cage and CO_2, the fact that carbon dioxide molecules in this case are stabilized in the small cages indicate that the hydrate structure formed epitaxially to the (THF) type II hydrate is structure II and not structure I as seen in Fig. 40. The spectra thus must reflect a lack of stabilizing interactions between the hexacaidecahedral cages and the CO_2 molecules, probably caused by the difference in size between the particular large cavity and small guest in question. These results disagree with what is seen in the case of small molecules occupying the large cages in the structure II hydrates (2, 24, 28). This disagreement could be explained by the difference in sample preparation, because in other laboratories the clathrate hydrate preparation is performed at higher temperatures, and especially at high guest pressure (~138 atm.), which forces the guests in the cages; whereas during this work, the pressure in the system is quite low as listed in Tables 10, 11, and 12.

The presence of the 4% HOD in the H_2O:CO_2 gas phase mixture helped identify the clathrate hydrate spectrum. The O-D stretching band of Fig. 41 curve (a) has a maximum at 2415 cm^{-1}, and its FWHM is 50 cm^{-1}, which combined with the fact that the bending-torsional mode overtone band of the host ice lattice shows a maximum at 1600 cm^{-1} as expected for all crystalline clathrate hydrates, indicates that the CO_2 sample is a clathrate hydrate and not CO_2 diluted in crystalline ice or amorphous ice; especially since the latter does not exist at 150 K. Figure 42 presented for comparison purposes shows that the

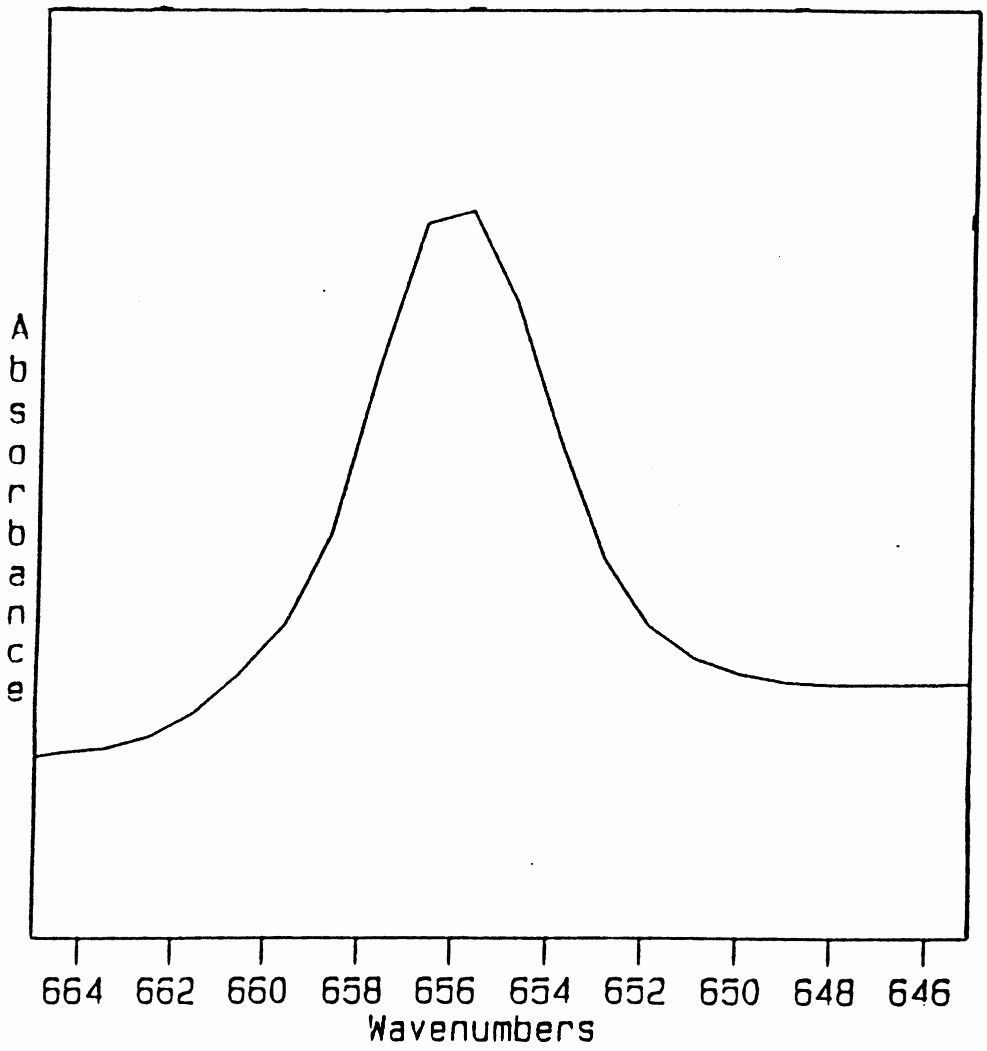
Absorbance
664
662
660
658
656
654
652
650
648
646
Wavenumbers

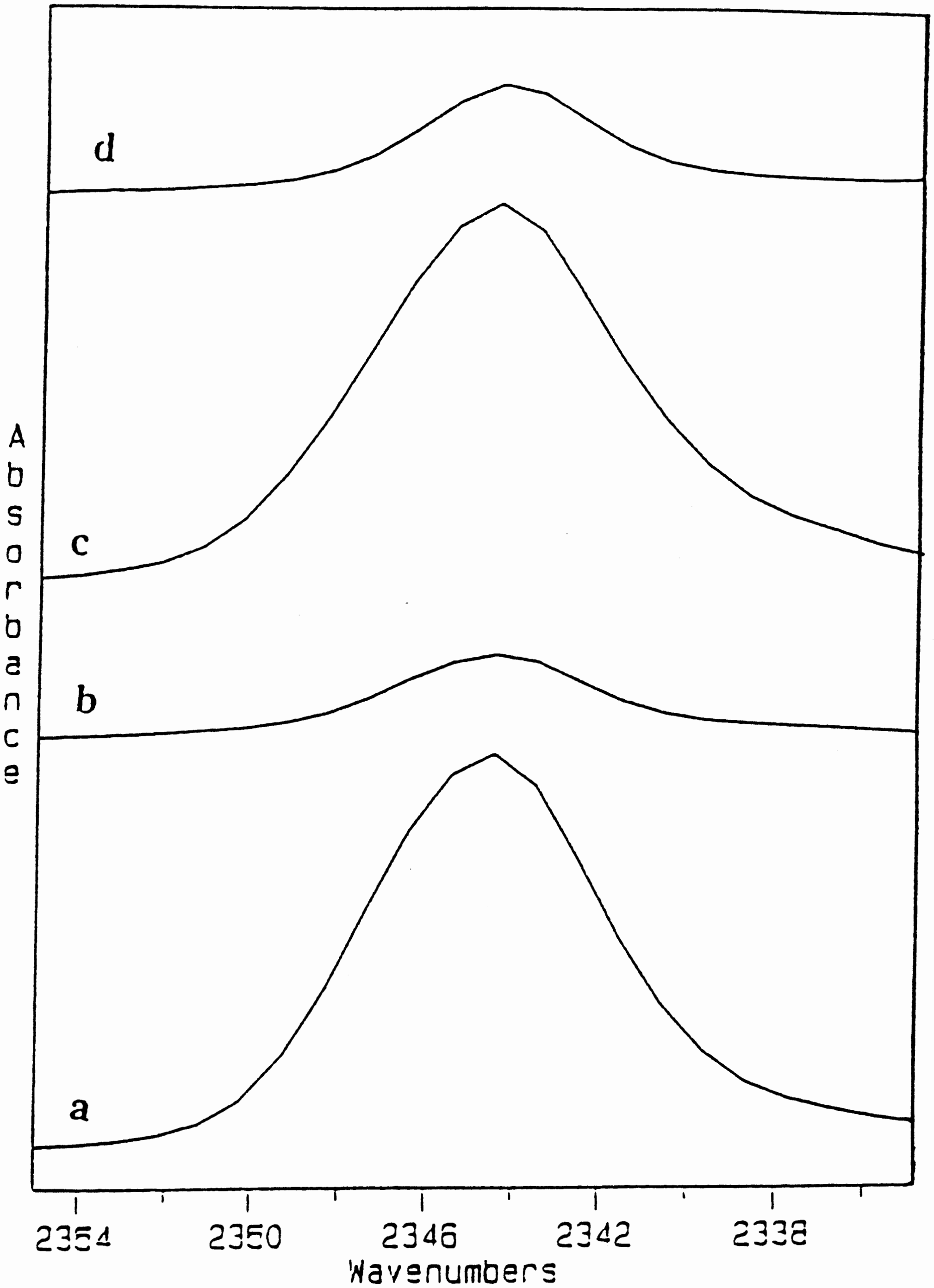
d
c
b
a
Absorbance
2354
2350
2346
2342
2338
Wavenumbers

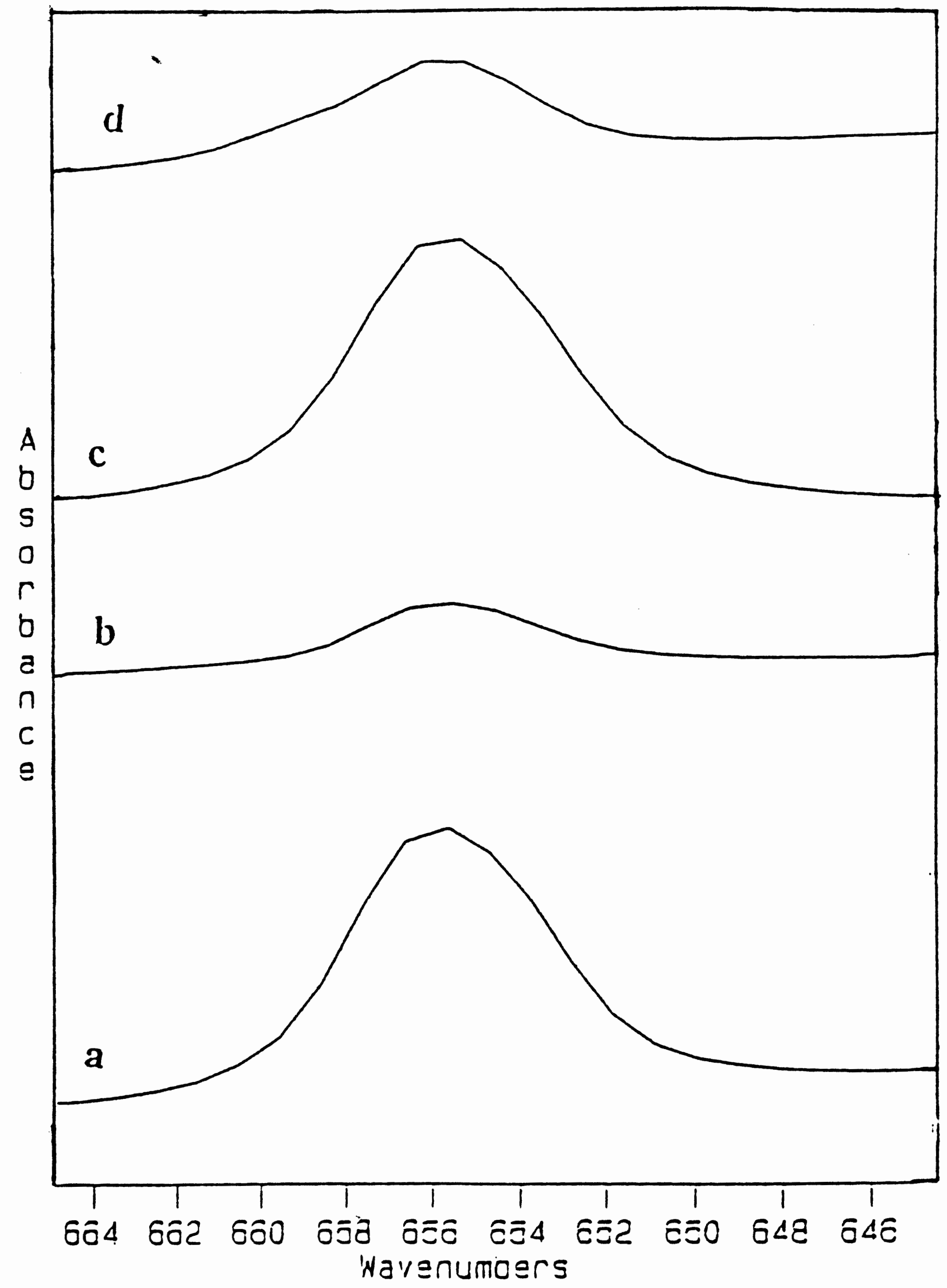
d
c
b
a
Absorbance
664
662
660
658
656
654
652
650
648
646
Wavenumbers

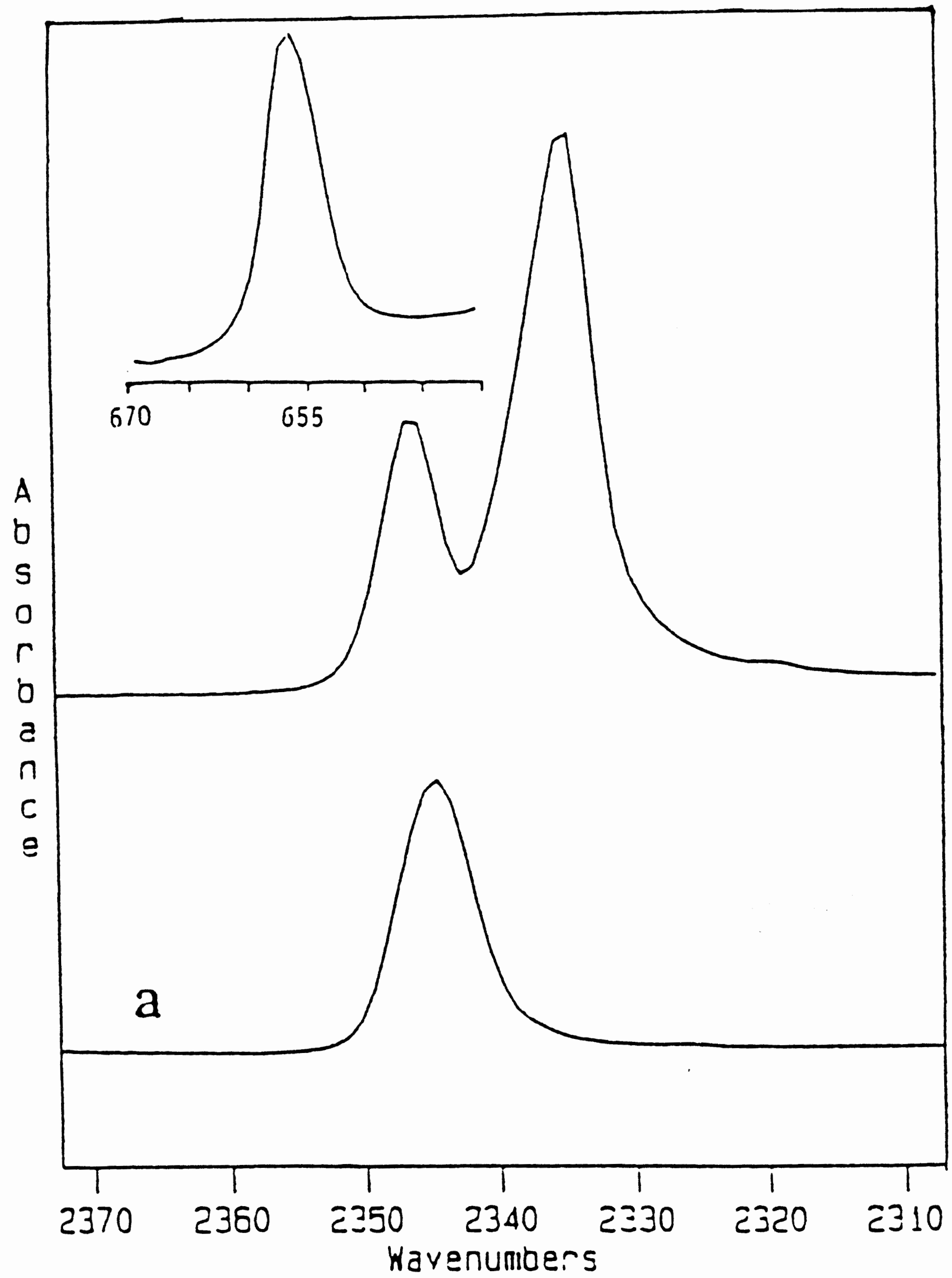
670
655
Absorbance
a
2370
2360
2350
2340
2330
2320
2310
Wavenumbers

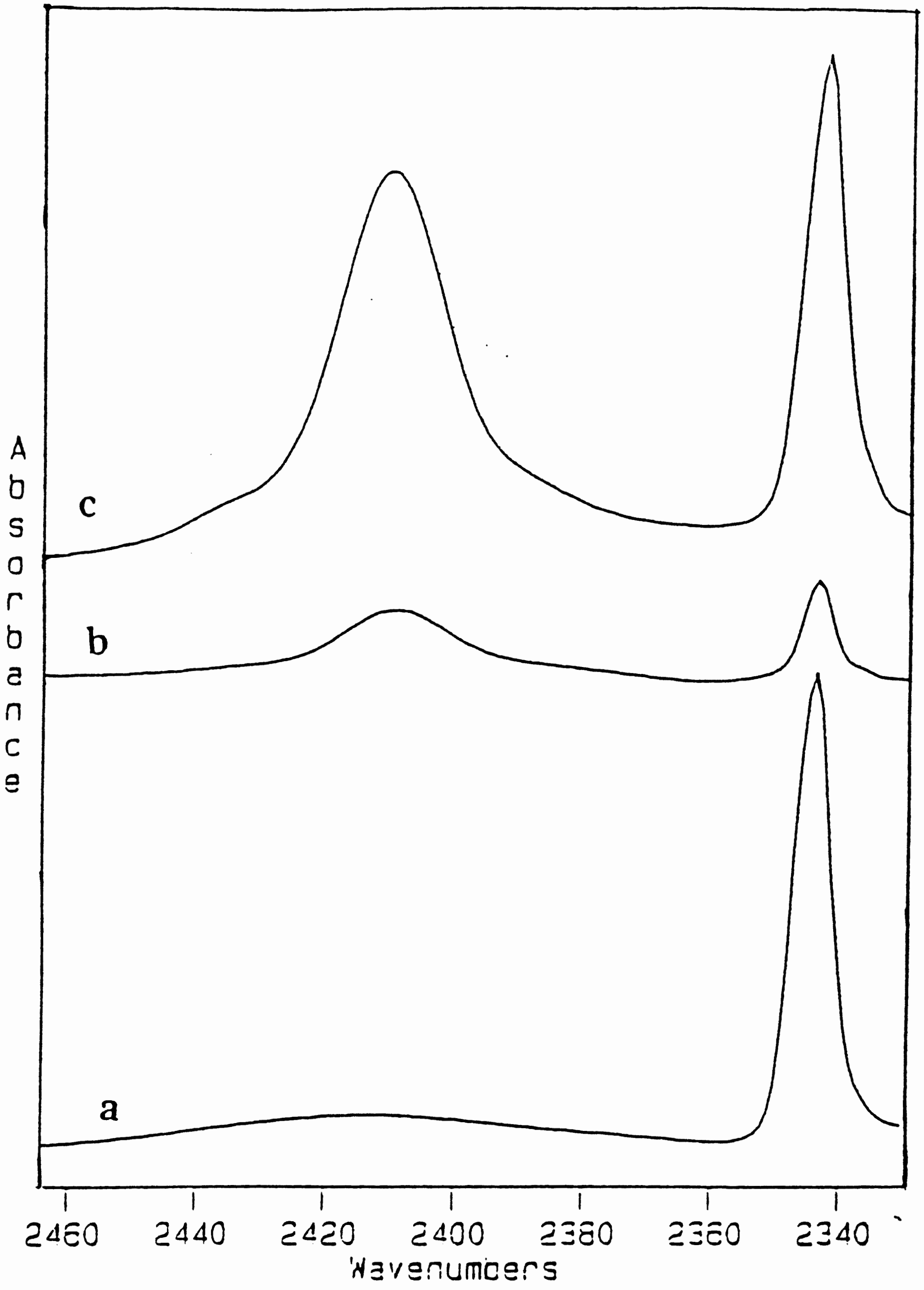
Absorbance
c
b
a
2460
2440
2420
2400
2380
2360
2340
Wavenumbers

Figure 42. Infrared spectra (13 K) of the isolated HOD molecules. (a) in the structure II of the CO_2 clathrate hydrate, (b) in CO_2 diluted in crystalline ice sample.

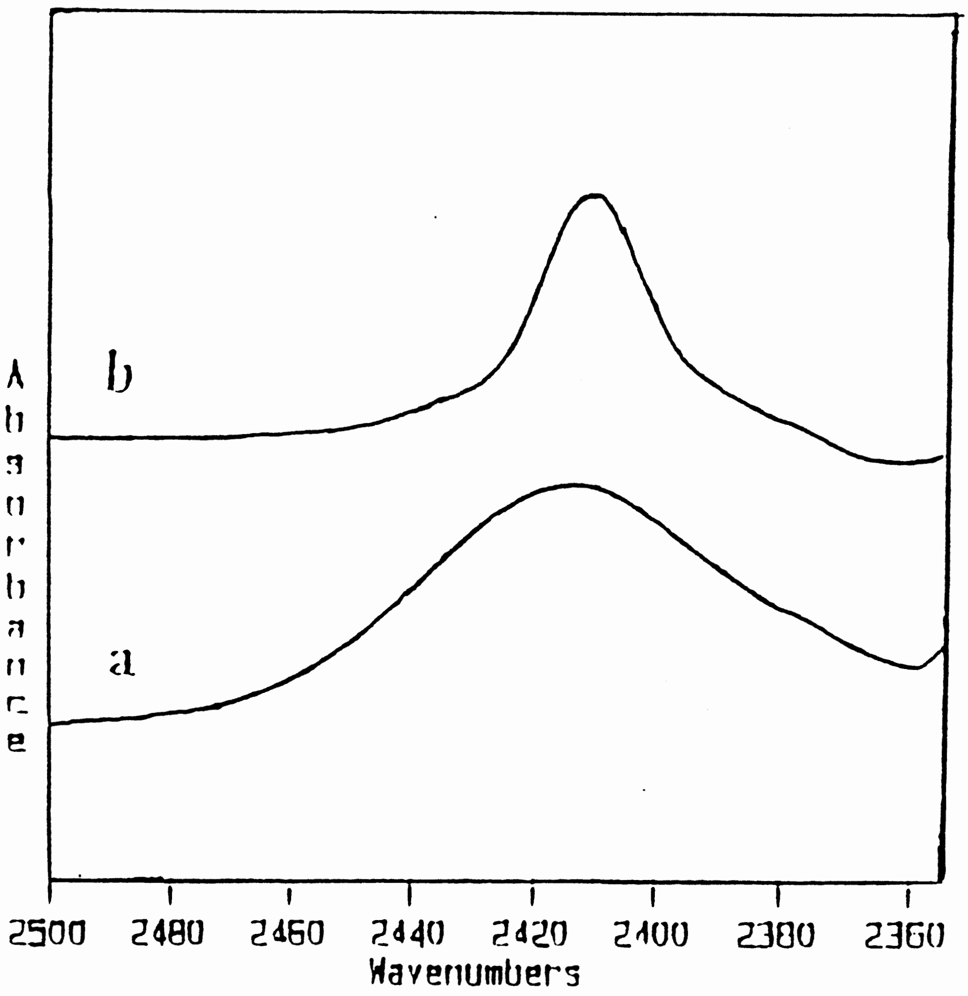
Absorbance
b
a
2500
2480
2460
2440
2420
2400
2380
2360
Wavenumbers

HOD band for CO_2 clathrate hydrate (curve a) and CO_2 diluted in crystalline ice for which the FWHM is 18 cm^{-1} (curve b). Since at 150 K CO_2 has a significant vapor pressure, the one minute overlap period between the H_2O:THF and the H_2O:CO_2 vapor beams incident at the ether-clathrate substrate created a slight ambient CO_2 pressure that suppressed the CO_2 escape, and thus facilitated the epitaxial formation of the CO_2 clathrate hydrate. The distinguishing features of the data, obtained after epitaxially depositing the vapor beam of H_2O:CO_2 onto the (THF) clathrate layer at 150 K, confirm that the clathrate hydrate of CO_2 nucleates on the substrate to form a simple type II hydrate structure, in which only the small cages are occupied.

The formation of the structure II CO_2 clathrate hydrate to the (THF) hydrate substrate again did not help the separation of the nucleation process from the Bjerrum-defect activity in the samples. Therefore, the same experiments in the (EO) clathrate hydrate case are also conducted in the (THF) hydrate case. The variation of the deposition temperature of the H_2O:THF mixture did not aid this study since (THF) clathrate hydrate itself is difficult to form at lower temperatures. Therefore, this study was restricted only to the variation of substrate thickness by varying substrate deposition times. Figs. 38 and 41 curve (a) and curve (b) correspond to the samples having a H_2O:THF and H_2O:CO_2 deposition times of (6 min., 6 min.) and (1 min., 6 min.) respectively. In curve (c) the deposition times of H_2O:THF and H_2O:CO_2 are (6 min., 25 min.), and in. curve (d), presented in Fig. 38, and not shown in Fig. 41, the deposition time of H_2O:THF is 6 min., but no H_2O:CO_2 mixture is deposited besides the one minute overlap period.

The CO_2 absorption bands in Fig.38 curves (a) and (c) match exactly, and also the ones in curves (b) and (d). Since the 6 min. H_2O:CO_2 deposit did not contribute to the band intensity in curve (d), it was deduced that the CO_2 of the 6 min. H_2O:CO_2 deposit in curve (b) did not stick on the substrate, and the only CO_2 remaining was what had come from the one minute overlap period. By comparing the HOD band in Fig.41 curves (a) and (b), the FWHM in the first curve is 50 cm^{-1} and in the second curve is 18 cm^{-1}. The only difference between curves (a) and (b) was the thickness of (THF) clathrate hydrate substrate. Therefore, it is concluded that CO_2 clathrate hydrate fails to grow epitaxially on a thin (THF) clathrate substrate, whereas it grows perfectly on a thick (THF) clathrate substrate.

By comparing curves (a) and (c) the absorption intensity is the same. However, in curve (a) the HOD FWHM is 50 cm^{-1} as mentioned earlier, but in curve (c) it is 18 cm^{-1}. By subtracting exactly 100% of the IR spectrum of the sample in curve (a) from the IR spectrum of the sample in curve (c), the only remaining band is the ice band as shown in Fig. 43. This particular result suggests that the clathrate hydrate of CO_2 grows epitaxially to the (THF) substrate up to a certain point, corresponding to 6 min. in deposition time or to 1 micron in thickness then stops, and ice formation occurs thereafter.

Assuming that (THF) clathrate hydrate substrate is a source of L-defects, it is clearly shown that the contribution of defects in the samples of curves (a) and (c) are enough to grow the CO_2 clathrate hydrate, whereas there is insufficient contribution from the (THF) clathrate hydrate substrate of curve (b). Also, since at 150 K L-defects are known to be mobile in ice, they must possess a translational motion that allows them to migrate through the crystal, which evidently makes the thicker (THF) hydrate samples a better clathrate substrate than the thinner samples, since the thicker the substrate the more defects can pass into the CO_2 clathrate hydrate layer. The results seen from curve (c) in Fig. 41 indicates that the L-defects are penetrating the CO_2 clathrate hydrate for at least 1 micron (corresponding to about 6 min. in deposition), but not enough L-defects are available to grow 4 microns of CO_2 clathrate hydrate sample, (corresponding to 25 min. deposit). This suggests that the defects are available to form the early part of the CO_2 sample, while a deficiency in defects forces the rest of the sample to grow as crystalline ice, as in the case of a regular H_2O:CO_2 deposit on a CsI plate. This conclusion is confirmed by the amount of unreacted CO_2 gas pumped out after each deposit. For samples in curves

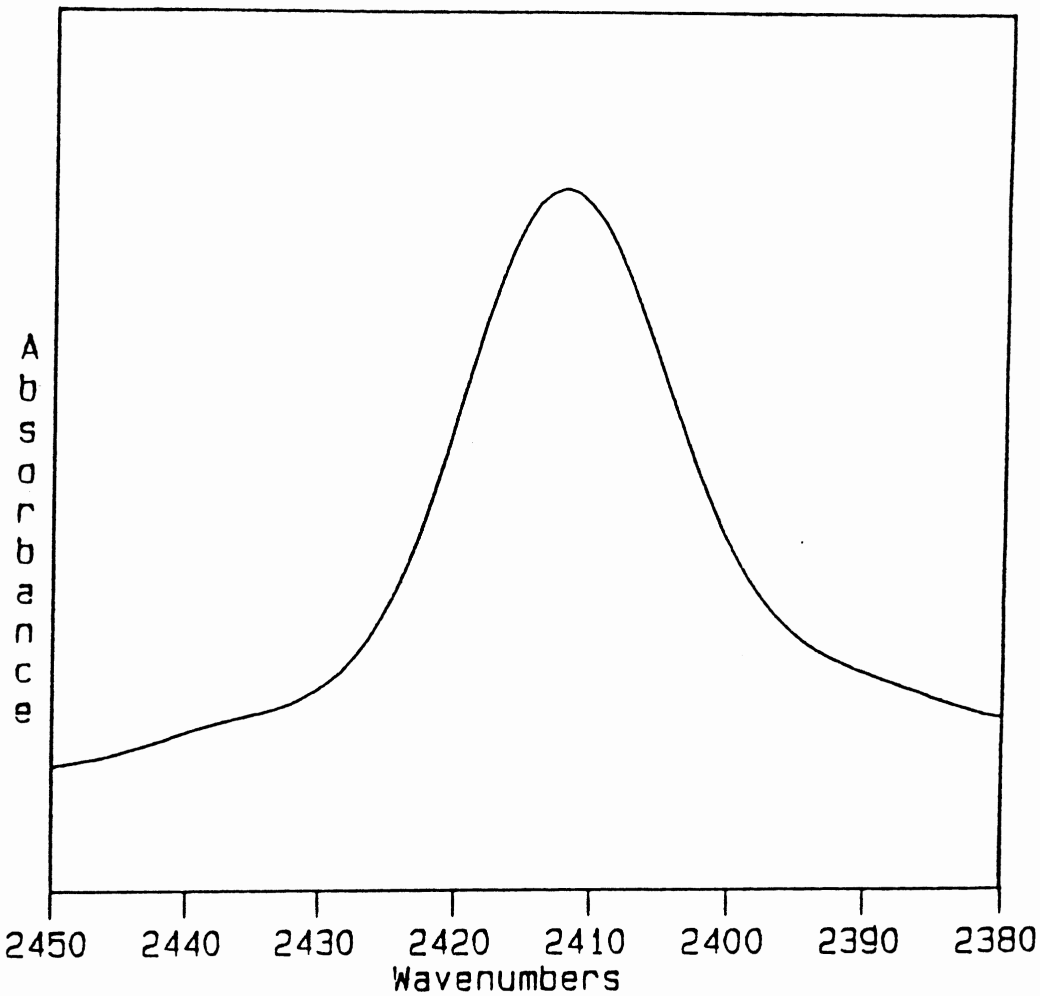
Absorbance
2450
2440
2430
2420
2410
2400
2390
2380
Wavenumbers

(b) and (c) the dynamic pressure increased to 60 microns, whereas for the sample in curve (a) the pressure increased to 15 microns.

A physical model is presented in Figs.44, 45, and 46 to describe what happens to the L-defects while migrating from a substrate through a boundary, and why it happens. To simplify the problem it is assumed that: a) the system is at equilibrium, b) the L-defects move forward, c) the D-defects are frozen in the 100-150K temperature range, and d) the L-defects are the negative charge carriers, and the D-defects are the positive charge carriers (45). In Fig.44 a barrier is placed, so the L-defects fail to cross the boundary. Since the system is at equilibrium:

$$(12)\quad [D][L] = \text{constant}$$

therefore charge separation does not exist in the system, and thus the curve in Fig.44 representing the concentration of L-defects per unit thickness is a straight line.

In Fig.45 the barrier is removed. Therefore, some L-defects generated from an infinitely thin substrate could migrate across the boundary. The migration of the L-defects causes an increase in the D-defect concentration in that substrate in order to maintain equilibrium. Since the D-defects are the positive charge carriers and the L-defects are the opposit, and since the volume of the ultrathin substrate is small, thus there would be an extensive charge separation caused by the positive charge concentration in the substrate, which would attract the L-defects and might limit their migration across the boundary. This limitation is presumed in this work to be the cause of the degradation in the clathrate hydrate quality. In Fig.46 when the substrate is considered to be thicker than the example above, indicates that more defects are migrating through the boundary. However, because of the increase in substate volume the positive charges in this case are not as concentrated as in the previous case, and thus the electrostatic attraction is weaker which explains why the curve represented beyond the boundary in Fig.46 does not decrease as fast as in the example above.

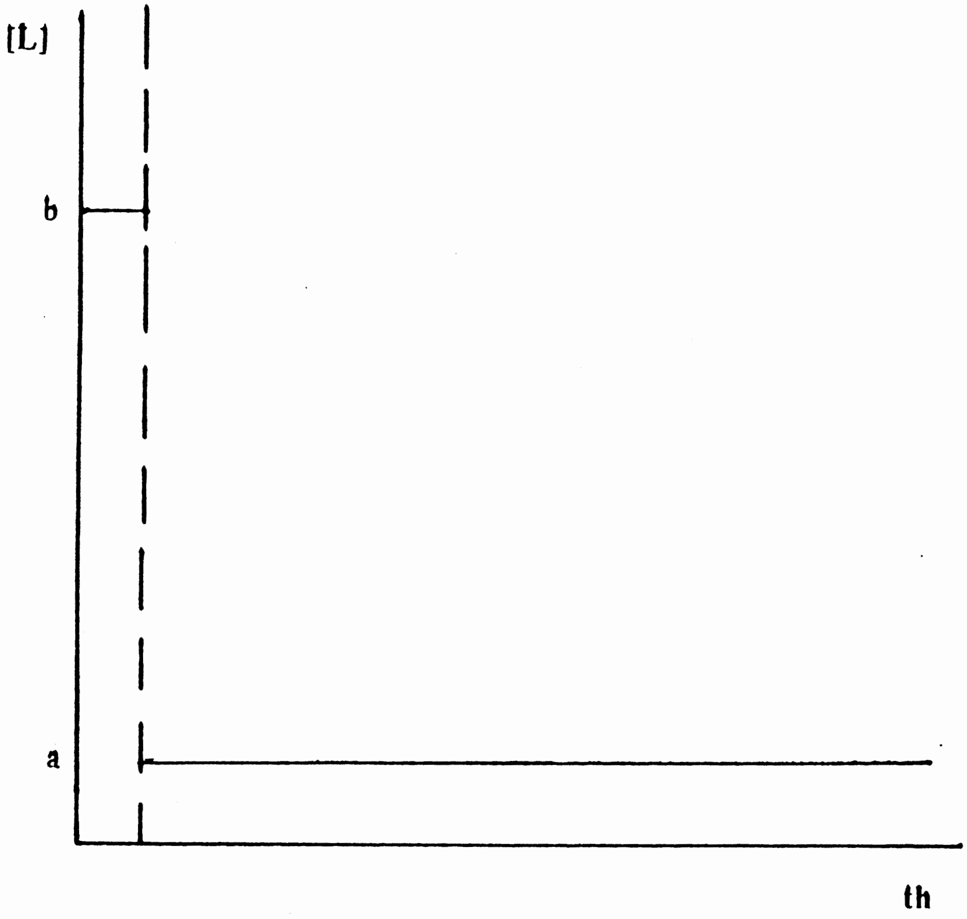
[L]
b
a
th

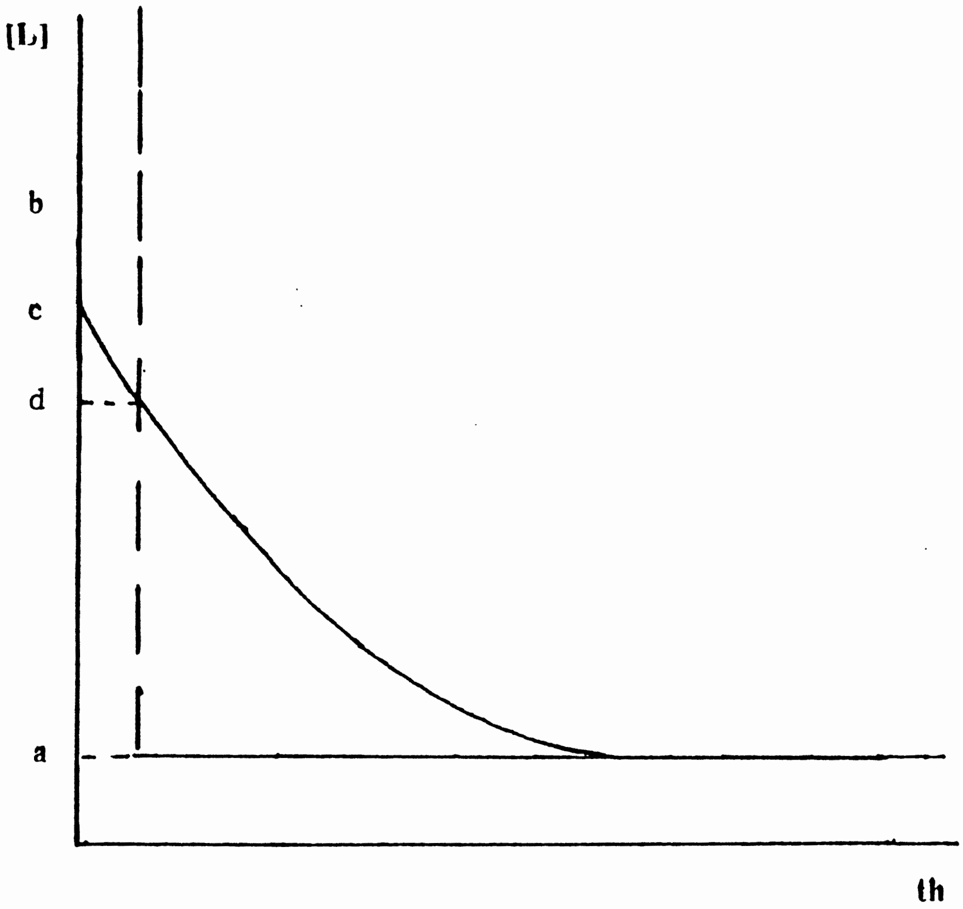
[L]
b
c
d
a
th

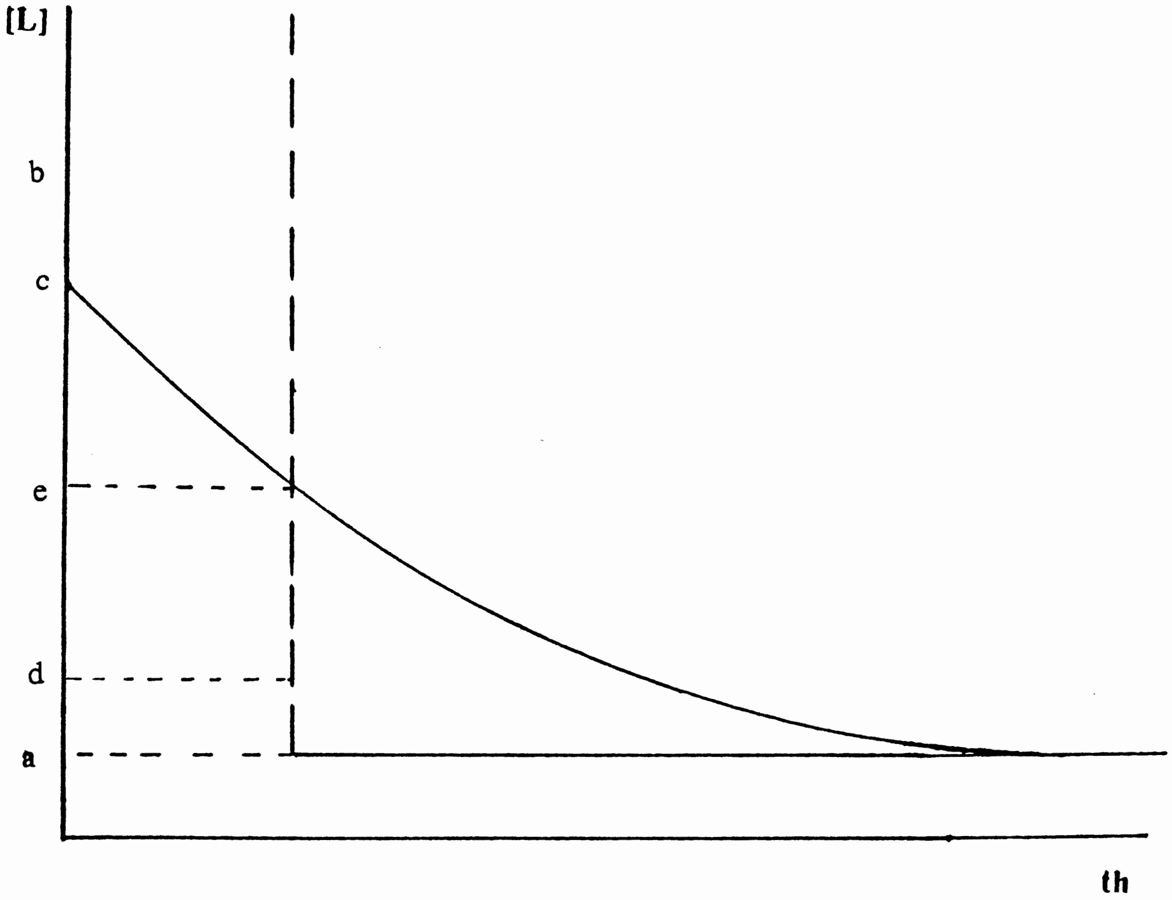
[L]
b
c
e
d
a
th

Similar to the (EO) case, upon warming the sample from 13 to 80 K as shown in Fig. 34 (a-d) the doublet of the (THF) ring C-O stretching mode band slowly merges to a single band to match the 90 K results, and the structured bands at 2865 and 2880 cm^{-1} in the clathrate hydrate stretching region merge together to form a singlet at 2870 cm^{-1}. Since these two modes are not degenerate, the gain in band symmetry is attributed to a possible shifting of the guest molecules to the center of the cages, away from nonequivalent sites, accompanied by the onset of rotational motion of the molecules inside the large cages of the lattice as suggested by Davidson (61) and White (54).

For the CO_2 molecules in the structure II clathrate hydrate no major thermal changes occurred, which seems consistent with the earlier results. Though the small cage $^{12}CO_2$ υ_3 band is symmetric for both structure I and structure II hydrates, the small-cage band of structure II is as broad as the large cage band of the structure I hydrate, while for the $^{13}CO_2$ the FWHM of the small cage bands for both types are much smaller (2-3 cm^{-1}) as listed in Table 14. This suggests that, in the structure II hydrate, the $^{12}CO_2$ molecules in the small cages are also subjected to dynamical coupling through dipole interactions caused by the large number of small cages in that structural type.

Structure II Simple Hydrate of Chloroform (CF) and CO_2

To advance the defect study in clathate hydrates the next step taken in this work was to introduce a D-defect promoter clathrate hydrate layer between the (THF) hydrate substrate and the H_2O:CO_2 deposit. The (CF) clathrate hydrate was chosen because the (CF) molecule is large enough to form a structure II hydrate, and in contrast to (THF) and (EO), the (CF) molecule is an electron acceptor, which might create a process inside the lattice cages, that is opposite to the one described by Whally and Davidson (51) for the electron donor molecules. Since the opposite process of L-defect formation in the lattice is the D-defect formation, it is safe to assume that the (CF) molecules inside the cages are

TABLE 14

FREQUENCIES [υ_3 and υ_2 (cm^{-1})] OF STRUCTURES I AND II $^{12}CO_2$ AND $^{13}CO_2$ HYDRATES IN THE SMALL AND THE LARGE CAGES, AND OF (THF) HYDRATE IN THE LARGE CAGES OF STRUCTURE II AT DIFFERENT TEMPERATURES.

Small cage/Large cage Structure I CO_2 Hydrate (cm^{-1}) υ_3			Small cage/Large cage Structure I CO_2 Hydrate (cm^{-1}) υ_2	
Temperature (K)	$^{12}CO_2$ (FWHM)	$^{13}CO_2$ (FWHM)	Temperature (K)	$^{12}CO_2$ (FWHM)
13	2347(4) / 2334(7)	2280(3) / 2271(3)	13	655(8) / 661, 659
60	2347(4) / 2335(7)			
90	2347(4) / 2336.5(8)	2281(3) / 2272(4)	90	655(8) / 661, 659
135	2347(4) / 2338(8)		135	655(8) / 661, 659

TABLE 14 (Continued)

Small cage Structure II CO_2 Hydrate (cm^{-1}) υ_3/υ_2			Large cage THF Structure II Hydrate (cm^{-1}) υ_3	
Temperature (K)	$^{12}CO_2$ (FWHM)	$^{13}CO_2$ (FWHM)	Temperature (K)	THF (FWHM)
13	2345(7) / 656(5)	2278(2)	13	1071 / 1076(5)
10	2345(7) / 656(5)	2278(2)	40	1072 / 1076
90	2346(7) / 657(5)	2279(2)	90	1074
135	2346(7) / 657(5)	2279(2)		

The numbers in parenthesis are the full width at half maximum.

D-defect promoters. This is justified by the fact that (CF) suppresses the (THF) clathrate hydrate formation when mixed with H_2O:THF (results not shown but noted in Table 11)

During this series of experiments the thickness of the (CF) clathrate layer varied, while the (THF) clathrate hydrate layer thickness was held constant. The (CF) clathrate hydrate was found to grow very easily as structure II hydrate to the (THF) clathrate layer epitaxially. Figs. 47 and 48 show the C-H and the C-Cl stretching modes for the (CF) molecules respectively inside the large cavities.

At 13 K, in the C-H bending region the band is at 1217 cm^{-1} and a small shoulder at 1220 cm^{-1} appears, and the C-Cl frequency is listed at 673 cm^{-1}. Similar to the (THF) molecules, the (CF) molecules are also believed to occupy inequivalent sites in the hydrate cages, and by increasing the sample temperature they develop a rotational motion and the shoulder vanishes.

From Fig. 49 (a-d) the major CO_2 band has the same frequency reported earlier, 2345 cm^{-1}, which suggests that the CO_2 resides in the small cages of the type II hydrate lattice. Unfortunately, not enough information about a weak 2336 cm^{-1} band is known, but its presence is directly related to the (CF) clathrate hydrate layer.

Also, it is observed in Fig. 49 that the CO_2 clathrate hydrate samples grow better epitaxially to the two layered clathrate hydrate substrate as the (CF) clathrate sample thickness decreases. This is seen from the absorption intensity variation of the CO_2 band and in the FWHM of the O-D stretching band. Curve (d) is a spectrum of the best CO_2 clathrate hydrate sample obtained during this particular series. In this experiment only 0.5 min. H_2O:CF is deposited on the (THF) clathrate hydrate layer, which means that the surface of contact between the two layered clathrate substrate and the H_2O:CO_2 layer is still rich in L-defects that migrate from the (THF) clathrate hydrate substrate through the ultrathin (CF) hydrate layer to reach the growing CO_2 clathrate hydrate phase. In curve (c) no major changes occurred, which indicates that the defects also can migrate through a 0.5 micron thickness of (CF) hydrate (corresponding to 3 min. in deposition time). The major

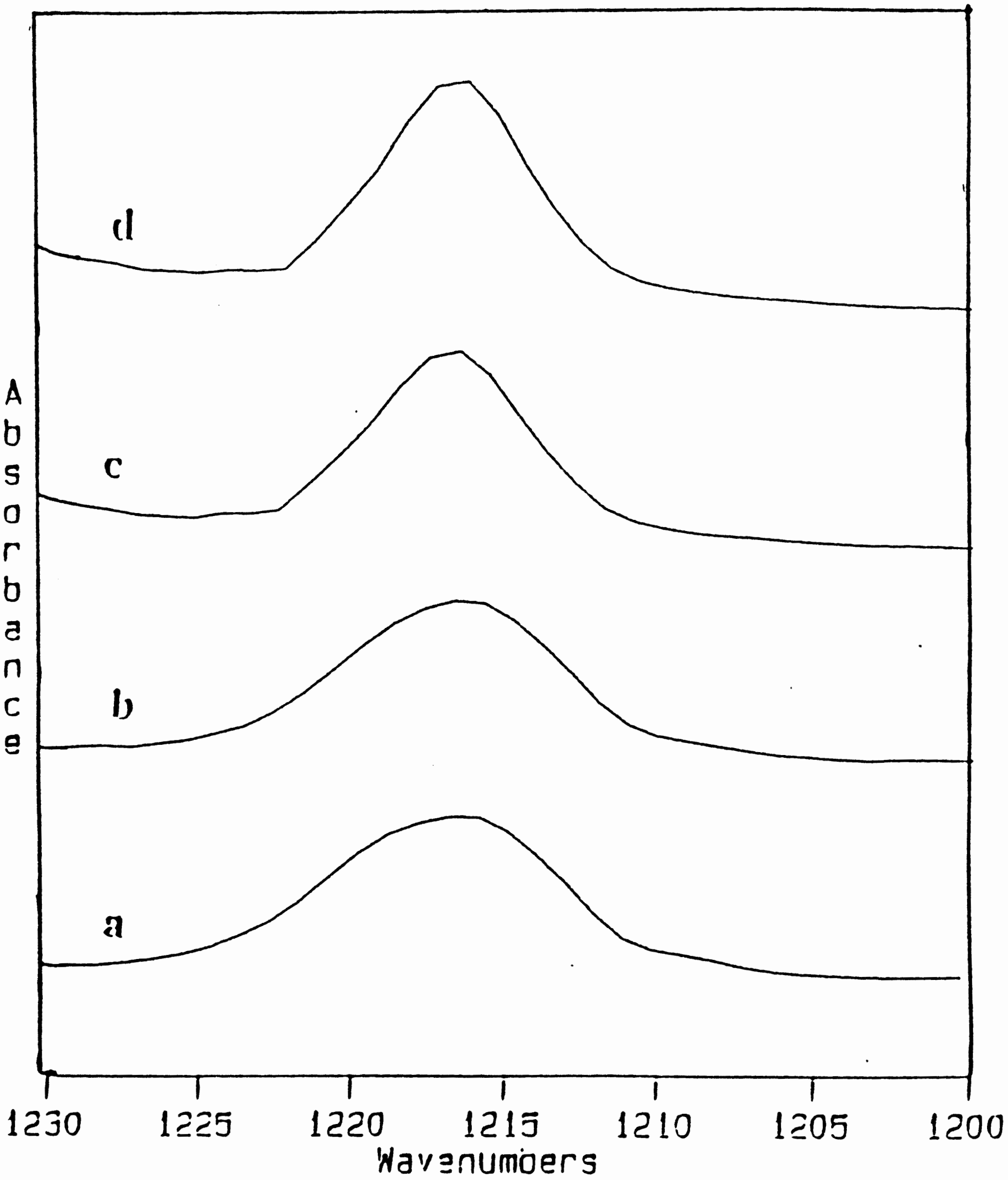
d
c
b
a
Absorbance
1230
1225
1220
1215
1210
1205
1200
Wavenumbers

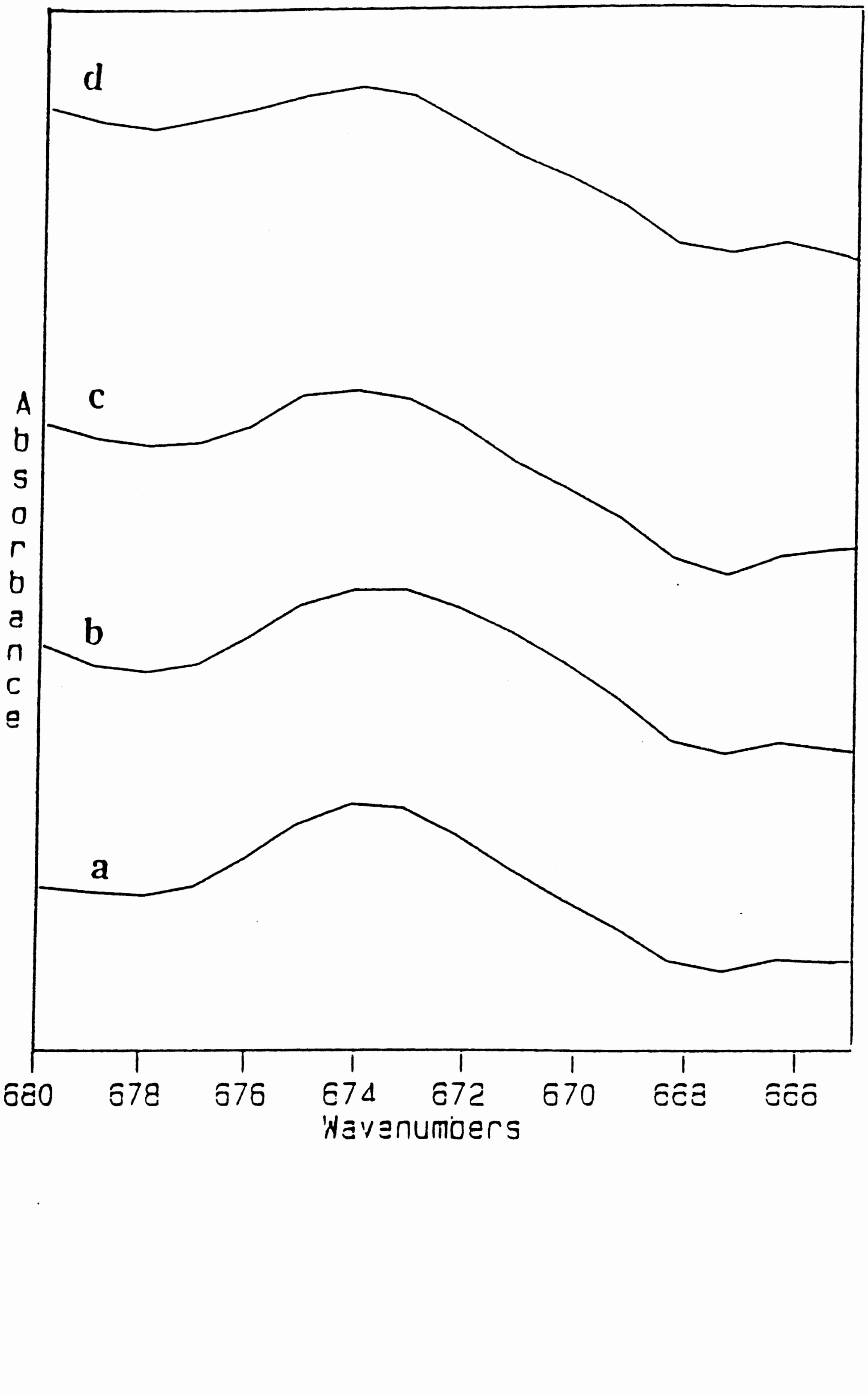
d
c
b
a
Absorbance
680
678
676
674
672
670
668
666
Wavenumbers

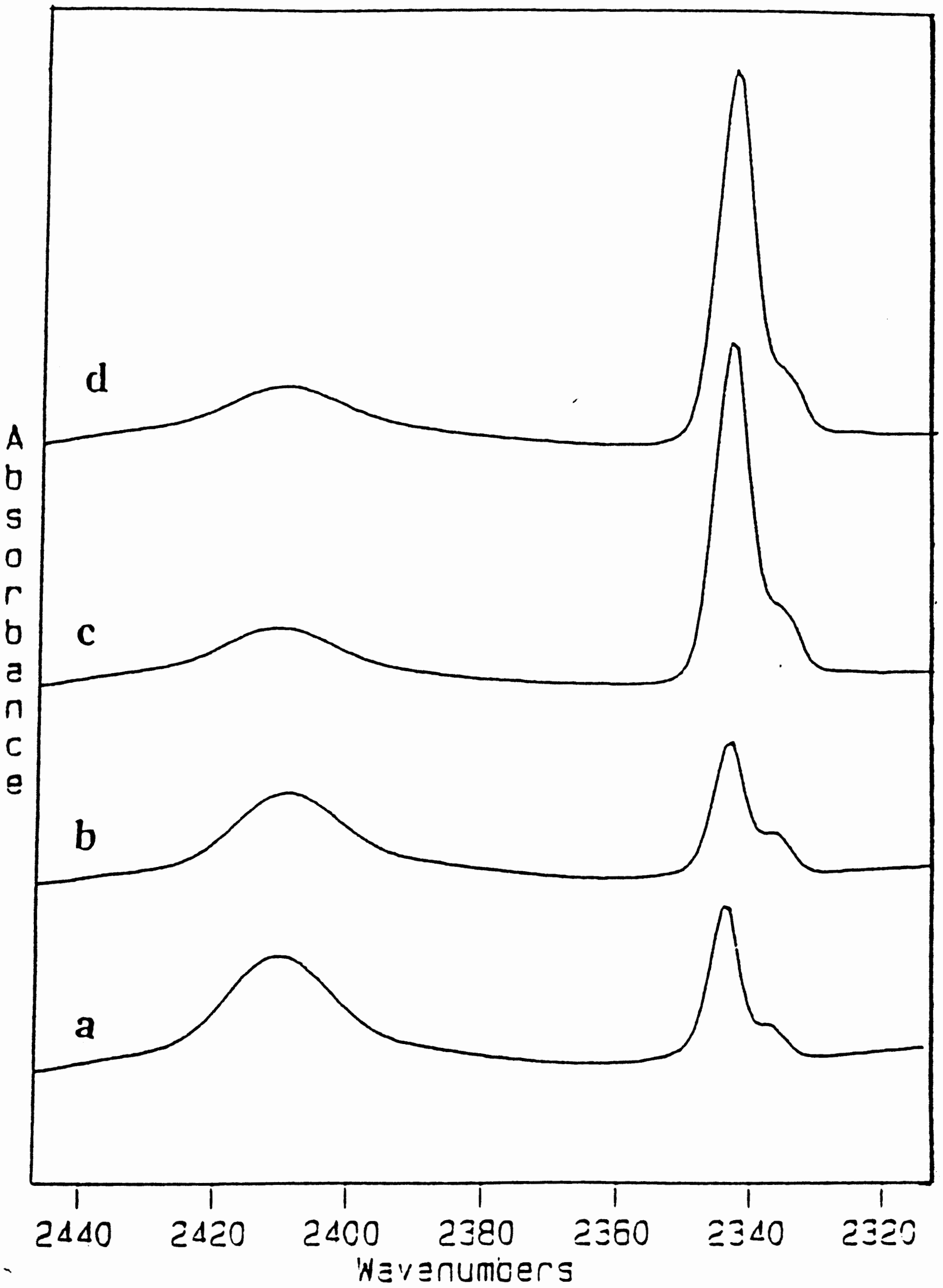
d
c
b
a
Absorbance
2440
2420
2400
2380
2360
2340
2320
Wavenumbers

change occurred in curve (b), where the deposition time of the (CF) hydrate is 6 min., leading to a very weak CO_2 band intensity, and a narrow HOD band. This suggests that there is no epitaxial growth on the hydrate substrate and most of the CO_2 hydrate formed is from the one minute overlap. This is justified by realizing that the (CF) deposition time in the sample corresponding to the spectrum in curve (b) is 6 min., which means that there is approximately 12 times more L-defect traps in this sample than the one represented by curve (d). The sample presented in curve (a) indicates that less L-defects are reaching the $H_2O:CO_2$ phase. Therefore, by increasing the thickness of the (CF) hydrate layer we directly increase the number of L-defect traps (or D-defect), and thus the effect between the substrate and the CO_2 growing phase will diminish. No major changes are seen between curve (b) and curve (a), the latter curve corresponding to a 9 min. deposit of H_2O:CF layer. Therefore, it is suggested that after 6 min. almost all the L-defects are trapped in the sample, and only ice grows after the one minute overlap period.

Methylchloride (meCl) Clathrate Hydrate

Similar to CO_2 and (CF), the methylchloride (meCl) clathrate hydrate fails to grow when deposited by itself on a CsI plate. However, by using the (EO) as a help gas, it was possible to form the (meCl) hydrate at 127 K. The frequency assignments shown in Table 15 are deduced from Figs. 50-52. Figs 50, 51, and 52 represent the C-H stretch, the CH_3 deformation, and the C-Cl stretch, respectively.

In order to understand the frequency assignments, one should be familiar first with the normal vibrations of the molecule (74). The (meCl) molecule has a $C_{3\upsilon}$ point group. This molecule contains nine fundamentals, of which three are totally symmetric (A_1) and six are degenerate (E). The fundamentals are shown in Fig. 53. The totally symmetric vibrations are υ_1, υ_2, and υ_3 and the degenerate vibrations are υ_4,υ_5, and υ_6. The fundamentals υ_1 and υ_4 represent the symmetric and the antisymmetric C-H stretching respectively, whereas the fundamentals υ_2 and υ_5 represent the symmetric and the

TABLE 15

FREQUENCIES AT (cm^{-1}) IN THE INFRARED SPECTRA OF (meCl) CLATHRATE HYDRATE

Fundamental	Vapor phase	Clathrate Hydrate
υ_1 (a_1)	2966.2 (vs)	2959/2986
υ_2 (a_1)	1354.9 (s)	1354/1348
υ_3 (a_1)	732.1 (vs)	733/717
υ_4 (e)	3041.8 (s)	3030
υ_5 (e)	1454.6 (m)	1446
υ_6 (e)	1015.0 (m)	------
2 υ_5	2878.8 (s)	2862
$\upsilon_5 + \upsilon_6$	2461 (w)	------

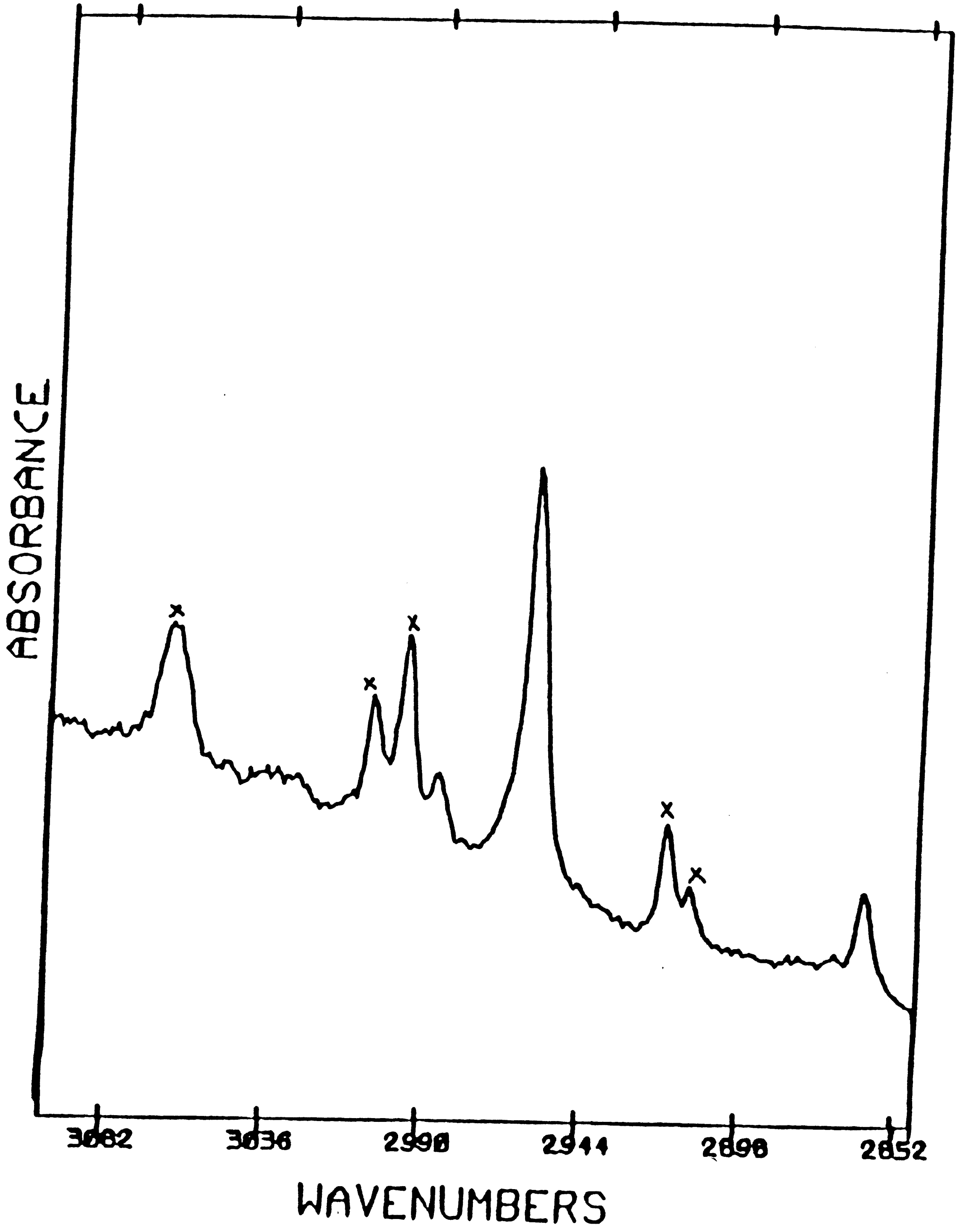
ABSORBANCE
3082
3036
2990
2944
2898
2852
WAVENUMBERS

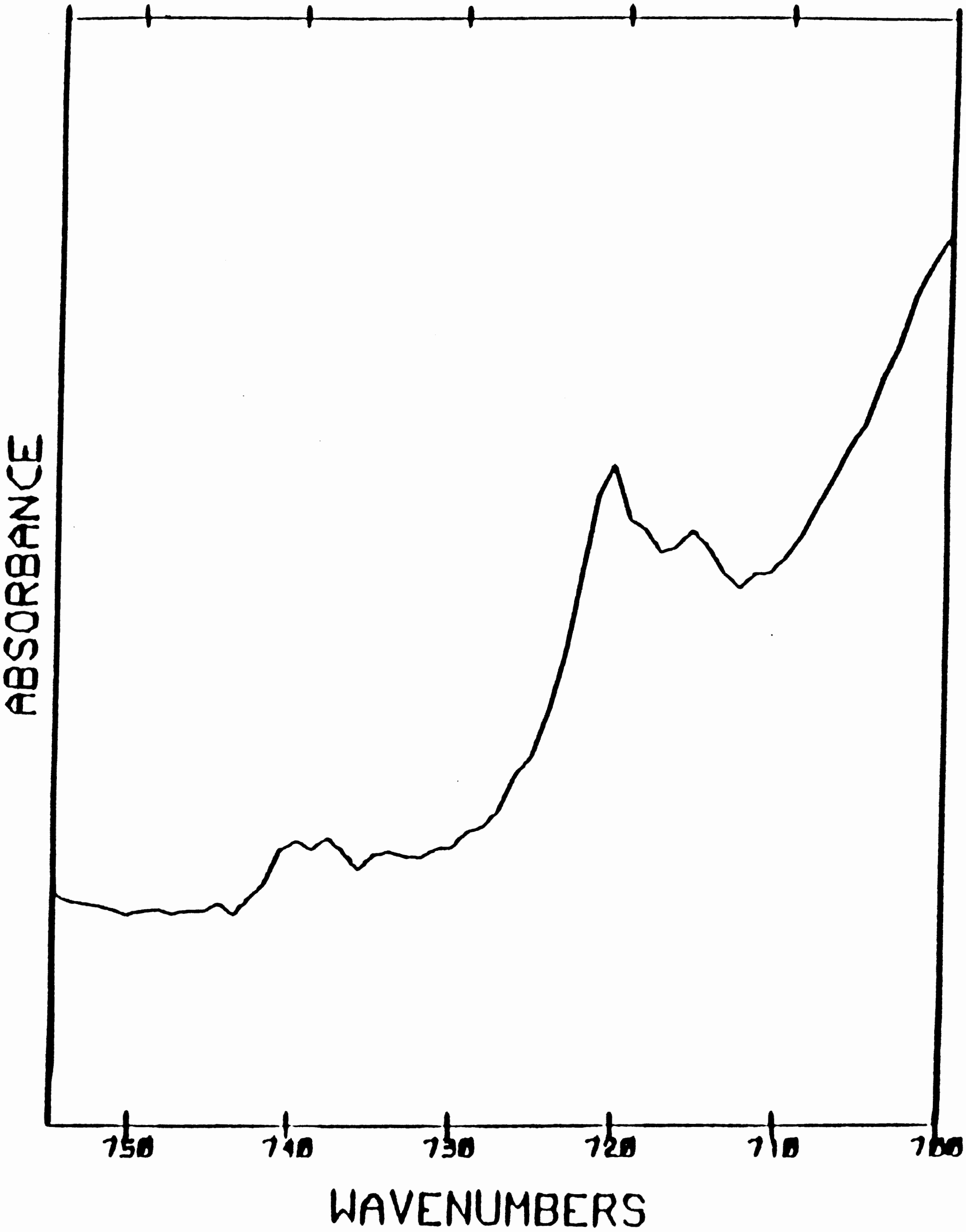
ABSORBANCE
750
740
730
720
710
700
WAVENUMBERS

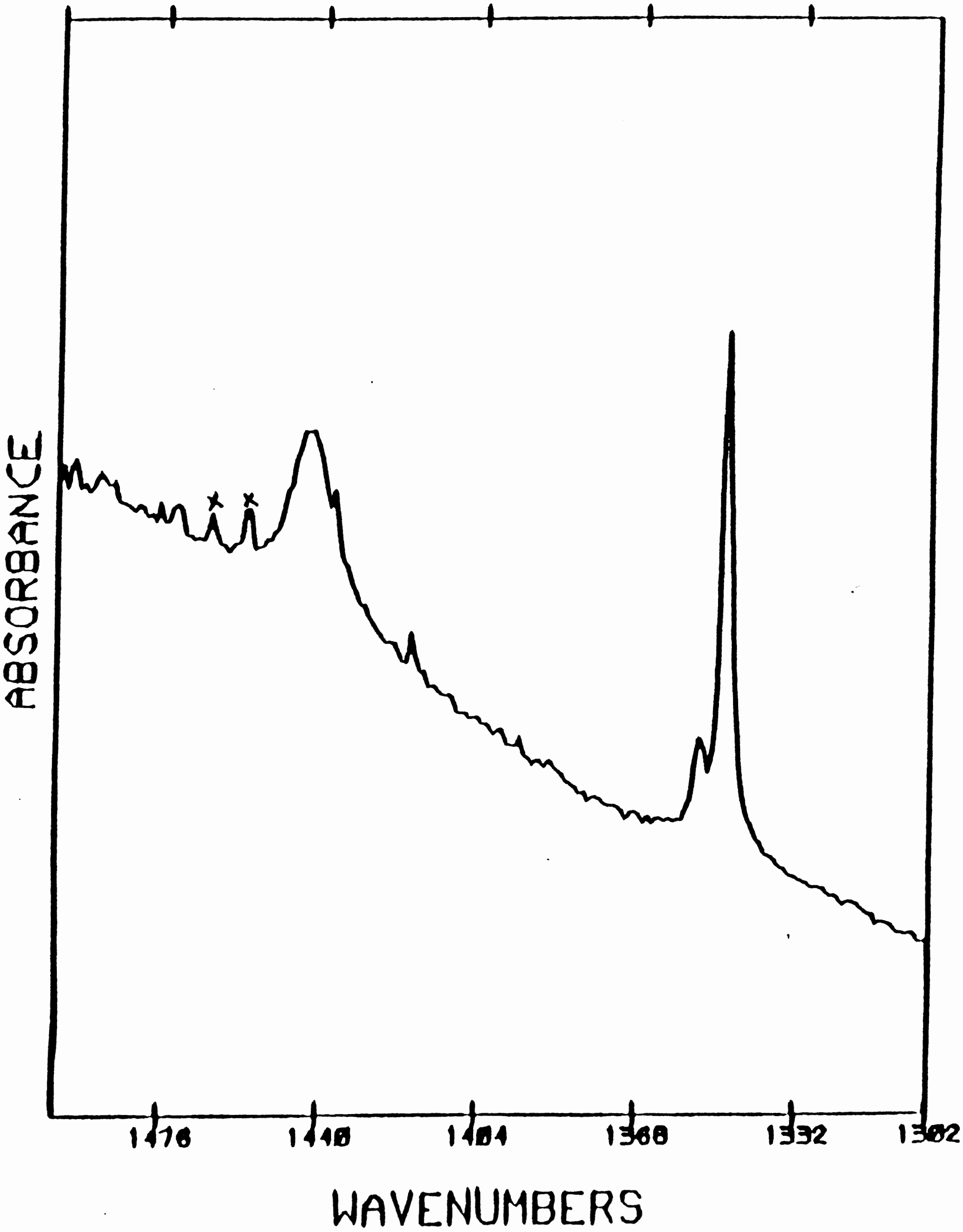
ABSORBANCE
x
x
1476
1440
1404
1368
1332
1302
WAVENUMBERS

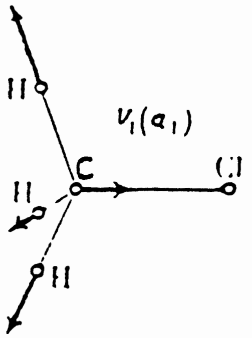
H
$\nu_1(a_1)$
C
Cl
H
H

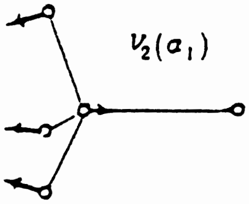
$\nu_2(a_1)$

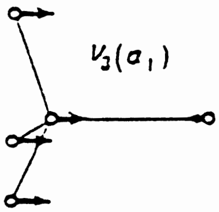
$\nu_3(a_1)$

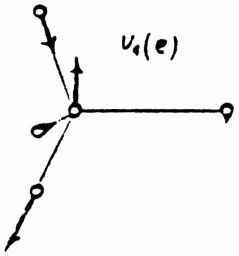
$\nu_4(e)$

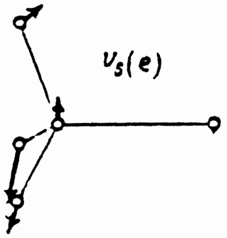
$\nu_5(e)$

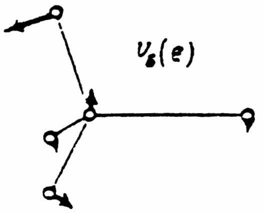
$\nu_6(e)$

antisymmetric bending mode of CH_3, respectively. The other two normal modes υ_3 and υ_6 represent the C-Cl stretching mode and the C-Cl bending mode, respectively. The symmetric methyl group deformation mode υ_2 as in Fig. 52 and the C-Cl stretching mode, υ_3 as in Fig. 51 show a doublet at 1354/1348 cm^{-1} (6 cm^{-1} splitting), and 740/721 cm^{-1} (19 cm^{-1} splitting). Since the splitting of the primary doublets resembles the (EO) small cage/large cage splitting, the result is attributed to a significant guest occupation of the small cages as well as the large cages, with the weak high frequency component representing the (meCl) molecules in the small cages. The secondary components of υ_3 at 734 and 714 cm^{-1} are caused by the natural abundance of the Chlorine isotopes. This is confirmed since the 7 cm^{-1} splitting (740-734 cm^{-1}) or (721-714 cm^{-1}) observed agrees with the value reported by Hertzberg (74). The two bands at 2959 and 2986 cm^{-1} in Fig. 50 are assigned to the υ_1 (a_1) of the (meCl) clathrate hydrate. The 2959 cm^{-1} is the frequency of the (meCl) occupying the large cages, and the 2986 cm^{-1} is the frequency of the (meCl) occupying the small cages. The υ_6 (e) methyl rocking mode absorption bands loses its intensity upon enclathration because of a dominating water band in this region. Since the band at 1446 cm^{-1} in Fig. 52 is very close to the vapor phase value of 1454 cm^{-1} (74), the mode is assigned to be the υ_5 (e), which leaves the weak band at 3030 cm^{-1} in Fig. 50 to correspond to the υ_4 (e) absorption band. The remaining band at 2862 cm^{-1} Fig. 50 is apparently caused by the overtone of the degenerate methyl group bending mode.

To confirm that the doublets observed in the (meCl) clathrate hydrate spectra are caused by small cage/large cage occupation, it is suggested to study the variation in the υ_2 frequency with respect to dilution factor, and relative guest concentration. The frequency υ_2 is chosen because it is the closest to the (EO) 1280 region, which allows a simultanous comparison of both modes. In Fig. 54 the total H_2O:Guest ratio is 6:1, where all the large cages are supposed to be occupied, in this mixture the relative concentration of meCl:EO is 4:1 (6: 0.8: 0.2). In Fig. 55 the same relative ratio of 4:1 meCl:EO is used, however the dilution factor is 6: 0.8.

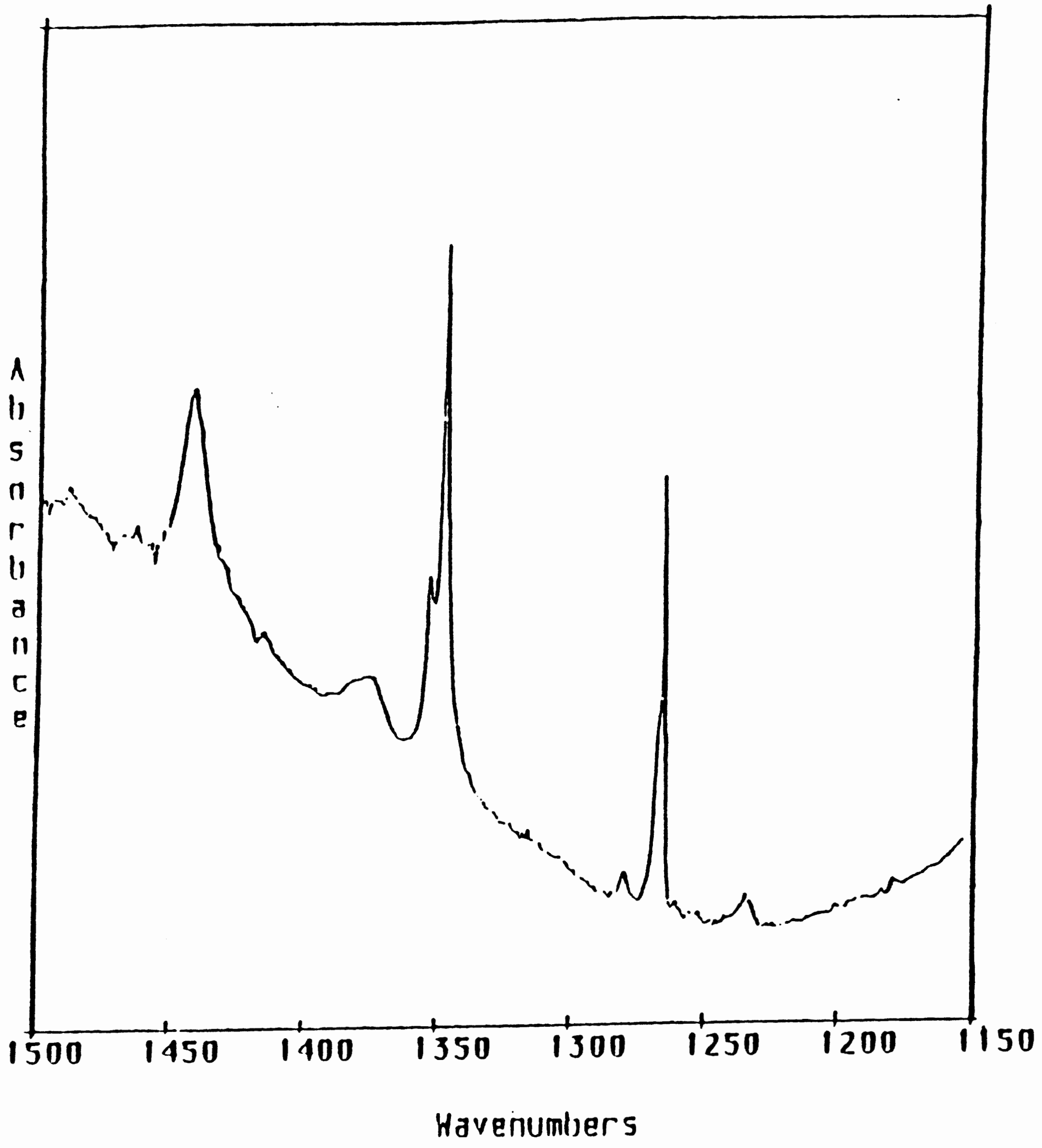
Absorbance
1500
1450
1400
1350
1300
1250
1200
1150
Wavenumbers

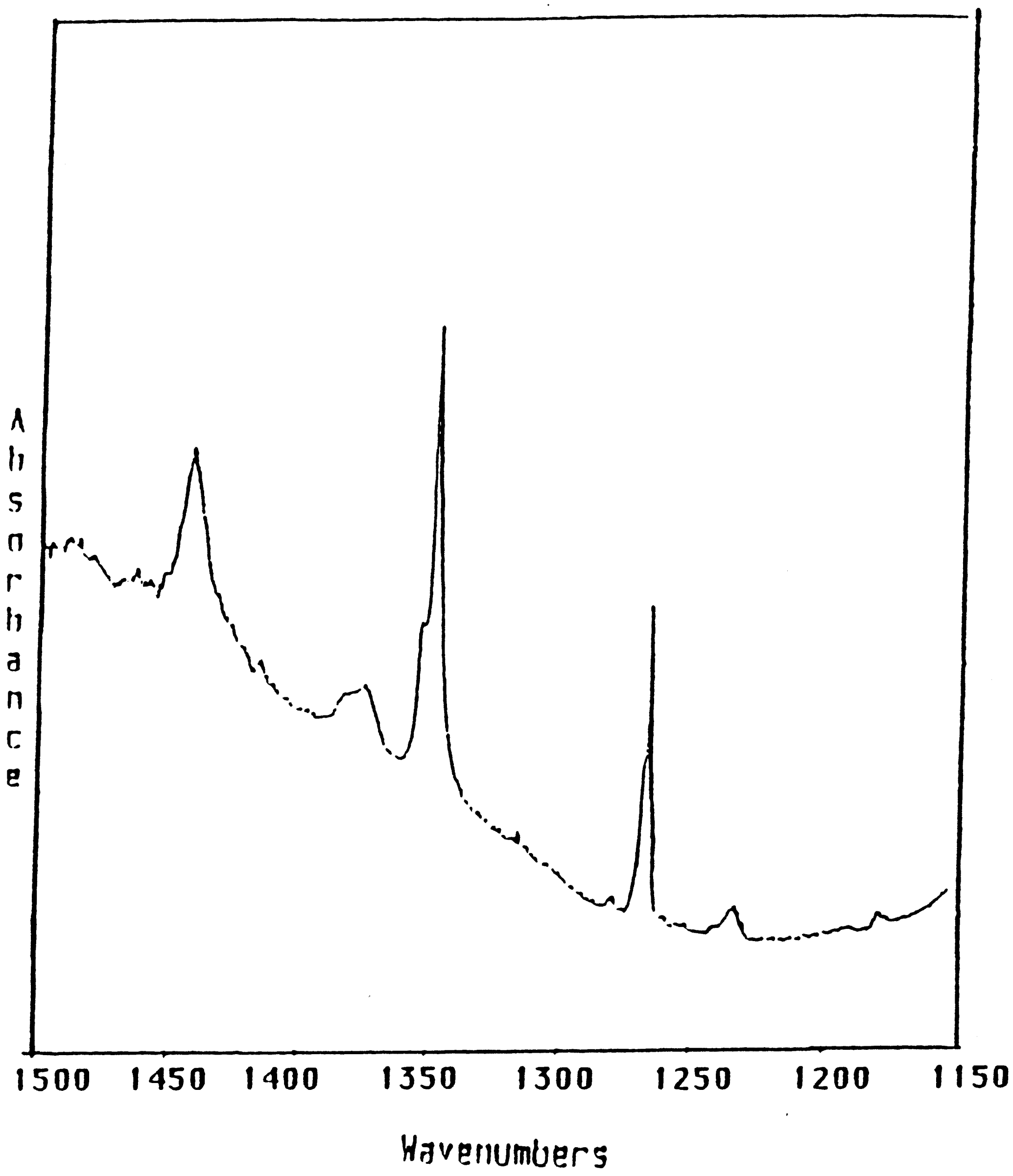
Absorbance
1500
1450
1400
1350
1300
1250
1200
1150
Wavenumbers

By comparing Figs. 54 and 55 it is noticeable that the small-cage band intensity decreased very rapidly compared to the decrease in the large-cage band intensity, which indicates that the population in the small-cage is decreasing faster than in the large-cage. This behavior is attributed to the fact that both (meCl), and (EO) have an approximate van der Waals size of 5.1 A°, which favors the large-cage occupation. This behavior is also seen in Fig. 56, where a deposition by an alternating-layer approach of 10:1:H_2O:EO and 6:1:H_2O:meCl mixtures was used. In this latter sample very few (EO) molecules occupied the small cages. This agrees totally with the clathrate hydrate structural geometries because by increasing the dilution factor of H_2O:EO we are automatically increasing the amount of water in the system, which leads to the rapid decrease of the population of small-cages vs. the large-cages, since the ratio of the cages is 1:3 respectively for the structure I hydrates.

Also, comparing Figs. 55 and 57, where the relative ratio of the sample represented by Fig. 57 is 3:1 meCl:EO, it is seen that less (EO) goes into the small-cages, which again supports the idea of the (EO) and (meCl) competing for the large-cage occupation. Since the υ_2 band of the (meCl) varies with the relative concentration of the guests, and also varies with the overall dilution factor, it is then concluded that the doublet seen in the region represents the small-cage/large-cage bands with the small-cage frequency being on the higher side.

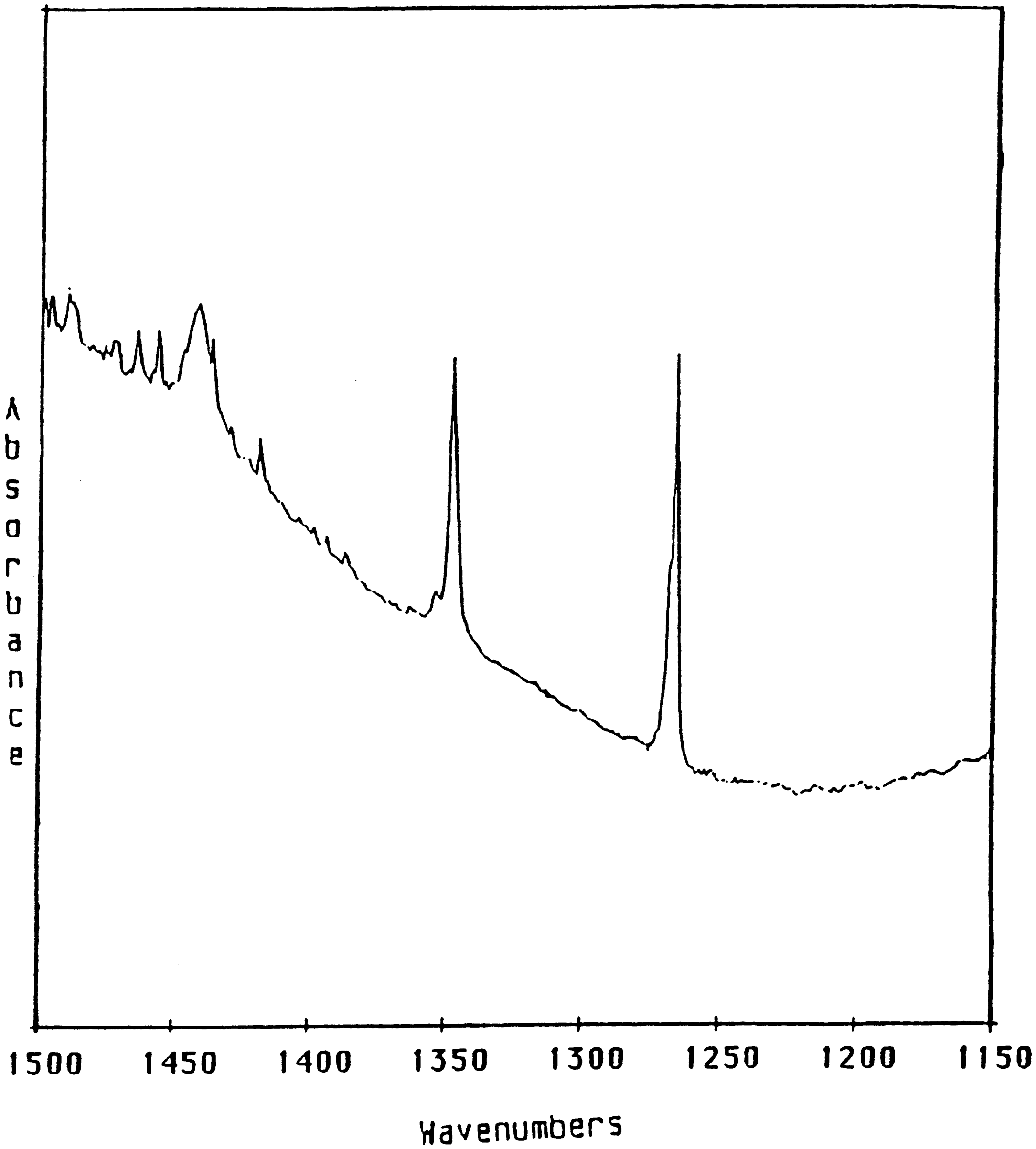
Absorbance
1500
1450
1400
1350
1300
1250
1200
1150
Wavenumbers

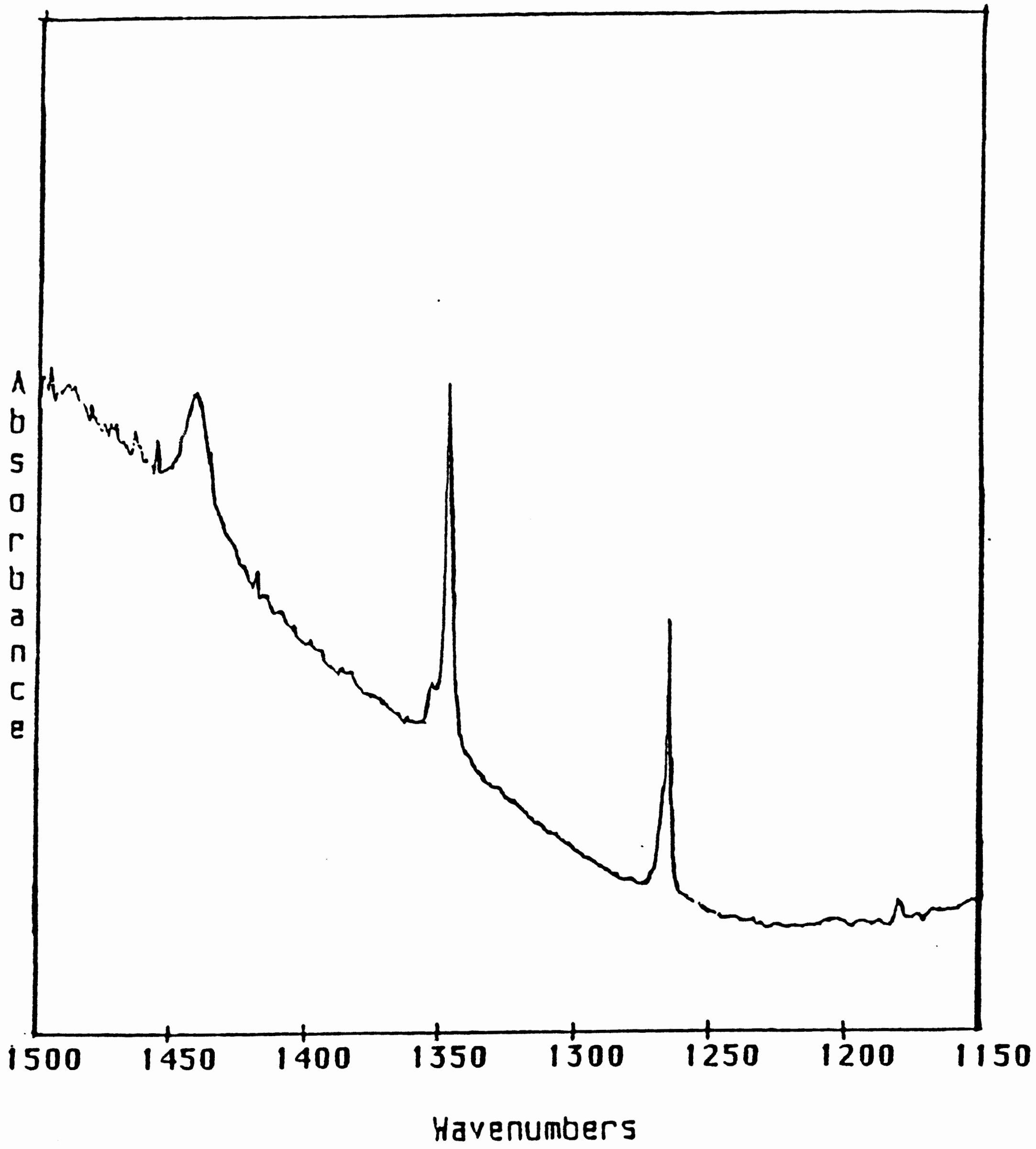
Absorbance
1500
1450
1400
1350
1300
1250
1200
1150
Wavenumbers

CHAPTER IV

CONCLUSION AND FUTURE RESEARCH

The results of spectroscopic study of the growth of CO_2 clathrate hydrates on (EO) and (THF) clathrate hydrate substrates, and the growth of (meCl) clathrate hydrate by using (EO) as a help gas have been presented. The orientational motion of the guest molecules have been investigated by varying the hydrate samples temperature. Also, the Bjerrum defect activity in the clathrate hydrate samples has been probed by varying the thickness of ether clathrate hydrate substrate, and the amount of help gas, required to form the clathrate hydrate samples, assuming that the help gas is an L-defect promoter when enclathrated.

The IR spectrum provides new evidence of the formation of the mixed CO_2 and (meCl) clathrate hydrate using (EO) as help gas, and the (EO) clathrate hydrate as a substrate, despite the fact that CO_2 and (meCl) are too volatile to allow direct deposition on a CsI plate to form the crystalline hydrate at higher temperatures. The primary conclusion drawn from the spectra of the guest molecules examined in this study supports the earlier conclusion of Bertie and Wright (38), which indicates that the small-cage stretching-mode frequencies, in general, are always at higher values than the large-cage frequencies.

The results of CO_2 clathrate hydrate grown epitaxially to the (EO) hydrate substrate *in vacuo*, under cryogenic conditions, show that the CO_2 occupy both the small and the large cages.

Despite the fact that a simple structure II hydrate normally contains polyatomic guest molecules having a maximum van der Waals diameter varying between 5.5 and 6.6 A°, the CO_2 molecules, with a maximum diameter of 4.7 A°, disobey that rule to form the type II hydrate grown epitaxially to the (THF) clathrate substrate at 150 K. This particular structure, which is stabilized by CO_2 molecules in the small type II cages only, is interesting considering that SO_2, having a maximum diameter of 5.0 A° (19), fails to grow a structure II hydrate under similar conditions (75). This makes the CO_2 molecule a possible candidate as the "largest" small molecule to form a type II hydrate. It is also interesting that the CO_2 molecules are limited to the small cages only, in contrast to the case for type II hydrates of small atomic and diatomic molecules (2, 24, 28).

During warming of the structure I hydrate sample the $^{12}CO_2$ large cage υ_3 band changed appearance; shifting to higher frequencies and broadening, whereas the corresponding $^{13}CO_2$ band did not show a comparable change. This is strong evidence that the $^{12}CO_2$ molecules in the large cages are subject to significant dynamical dipole-dipole interactions. In the structure II hydrate also, a similar conclusion was drawn for the $^{12}CO_2$ molecules occupying the small cages, which, for that structure, outnumber the large cages. The spectroscopic evidence of intermolecular coupling of guest molecules, from the behavior of a fundamental mode absorption band of a clathrate hydrate, is unique. However, evidence of intermolecular vibrational coupling has also been noted in the overtone region of the (EO) clathrate hydrate (36). In the bending mode region, obtaining evidence of the coupling was not possible as the $^{13}CO_2$ band was difficult to monitor. However, the increased rotational motion of the CO_2 guest molecules inside the large cages at high temperature was evidenced by a change in the "degeneracy" splitting at high temperatures.

The mechanism of formation of the (meCl) structure I clathrate hydrate and CO_2 structures I and II are believed to relate directly to the activity of Bjerrum defects in ice and ice-like materials. One very important result is the dependence of the clathrate hydrate growth on the thickness of the substrate. From the IR spectra it is shown that the clathrate hydrate quality degraded when the thickness of the L-defect promoter substrate is decreased, or when the thickness of an intermediate layer of a D-defect promoter is increased.

Finally, these results did not conclusively separate the nucleation process from the L-defect mechanism, but they apparently showed that if L-defects are not present in a minimum amount, by either migrating from a substrate to a new growing phase, or contributed from a help gas in a mixture, the non-polar guest clathrate hydrate fails to grow.

As for future research four interesting suggestions are summarized below:

1. Spectroscopic study is suggested to investigate the clathrate hydrate growth of alcohol, in particular methanol, since it is the chemical used in industry as an inhibitor to stop the natural gas clathrate hydrate formation in pipelines.
2. In order to have a better understanding of L-defect activity in CO_2 clathrate hydrate, it is suggested to conduct an isotopic exchange experiment by introducing isolated D_2O into the CO_2 clathrate hydrate layer, then irradiate the sample using electron bombardment, and then warm up the sample so the exchange from $(HOD)_2$ to HOD,which requires active L-defects, can be spectroscopically detected.
3. Perform a theoretical calculation to study the change in the transition-dipole coupling constant and in the υ_3 splitting of the CO_2 molecules occupying the clathrate hydrate large cavities.
4. Develop information about the 2337 cm^{-1} band in the C-O stretching region of CO_2, where the H_2O:CO_2 mixture is deposited epitaxially to a double layered clathrate hydrate substrate of H_2O:THF and H_2O:CF.

BIBLIOGRAPHY

1. J. H. van der Walls and J. C. Platteeuw, *Adv. Chem. Phys.* **2**, *1*, **(1959)**.

2. J. Nakahara, Y. Shigesato, A. Higashi, T. Hondoh and C. C. Langway, *Phil. Mag. B.* **57**, *No. 3, 421*, **(1988)**.

3. D. W. Davidson, S. K. Garg, S. R. Gough, Y. P. Handa, C. I. Ratcliff, J. A. Ripmeester and J. S. Tse, *Geochimica et Cosmochianica Acta.* **Vol. 50**, *619*, **(1986)**.

4. J. Lunine and D. Stevenson, *Icarus* **70**, *61*, **(1987)**.

5. D. L. Chandler, "*The Boston Globe*" July 11, **(1988)**.

6. C. F. Pearson, P. M. Halleck, P. L. McGuire, R. Hermes and M. Mathews, *J. Phys. Chem.* **87**, *4180*, **(1983)**.

7. P. B. Dharmawardhama, W. R. Parrish and E. D. Sloan, *Ind. Eng. Chem. Fundam.* **19**, *No. 4, 411*, **(1980)**.

8. J. W. Ullerich, M. S. Selim and E. D. Sloan, *J. AICHE* **33**, *No. 5, 747*, **(1987)**.

9. P. D. Menten, W. R. Parrish and E. D. Sloan, *Ind. Eng. Chem. Process Des. Dev.* **20**, *No. 2, 399*, **(1980)**.

10. E. G. Hammerschmidt, *Ind. Eng. Chem.* **26**, *851*, **(1934)**.

11. E. G. Hammerschmidt, *Oil Gas J.* **37**, *66*, **(1939)**.

12. H. Matsui and H. Nakayama, *Bull. Chem. Soc. Jpn.* **57**, *2663*, **(1984)**.

13. A. D. Potts and D. W. Davidson, *J. Phys. Chem.* **69**, *996*, **(1965**.

14. B. Z. Gorbunov and Y. I. Naberukhin, *Chem. Phys. Lett.* **19**, *215*, **(1972)**.

15. A. Davy, *Phil. Trans. Roy. Soc.* (London) **101**, *1*, **(1811)**.

16. M. Faraday, *Quart. J. Sci.* **15**, *71*, **(1823)**.

17. D. N. Glew and N. S. Rath, *J. Chem. Phys.* **44**, *1710*, **(1966)**.

18. H. M. Powell, *J. Chem. Soc.*, London, *61*, **(1948)**.

19. D. W. Davidson, "Water, a Comprehensive Treatise", F. Franks, Ed., Plenum Press, New York, **Vol. 3**, Chapt. 2, **(1972)**.

20. R. K. McMullan and G. A. Jeffery, *J. Chem. Phys.* **42**, *2725*, (**1965**).

21. T. C. W. Mak and R. K. McMullan, *J. Chem. Phys.* **42**, *2732*, (**1965**).

22. G. P. Johari, *J. Chem. Phys.* **74**, *1326*, (**1981**).

23. G. D. Holder and D. G. Manganiello, *Chem. Eng. Sci.* **9**, *37*, (**1982**).

24. D. W. Davidson, S. R. Gough, Y. P. Handa, C. I. Ratcliffe, J. A. Ripmeester and J. S. Tse, *J. de Physique*, Colloque C 1, Supplement to No. 3, **Vol. 48**, C 1-537, (**1987**).

25. J. S. Tse and M. L. Klein, *J. Phys. Chem.* **91**, *5789*, (**1987**).

26. E. Mayer and A. Hallbrucker, *J. Chem. Soc. CHEM COMMUN*, **No. 12**, *749*, (**1989**).

27. J. S. Tse, Y. P. Handa, C. I. Ratcliffe and B. M. Powell, *J. of Incl. Phenom.* **4**, *235*, (**1986**).

28. D. W. Davidson, Y. P. Handa, C. I. Ratcliffe, J. S. Tse and B. M. Powell, *Nature* **311**, *142*, (**1984**).

29. D. F. Sargent and L. D. Calvert, *J. Phys. Chem.* **70**, *2689*, (**1966**).

30. E. D. Sloan, Presented at 69th Annual GPA Convention, March 12-13, (**1990**).

31. J. E. Bertie and D. A. Othen, *Can. J. Chem.* **51**, *1159*, (**1972**).

32. J. E. Bertie and S. M. Jacobs, *J. Chem. Phys.* **68**, *97*, (**1977**).

33. J. E. Bertie and S. M. Jacobs, *Can. J. Chem.* **55**, *1777*, (**1976**).

34. J. E. Bertie and D. A. Othen, *Can. J. Chem.* **50**, *3443*, (**1972**).

35. J. P. Devlin, *J. Chem. Phys.* **91**, *5850*, (**1989**).

36. H. H. Richardson, P. J. Wooldridge and J. P. Devlin, *J. Chem. Phys.* **83**, *4387*, (**1985**).

37. J. E. Bertie and S. M. Jacobs, *J. Chem. Phys.* **69**, *4105*, (**1978**).

38. P. G. Wright, Ph.D. Thesis, University of Alberta, (**1976**).

39. J. E. D. Davies "Inclusion Compounds III", *Academic Press*, London, *Chapt. 2*, (**1984**).

40. J. E. Bertie and J. P. Devlin, *J. Chem. Phys.* **78**, *6340*, (**1983**).

41. H. H. Richardson, P. J. Wooldridge and J. P. Devlin, *J. Phys. Chem.* **8**, *3552*, (**1985**).

42. P. W. Atkins, "*Physical Chemistry*", University Press, Oxford, *Chapt. 17*, **(1978)**.

43. P. J. Wooldridge, H. H. Richardson, and J. P. Devlin, *J. Chem. Phys.* **87**, *4126*, **(1987)**.

44. K. Consani and C. Pimentel, *J. Phys. Chem.* **91**, *289*, **(1987)**.

45. P. V. Hobbs, "*Ice Physics*", Clarendon Press, Oxford,Chapt. 2, **(1974)**.

46. F. Franks, "*Water a Comprehensive Treatise*", F. Franks, Ed., Plenum Press, New York, **Vol. 1**, *Chapt. 4*, **(1972)**.

47. E. Whally and J. B. R. Heath, *J. Chem. Phys.* **45**, *3976*, **(1966)**.

48. L. Pauling, *J. Am Chem. Soc.* **57**, *2680*, **(1935)**.

49. P. R. Camp, W. Kiszenick and D. A. Arnold, *Electrical Conduction in Ice*, in "Physics of Ice", *450*, **(1969)**.

50. D. W. Davidson and J. A. Ripmeester, "*Inclusion Compounds III*", Chapt. 3, **(1984)**.

51. S. R. Gough, E. Whalley and D. W. Davidson, *Can. J. of Chem.* **46**, *1673*, **(1967)**.

52. S. K. Garg, D. W. Davidson and J. A. Ripmeester, *J. of Magn. Reson* **15**, *295*, **(1974)**.

53. D. G. Leaist, J. J. Murray, L. Post and D. W. Davidson, *J. Phys. Chem.* **86**, *4175*, **(1982)**.

54. M. A. White and M. T. MaClean, *J. Phys. Chem.* **89**, *1380*, **(1984)**.

55. O. Yamamuro, M. Oguni, T. Matsuo and H. Suga, *Sol. State Com.* **62**, *No. 4*, *289*, **(1987)**.

56. O. Yamamuro, M. Oguni, T. Malsuo and H. Suga, *J. Phys. Chem.* **49**, *425*, **(1987)**.

57. F. Fujara, S. Wefing and W. F. Kuhs, *J. Chem. Phys.* **88**, *6801*, **(1988)**.

58. "The Interpretation of Vapor - Phase Infrared Spectra" (Sadtler Research Laboratories, Philadelphia, **Vol. 2**, p. 330, **(1984)**.)

59. C. J. Pouchert, "The Aldrich Library of Infrared Spectra" Ed. III 139G, **(1981)**.

60. J. S. Tse and W. R. McKinnon, *J. Phys. Chem.* **91**, *4188*, **(1987)**.

61. D. W. Davidson and G. J. Wilson, *Can J. of Chem.* **41**, *1424*, **(1963)**.

62. C. I. Ratcliffe and J. A. Ripmeester, *J. Phys. Chem.* **90**, *1259*, **(1986)**.

63. B. Schmitt, Ph. D. Thesis, University of Grenoble, **(1986)**.

64. M. Falk, *J. Chem. Phys.* **86**, *560*, **(1987)**.

65. M. Falk and P. F. Seto, *Can. J. Spectrasc.* **31**, *134*, **(1986)**.

66. F. Fleyfel and J. P. Devlin, *J. Phys. Chem.* **93**, *7292*, **(1989)**.

67. J. A. Barnes and T. E. Gough, *J. Chem. Phys.* **86**, *6012*, **(1987)**.

68. G. E. Ewing and D. T. Sheng, *J. Phys. Chem.* **92**, *4062*, **(1988)**.

69. H. H. Richardson, Ph.D. Thesis, Oklahoma State University, **(1985)**.

70. J. C. Decius, *J. Chem. Phys.* **23**, *1290*, **(1955)**.

71. C. H. Haas and D. F. Hornig, *J. Chem. Phys.* **32**, *1763*, **(1960)**.

72. R. Desselkamp and G. E. Ewing, *J. Chem. Soc. Faraday Trans.* **86**, *1*, **(1990)**.

73. H. Yamada and W. B. Person, *J. Chem. Phys.* **41**, *2478*, **(1964)**.

74. G. Herzberg, F.R.S.C., in "Infrared and Raman Spectra", D. Van Nostrand Company, Inc.; Princeton, New Jersey **(1956)**.

75. F. Fleyfel, H. H. Richardson and J. P. Devlin, *J. Phys. Chem.*, submitted for publication, **(1990)**.

APPENDIX A

NOMENCLATURE

τ : relaxation time

A: Arrhenius constant

Ea: activation energy

k : Boltzmann constant

T : temperature

N : normal hydrogen bond

M : guest molecule

υ : angular frequency

T_d: deposition temperature

T_s: scanning temperature

P : pressure of the system

t_d: deposition time (min.)

f : flowrater setting

s : substrate

L : layer

SI: Structure I

SII: Structure II

D : Debye

C: Coulomb

cm: centimeter

e : charge of electron

a_0: Bohr radius

A°: angstroms

J : joules

KE: kinetic energy

V: potential energy

x : cartesian coordinates

x· : derivation of the coordinate with respect to time

q : new coordinates

m : mass of the molecule

P_1: momentum of molecule

P_2: momentum of molecule 2

α : coupling constant

β : bond constant

E : energy of molecule 1

H : Hamiltonian

μ : 0.5 x mass

$\Delta\upsilon$: frequency splitting

M (L): mixture of a layer

APPENDIX B

UNIT CONVERSIONS FROM N/m TO $D^2/A°5$

Knowing that:

$1D = 3.33564 \text{ X } 10^{-28}$ C.m

$1D = 10^{-18}$ statC.cm

$e = 4.803207 \text{ x } 10^{-10}$ statC

Therefore:

$$1D = \left(\frac{10^{-18}}{4.803207 \text{ x } 10^{-10}}\right) \text{e cm}$$

Which leads to:

$$e = \left(\frac{4.803207 \text{ x } 10^{-10}}{10^{-18}}\right) \text{ D/cm, or}$$

$$\boxed{e = 4.803207 \text{ x } 10^{8} \text{ D/cm}}$$

But since:

$$e = 4.803207 \text{ x } 10^{8} \frac{D}{cm} \text{ x } \frac{1cm}{10^{8}A°} ,$$

$$e = 4.803207 \frac{D}{A°}$$

Using Hartree equation:

$$27.212 \text{ ev} = \frac{e^2}{a_o}$$

Substituting e in the equation leads to:

$$27.212\ \mathrm{ev} = \frac{(4.803207)^2}{0.5292} D^2/A^{\circ 3}$$

Therefore:

$$1\ \mathrm{ev} = 1.602073\ D^2/A^{\circ 3}$$

Thus,

$$1\ \mathrm{ev} = 1.602177 \times 10^{-19}\ \mathrm{J}$$

$$\Rightarrow 1_J = \left(\frac{1.602073}{1.602177 \times 10^{-19}}\right) D^2/A^{\circ 3} \Rightarrow 1J = 9.99935 \times 10^{18}\ D^2/A^{\circ 3}$$

Knowing that:

$$1_J = 1\ \mathrm{N.m} = 10^{10}\ \mathrm{N.A^\circ}$$

gives:

$$10^{10}\ \mathrm{N.A^\circ} = 9.99935 \times 10^{18}\ D^2/A^{\circ 3}$$

Therefore,

$$1\ \mathrm{N} = 9.99935 \times 10^{8}\ D^2/A^{\circ 4}$$

$$1\frac{N}{m} = 9.99935 \times 10^{8}\ D^2/A^{\circ 4} \times \frac{1}{10^{10}\ A^\circ}$$

$$\boxed{\frac{1N}{m} = 9.99935 \times 10^{-2}\ D^2/A^{\circ 5}}$$

As an example, the numerical value for the coupling constant $\alpha = 14.2 \times 10^5$ dynes/cm.

But:

$1N = 10^5$ dynes

Therefore:

$$\alpha = 14.2 \times 10^5 \frac{\text{dynes}}{\text{cm}} = 14.2 \frac{\text{N}}{\text{cm}} = 14.2 \frac{\text{N}}{\text{cm}} \times \frac{100\text{cm}}{\text{m}}$$

Thus, $\alpha = 1420 \frac{\text{N}}{\text{m}}$

Using the conversion factor found earlier gives:

$\alpha = 1420 \times 9.99935 \times 10^{-2} = 141.99077\ D^2/A^{\circ 5}$

APPENDIX C

DERIVATION OF THE FREQUENCY SPLITTING EQUATION

In cartesian coordinates the kinetic energy of the system is:

$$T = \frac{m}{2} (\dot{x}_1^2 + \dot{x}_2^2)$$

The potential energy of the system is:

$$V = \frac{1}{2} \beta (x_1^2 + x_2^2) + \alpha x_1 x_2$$

Introducing two new coordinates q_1 and q_2

$$q_1 = x_1 - x_2 \qquad q_2 = x_1 + x_2$$

$$x_1 = \frac{q_1 + q_2}{2} \qquad x_2 = \frac{q_2 - q_1}{2}$$

$$x_1^2 = \frac{1}{4} [q_1^2 + q_2^2 + 2q_1q_2] \qquad x_2^2 = \frac{1}{4} [q_1^2 + q_2^2 - 2q_1q_2]$$

$$\dot{x}_1 = \frac{1}{2} (\dot{q}_1 + \dot{q}_2) \qquad \dot{x}_2 = \frac{1}{2} (\dot{q}_2 - \dot{q}_1)$$

$$\dot{x}_1^2 = \frac{1}{4} (\dot{q}_1^2 + \dot{q}_2^2 + 2\dot{q}_1\dot{q}_2) \qquad \dot{x}_2^2 = \frac{1}{4} (\dot{q}_2^2 + \dot{q}_1^2 - 2\dot{q}_2\dot{q}_1)$$

Writing the Kinetic energy as a function of the new coordinates, and the momenta:

$$T = \frac{m}{4} (\dot{q}_1^2 + \dot{q}_2^2)$$

Therefore:

$$\dot{q}_1^2 = \frac{4\,P_1^2}{m^2} \qquad \dot{q}_2^2 = \frac{4\,P_2^2}{m^2}$$

$$T = \frac{m}{4}\left(\frac{4\,P_1^2}{m^2} + \frac{4\,P_2^2}{m^2}\right) \qquad \boxed{T = \frac{P_1^2}{m} + \frac{P_2^2}{m}}$$

Writing the potential energy in terms of the new coordinates:

$$V = \frac{\beta}{2}\,(x_1^2 + x_2^2) + \alpha\, x_1\, x_2$$

$$= \frac{\beta}{4}\,(q_1^2 + q_2^2) + \frac{\alpha}{4}\,(q_2^2 - q_1^2)$$

$$= q_1^2\left(\frac{\beta}{4} - \frac{\alpha}{4}\right) + q_2^2\left(\frac{\beta}{4} + \frac{\alpha}{4}\right)$$

The Hamiltonian is:

$H = T + V$

$$= \left(\frac{P_1^2}{m} + \frac{P_2^2}{m}\right) + \frac{\beta}{4}\left(1 - \frac{\alpha}{\beta}\right) q_1^2 + \frac{\beta}{4}\left(1 + \frac{\alpha}{\beta}\right) q_2^2$$

$$H = \left(\frac{P_1^2 + P_2^2}{m}\right) + \frac{\beta}{4}\,\left(1 - \frac{\alpha}{\beta}\right)q_1^2 + \frac{\beta}{4}\,\left(1 + \frac{\alpha}{\beta}\right) q_2^2$$

let $m = 2\mu$, $\frac{\beta'}{2} = \frac{\beta}{4}\left(1 - \frac{\alpha}{\beta}\right)$ $\frac{\beta''}{2} = \frac{\beta}{4}\left(1 + \frac{\alpha}{\beta}\right)$

Separating the Hamiltonian:

$$H_1 = \frac{P_1^2}{2\mu} + \frac{\beta'}{2}\,q_1^2$$

$$H_2 = \frac{P_2^2}{2\mu} + \frac{\beta''}{2} q_2^2$$

The corresponding energies:

$$E_1 = (n_1 + \frac{1}{2}) h\upsilon_1 \quad \upsilon_1 = \frac{1}{2\mu} \sqrt{\frac{\beta'}{\mu}}$$

$$E_2 = (n_2 + \frac{1}{2}) h\upsilon_2 \quad \upsilon_2 = \frac{1}{2\pi} \sqrt{\frac{\beta''}{\mu}}$$

Therefore, the Harmonic oscillator frequencies are:

$$\upsilon_1 = \frac{1}{2\pi} \left[\frac{2}{m} \text{ x } \frac{\beta}{2} \quad 1 - \frac{\alpha}{\beta} \right]^{1/2}$$

$$= \upsilon_o (1 - \frac{\alpha}{\beta})^{1/2} \qquad \upsilon_1 = \upsilon_o (1 - \frac{\alpha}{2\beta})$$

$$\upsilon_2 = \frac{1}{2\pi} \left[\frac{2}{m} \text{ x } \frac{\beta}{2} \quad 1 + \frac{\alpha}{\beta} \right]^{1/2}$$

$$= \upsilon_o (1 + \frac{\alpha}{\beta})^{1/2} \qquad \upsilon_2 = \upsilon_o (1 + \frac{\alpha}{2\beta})$$

Thus, the splitting equation is:

$$\boxed{\Delta\upsilon = \upsilon_o \frac{\alpha}{\beta}}$$

VITA

Fouad Fleyfel

Candidate for the Degree of

Doctor of Philosophy

Thesis: SPECTROSCOPIC INVESTIGATION OF SIMPLE, MIXED, AND DOUBLE CLATHRATE HYDRATES; PROBE OF DEFECT ACTIVITY

Major Field: Chemistry

Biographical:

Personal Data: Birthdate: March 11, 1961 in Beirut, Lebanon, the son of Adnan and Mona Fleyfel; Citizenship: Permanent Resident

Education: Graduated from Makassed High School, Beirut, Lebanon in May 1979; attended D. E. U. G. 'A' (Diplome D'étude Universitaire Général), at the'Université de Sciences et Techniques du Languedoc', Montpellier, France.from 1979-1981; recieved Bachelor of Science Degree from University of Tulsa, Tulsa, Oklahoma with a major in Chemical Engineering and a minor in Math in May, 1985; completed requirements for the Doctor of Philosophy Degree at Oklahoma State University, Stillwater, Oklahoma in Physical Chemistry in December, 1990.

Professional Experience: Graduate Teaching and Research Assistant 1986-90.